

Alma Mater Studiorum Università di Bologna
Archivio istituzionale della ricerca

The Long Noncoding RNA CCAT2 Induces Chromosomal Instability Through BOP1-AURKB Signaling

This is the final peer-reviewed author's accepted manuscript (postprint) of the following publication:

Published Version:

Chen, B., Dragomir, M.P., Fabris, L., Bayraktar, R., Knutsen, E., Liu, X.u., et al. (2020). The Long Noncoding RNA CCAT2 Induces Chromosomal Instability Through BOP1-AURKB Signaling. *GASTROENTEROLOGY*, 159(6), 2146-2162.e33-2162.e33 [10.1053/j.gastro.2020.08.018].

Availability:

This version is available at: <https://hdl.handle.net/11585/786069> since: 2020-12-30

Published:

DOI: <http://doi.org/10.1053/j.gastro.2020.08.018>

Terms of use:

Some rights reserved. The terms and conditions for the reuse of this version of the manuscript are specified in the publishing policy. For all terms of use and more information see the publisher's website.

This item was downloaded from IRIS Università di Bologna (<https://cris.unibo.it/>).
When citing, please refer to the published version.

(Article begins on next page)

This is the peer reviewed accepted manuscript of:

Chen B, Dragomir MP, Fabris L, Bayraktar R, Knutsen E, Liu X, Tang C, Li Y, Shimura T, Ivkovic TC, De los Santos MC, Anfossi S, Shimizu M, Shah MY, Ling H, Shen P, Multani AS, Pardini B, Burks JK, Katayama H, Reineke LC, Huo L, Syed M, Song S, Ferracin M, Oki E, Fromm B, Ivan C, Bhuvaneshwar K, Gusev Y, Mimori K, Menter D, Sen S, Matsuyama T, Uetake H, Vasilescu C, Kopetz S, Parker-Thornburg J, Taguchi A, Hanash SM, Girnita L, Slaby O, Goel A, Varani G, Gagea M, Li C, Ajani JA, Calin GA, The Long Noncoding RNA CCAT2 induces chromosomal instability through BOP1 - AURKB signaling, *Gastroenterology* (2020),

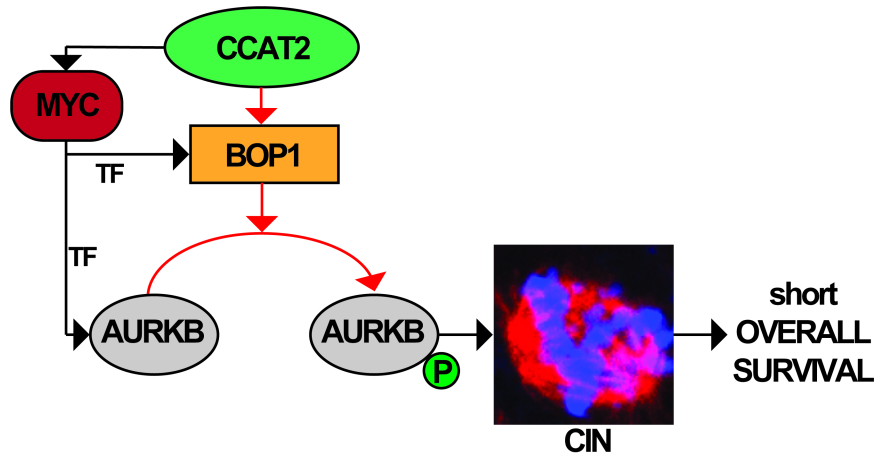
Final version available at: <https://doi.org/10.1053/j.gastro.2020.08.01>

Rights / License:

The terms and conditions for the reuse of this version of the manuscript are specified in the publishing policy. For all terms of use and more information see the publisher's website.

This item was downloaded from IRIS Università di Bologna (<https://cris.unibo.it/>)

When citing, please refer to the published version.



The Long Noncoding RNA *CCAT2* induces chromosomal instability through BOP1 - AURKB signaling

Baoqing Chen^{1,2,29*}, **Mihnea P. Dragomir**^{1,3*}, **Linda Fabris**^{1*}, **Recep Bayraktar**^{1*},
Erik Knutsen^{1,4}, *Xu Liu*^{1,5}, *Changyan Tang*⁶, *Yongfeng Li*¹, *Tadanobu Shimura*⁷, *Tina Catela Ivkovic*⁸,
*Mireia Cruz De los Santos*¹, *Simone Anfossi*¹, *Masayoshi Shimizu*¹, *Maitri Y. Shah*¹, *Hui Ling*¹,
Peng Shen^{1,9}, *Asha S. Multani*¹⁰, *Barbara Pardini*^{1,30,31}, *Jared K. Burks*¹¹, *Hiroyuki Katayama*¹²,
*Lucas C. Reineke*¹³, *Longfei Huo*¹⁴, *Muddassir Syed*¹⁴, *Shumei Song*¹⁴, *Manuela Ferracin*¹⁵, *Eiji Oki*¹⁶,
Bastian Fromm^{17,18}, *Cristina Ivan*^{1,19}, *Krithika Bhuvaneshwar*²⁰, *Yuriy Gusev*²⁰, *Koshi Mimori*²¹,
*David Menter*¹⁴, *Subrata Sen*²², *Takatoshi Matsuyama*²³, *Hiroyuki Uetake*²⁴, *Catalin Vasilescu*^{3,25},
*Scott Kopetz*¹⁴, *Jan Parker-Thornburg*¹⁰, *Ayumu Taguchi*²², *Samir M. Hanash*¹², *Leonard Girnita*²⁶,
Ondrej Slaby^{8,27}, *Ajay Goel*^{7,32}, *Gabriele Varani*⁶, *Mihai Gagea*²⁸, *Chunlai Li*¹ & *Jaffer A. Ajani*¹⁴ &
George A. Calin^{1,19,33} &

* - author names in bold designate shared co-first authorship.

& - co-corresponding authors;

¹ Department of Experimental Therapeutics, The University of Texas MD Anderson Cancer Center, Houston, TX 77030, USA.

² Department of Radiation Oncology, State Key Laboratory of Oncology in South China, Collaborative Innovation Center for Cancer Medicine, Sun Yat-sen University Cancer Center, Guangzhou, Guangdong, China;

³ Department of General Surgery, Fundeni Clinical Hospital, Carol Davila University of Medicine and Pharmacy, Bucharest, Romania.

⁴ Department of Medical Biology, Faculty of Health Sciences, UiT - The Arctic University of Norway, Tromsø, Norway.

⁵ Department of Thoracic Surgery, The First Affiliated Hospital of Xi'an Jiaotong University, Xi'an, China

⁶ Department of Chemistry, University of Washington, Seattle, WA 98195, USA.

⁷ Center for Gastrointestinal Research; Center for Translational Genomics and Oncology, Baylor Scott & White Research Institute, Charles A Sammons Cancer Center, Baylor University Medical Center, Dallas, USA.

⁸ Central European Institute of Technology, Masaryk University, Brno, Czech Republic

⁹ Department of Oncology, Nanfang Hospital, Southern Medical University, Guangzhou, China.

¹⁰ Department of Genetics, The University of Texas MD Anderson Cancer Center, Houston, TX, USA.

¹¹ Department of Leukemia, The University of Texas MD Anderson Cancer Center, Houston, TX, USA.

- ¹² Department of Clinical Cancer Prevention, University of Texas MD Anderson Cancer Center, Houston, TX, USA.
- ¹³ Department of Neuroscience, Baylor College of Medicine, Houston, TX, USA.
- ¹⁴ Department of Gastrointestinal Medical Oncology, The University of Texas MD Anderson Cancer Center, Houston, TX, USA.
- ¹⁵ Department of Experimental, Diagnostic and Specialty Medicine (DIMES), University of Bologna, 40126 Bologna, Italy.
- ¹⁶ Department of Surgery and Science, Graduate School of Medical Sciences, Kyushu University, Fukuoka, Japan.
- ¹⁷ Science for Life Laboratory, Department of Molecular Biosciences, The Wenner-Gren Institute, Stockholm University, Stockholm, Sweden
- ¹⁸ Department of Tumor Biology, Institute for Cancer Research, The Norwegian Radium Hospital, Oslo University Hospital, Oslo, Norway
- ¹⁹ Center for RNA Interference and Non-coding RNAs, The University of Texas MD Anderson Cancer Center, Houston, TX 77030, USA.
- ²⁰ Innovation Center for Biomedical Informatics, Georgetown University, Washington, DC, USA
- ²¹ Department of Surgery, Kyushu University Beppu Hospital, Beppu, Japan.
- ²² Department of Translational Molecular Pathology, The University of Texas MD Anderson Cancer Center, Houston, TX, 77030, USA.
- ²³ Department of Gastrointestinal Surgery, Tokyo Medical and Dental University Graduate School of Medicine, Tokyo, Japan.
- ²⁴ Department of Specialized Surgeries, Graduate School, Tokyo Medical and Dental University, Tokyo, Japan.
- ²⁵ “Carol Davila University of Medicine and Pharmacy”, Bucharest, Romania
- ²⁶ Department of Oncology-Pathology, Bioclinicum, Karolinska Institute and Karolinska University Hospital, SE-171 647 Stockholm, Sweden.
- ²⁷ Department of Biology, Faculty of Medicine, Masaryk University, Brno, Czech Republic
- ²⁸ Department of Veterinary Medicine and Surgery, The University of Texas MD Anderson Cancer Center, Houston Texas 77030, USA.
- ²⁹ Department of Thoracic Oncology, Cancer Center and State Key Laboratory of Biotherapy, West China Hospital, Sichuan University, Chengdu, Sichuan, China.
- ³⁰ present address: Italian Institute for Genomic Medicine (IIGM), Candiolo, Italy.
- ³¹ present address: Candiolo Cancer Institute, FPO-IRCCS, Candiolo, Italy.
- ³² present address: Department of Molecular Diagnostics and Experimental Therapeutics, Beckman Research Institute of City of Hope Comprehensive Cancer Center, Duarte, CA

Running title: *CCAT2* induces chromosomal instability via BOP1

Grant Support: Dr. Calin is the Felix L. Haas Endowed Professor in Basic Science. Work in Dr. Calin's laboratory is supported by National Institutes of Health (NIH/NCATS) grant UH3TR00943-01 through the NIH Common Fund, Office of Strategic Coordination (OSC), the NCI grants 1R01 CA182905-01 and 1R01CA222007-01A1, an NIGMS 1R01GM122775-01 grant, a U54 grant #CA096297/CA096300 – UPR/MDACC Partnership for Excellence in Cancer Research 2016 Pilot Project, a Team DOD (CA160445P1) grant, a Chronic Lymphocytic Leukemia Moonshot Flagship project, the UT MD Anderson Cancer Center Duncan Family Institute for Cancer Prevention and Risk Assessment, a Sister Institution Network Fund (SINF) 2017 grant, and the Estate of C. G. Johnson, Jr. Dr. Pardini is recipient of a Fulbright Research Scholarships (year 2018). Work at the University of Washington was supported by NIGMS R35 GM121487. The work of Dr. Baoqing Chen is supported by National Natural Science Foundation of China (No. 81902462). The work in Dr. Goel's lab is supported by the grants CA72851, CA181572 and CA202797 from the National Cancer Institute, National Institute of Health. The work of Dr. Parker-Thornburg was supported by the grants 5R50CA211121-03 and CCSG for the GEMF core.

Abbreviations: CIN, chromosomal instability; ncRNA, non-coding RNA; lncRNA, long non-coding RNA; *CCAT2*, colon cancer associated transcript 2 gene; CRC, colorectal cancer; BOP1, BOP1 ribosomal biogenesis factor; AURKB, aurora kinase B; MSS, microsatellite stable; MSI microsatellite unstable; MDS, myelodysplastic syndrome; GC, gastric cancer; DSB, double strand breaks; AOM, azoxymethane; DSS, dextran sulphate sodium; IPA, Ingenuity Pathway Analysis; GEA, gene expression analysis; MS, mass spectrometry; RIP, RNA immunoprecipitation; NLS, nuclear localization signal; CHX, cycloheximide; TF, transcription factor; AURKA, aurora kinase A; pAURKB, phosphorylated aurora B; PDX, patient derived xenograft; PDO, patient derived organoid; OS, overall survival; RFS, recurrence free survival.

Correspondence: George A. Calin, M.D., Ph.D. Professor, Department of Experimental Therapeutics, Center for RNA Interference and Non-Coding RNAs, Department of Experimental Therapeutics - Unit 1950, The University of Texas MD Anderson Cancer Center, P.O. Box 301429, Houston, Texas 77030-1429, gcalin@mdanderson.org, or to Jaffer Ajani, M.D., at jajani@mdanderson.org Department of Gastrointestinal Medical Oncology, The University of Texas MD Anderson Cancer Center, Houston, TX, USA, or to Chunlai Li, Ph.D. at CLi10@mdanderson.org, Department of Experimental Therapeutics, The University of Texas MD Anderson Cancer Center, Houston, TX, USA.

Disclosure: The authors declare no competing interests.

Transcript profiling: Gene expression Omnibus accession number from data used in this study (GSE106581, GSE133590).

Author contributions: Conceptualization B.C., M.P.D., and G.A.C.; Methodology, B.C, M.P.D., C.L., E.K., X.L., C.T, T.S., T.C.I, M.Y.S., H.L., P.S., A.S.M., B.P, J.K.B., H.K., L.C.R., Y.G., D.M., S.Sen, J.P.T., M.G., A.T, L.G. G.A.C.; Formal Analysis, B.C., M.P.D., E.K., C.T, T.S., T.C.I, A.S.M., L.C.R., M.F, B.F, C.I, K.B., Y.G., Investigation, B.C., M.P.D., C.L., L.F, R.B., E.K., Y.L., C.T, X.L., T.S., T.C.I., S.A., M.Shimizu, M.C.S., A.S.M., B.P, H.K., L.C.R., L.H., M.Syed, S.Song, M.F, E.O., T.M., H.U., A.T, Writing – Original Draft, B.C., M.P.D., and G.A.C.; Writing – Review & Editing, all authors.; Supervision, C.V., S.K., S.M.H., L.G., K.M., A.G., O.S., G.V., J.A.A., and G.A.C.; Funding Acquisition, J.A.A. and G.A.C..

Acknowledgements: We thank the MDACC Cytogenetics and Cell Authentication Core for technical assistance in the cytogenetic analysis.

Abstract

Background & Aims: Chromosomal instability (CIN) is a carcinogenesis event that promotes metastasis and resistance to therapy, by unclear mechanisms. Expression of the colon cancer associated transcript 2 gene (*CCAT2*), which encodes a long noncoding RNA (lncRNA), associates with CIN, but little is known about how *CCAT2* lncRNA regulates this cancer enabling characteristic.

Methods: We performed cytogenetic analysis of colorectal cancer (CRC) cell lines (HCT116, KM12C/SM, and HT29) overexpressing *CCAT2* and colon organoids from C57BL/6N mice with the *CCAT2* transgene and without (controls). CRC cells were also analyzed by immunofluorescence microscopy, γ -H2AX, and senescence assays. *CCAT2* transgene and control mice were given azoxymethane and dextran sulphate sodium (DSS) to induce colon tumors. We performed gene expression array and mass spectrometry to detect downstream targets of *CCAT2* lncRNA. We characterized interactions between *CCAT2* with downstream proteins using MS2 pulldown, RNA immunoprecipitation, and SHAPE analyses. Downstream proteins were overexpressed in CRC cells and analyzed for CIN. Gene expression levels were measured in CRC and non-tumor tissues from 5 cohorts, comprising more than 900 patients.

Results: High expression of *CCAT2* induced CIN in CRC cell lines and increased resistance to 5-fluorouracil and oxaliplatin. Mice that expressed the *CCAT2* transgene developed chromosome abnormalities, and colon organoids derived from crypt cells of these mice had a higher percentage of chromosome abnormalities compared to organoids from control mice. The transgenic mice given azoxymethane and DSS developed more and larger colon polyps than control mice given these agents. Microarray analysis and mass spectrometry indicated that expression of *CCAT2* increased expression of genes involved in ribosome biogenesis and protein synthesis. *CCAT2* lncRNA interacted directly with and stabilized BOP1 ribosomal biogenesis factor (BOP1). *CCAT2* also increased expression of MYC, which activated expression of BOP1. Overexpression of BOP1 in CRC cell lines resulted in chromosomal missegregation errors, and increased colony formation, and invasiveness, whereas BOP1 knockdown reduced viability. BOP1 promoted CIN by increasing the active form of aurora kinase B (AURKB), which regulates chromosomal segregation. *BOP1* was overexpressed in polyp tissues from *CCAT2* transgenic mice, compared to healthy tissue. *CCAT2* lncRNA and BOP1 mRNA or protein were all increased in microsatellite stable tumors (characterized by CIN), but not in tumors with microsatellite instability, compared with non-

tumor tissues. Increased levels of *CCAT2* lncRNA and *BOP1* mRNA correlated with each other and with shorter survival times of patients.

Conclusions: We found that overexpression of *CCAT2* in colon cells promotes CIN and carcinogenesis, by stabilizing and inducing expression of BOP1 an activator of AURKB. Strategies to target this pathway might be developed for treatment of patients with microsatellite stable colorectal tumors.

KEY WORDS: MSS, aneuploidy, tumorigenesis, non-coding RNA

Introduction

Considered one of the initial molecular events and one of the most noticeable pathogenic feature of cancer, genomic instability ¹, was predicted by Theodore Boveri, over 100 years ago ². Chromosomal instability (CIN) is one of the most common forms of genomic instability, and is characterized by high rates of structural and numerical chromosomal aberrations ³. By constantly making new aneuploid genomes, CIN causes tumor cell heterogeneity, upon which clonal selection can act ⁴.

One of the main causes of CIN is the asymmetrical segregation of chromosomes during the metaphase as a consequence of abnormal spindle formation ⁵ that will also induce anaphase bridges during mitosis, which is a key feature of CIN ⁶. CIN is associated with poor survival, metastases, and therapy resistance in cancer ⁷. Yet, the complex molecular mechanism(s) underlying the process remains unclear. Tens of protein coding genes and only few non-coding RNAs (ncRNAs) have been associated with the occurrence of CIN ⁸. Nonetheless, all these genes are altered in a small fraction of patients and their involvement in CIN has been studied mainly in *in vitro* systems.

The long-non-coding RNA (lncRNA) colon cancer associated transcript 2 (*CCAT2*), is up-regulated in microsatellite stable (MSS) colorectal cancers (CRC), tumors characterized by CIN and in which *CCAT2* promotes metastases ⁹ and influence glutamine metabolism ¹⁰. Additionally, *CCAT2* lncRNA was also reported to be involved in the initiation of myelodysplastic syndrome (MDS) ¹¹, a premalignant condition associated with abnormal chromosomes ¹². These findings imply that *CCAT2* plays a role in early stages of carcinogenesis. Despite its proven clinical value, the exact molecular mechanisms by which *CCAT2* lncRNA induces CIN are unexplored. Here, we have analyzed, for the first time, the molecular pathways through which a lncRNA induces CIN both *in vitro* and *in vivo*, and we identify *CCAT2* as a regulator of MYC-BOP1-AURKB pathway causing CIN.

Materials and Methods

Patient sample collection

For this study we used five different patient cohorts (**Supplementary Tables 1-4**): **Cohort A** (TCGA colorectal cancer cohort) was used for screening of the PES1, BOP1, and WDR12 (PeBoW) complex expression in MSS versus MSI subtypes of CRC; **Cohort B** for validating *CCAT2* lncRNA and

PeBoW complex mRNA overexpression in CRC; **Cohort C** for validating *CCAT2* lncRNA and *BOP1* mRNA role in MSS CRC subtype; **Cohort D** for further validation and prognosis analysis of *CCAT2* lncRNA and PeBoW complex mRNA expression in CRC; and **Cohort E** (described previously in ¹⁰) for validation of the mechanism at the protein level. Written informed consent was obtained from each patient, and the study was approved by the institutional review boards of all the involved institutions.

Additional methods are available in Supplementary material and methods. Primers and antibody information are available in **Supplementary Tables 5 and 6**.

RESULTS

***CCAT2* lncRNA induces CIN and activates pathways associated with ribosomal proteins**

We decided to investigate the causal relationship between *CCAT2* and CIN in cancer because of multiple lines of evidence. First, in multiple CRC and gastric cancer (GC) cell lines used, we observed that an aberrant chromosomal number is associated with high levels of *CCAT2* lncRNA (**Supplementary Figure 1A and Supplementary Table 7**). Second, cytogenetic analysis suggested that HCT116 clones with exogenous *CCAT2* over-expression (named here HCT116^{CCAT2}) have a higher percentage of chromosome abnormalities (including breaks, fusion, and polyploidy) compared to HCT116 cells transduced with an empty vector (HCT116^{Empty}) (31.0% versus 11.9%, $P = .001$). Similar results were found in the KM12SM cells (highly metastatic) compared to KM12C (poorly metastatic, from same patient) (44.5% versus 33.3%, $P = .1099$) (**Figure 1A and 1B**) KM12SM, with two times higher *CCAT2* levels as KM12C, presents also higher degree of CIN (**Supplementary Figure 1A and Supplementary Table 7**). Third, by double strand breaks (DSB) analysis using γ -H2AX, the number of cells with DSBs was higher in HCT116^{CCAT2} (39/152, 25.7%) compared to HCT116^{Empty} (2/162, 1.2%) ($P < .0001$) (**Supplementary Figure 1B**). Next, when we treated the cells with the DNA strand breaks inducer bleomycin, the number of DSBs was 42/126 in HCT116^{CCAT2} cells (33.3%) and 28/138 in HCT116^{Empty} cells (20.3%) ($P = .0165$) (**Supplementary Figure 1C**). Additionally, we observed that HCT116^{CCAT2} showed significantly lower chemosensitivity to 5-Fluorouracil ($P = .003$, $P = .006$ and $P = .0001$, respectively) (**Supplementary Figure 1D**) and to oxaliplatin ($P < .0001$ for all three concentrations) (**Supplementary Figure 1E**) compared to HCT116^{Empty}. One of the possible mechanisms through which cells tolerate DNA damage and stop CIN, is senescence ¹³. We observed that HCT116^{CCAT2}

clones had ten times lower number of senescent cells compared to HCT116^{Empty} ($P = .0001$) (**Supplementary Figure 1F**). Fourth, HCT116^{CCAT2} clones had a significant increase in abnormal spindles, along with a higher percentage of anaphase bridges, indirect indicators of CIN ¹⁴, compared with HCT116^{Empty} (mean 13.9% versus 6.2%, $P = .009$ and 51.8% versus 24.7%, $P = .0052$, respectively) (**Figure 1C and 1D**).

Fifth, our recently developed mouse model ¹¹ indicates that *CCAT2* lncRNA can trigger CIN *in vivo* (**Supplementary Figure 1G**). We found that the karyotypes from the bone marrow tissue of *CCAT2* mice showed more chromosomal abnormalities compared to WT littermates (**Supplementary Figure 1H**). Finally, we developed normal colon organoid cultures from the crypt cells of *CCAT2* and WT mice. The *CCAT2* lncRNA expression remained significantly higher in *CCAT2* organoids compared to WT organoids (**Supplementary Figure 1I**). No important morphology differences were observed between *CCAT2* and WT mice derived organoids (**Supplementary Figure 1J**), but a more rapid growth rate was measured for the *CCAT2* organoids ($P = .001$) (**Supplementary Figure 1K**). After 3 passages we performed cytogenetic analysis, which showed that normal colon organoids from *CCAT2* mice had a significantly higher percentage of chromosome abnormalities compared to organoids from WT mice (68.6% versus 51.4%, $P = .0094$) (**Figure 1E and 1F**), denoting that CIN induced by *CCAT2* preceded tumor development.

To find out if *CCAT2* lncRNA plays a role in the acceleration and progression of colon tumors we used the azoxymethane/dextran sulphate sodium (AOM/DSS) model, which was previously reported to induce CIN ¹⁵. *CCAT2* transgenic and WT mice were injected with AOM and then subjected to four rounds of DSS (**Figure 1G**). Macroscopic analysis revealed that *CCAT2* mice had significantly higher number of polyps ($P = .0143$), the surface of colon mucosa covered by polyps was significantly larger ($P = .0088$), and the average polyp diameter was significantly longer ($P = .0009$) than WT mice (**Figure 1H and 1I**). Next, we performed Hematoxylin and Eosin (H&E) staining and histopathological evaluation of the colon of WT and *CCAT2* mice (**Figure 1J**). The size of the largest polyp was significantly greater in *CCAT2* mice compared to WT mice ($P = .0093$) (**Figure 1K**). Importantly in *CCAT2* mice the grade of hyperplasia of the colon glands was higher in comparison with WT mice (Grade 3-4: *CCAT2* - 71.4% versus WT - 50.0%, $P = .0024$) (**Figure 1L**) and the mice had a higher incidence of dysplastic colon glands in comparison with the control group (71.4% versus 50.0%, $P = .0024$) (**Figure 1M**).

We used microarray gene expression analysis (GEA) to identify downstream targets of *CCAT2*

on BM cells obtained from WT mice and CCAT2 transgenic mice (GSE106581). Ingenuity Pathway Analysis (IPA) revealed that EIF2, mTOR, and regulation of eIF4 and p70S6K pathways were all significantly up-regulated in the CCAT2 mouse model when compared to WT mice (**Figure 1N**). All these pathways are related to protein synthesis ¹⁶. Among the common genes involved in these pathways, those related to ribosomal proteins and ribosome biogenesis were enriched (**Figure 1N**). The deregulation of proteins involved in ribosome biogenesis or ribosomal proteins have been previously linked to CIN ¹⁷.

CCAT2 lncRNA interacts with BOP1

Considering that the lncRNA *CCAT2* is localized mostly in the nucleus (**Supplementary Figure 2A**), we performed Mass Spectrometry (MS) on HCT116 cells transiently transfected with *CCAT2*-MS2 vectors, and isolated *CCAT2* lncRNA interacting nuclear proteins. Again, we found an enrichment in proteins involved in protein translation and ribosomal biogenesis (**Supplementary Table 8**). By screening the literature, we found that, one of these candidate proteins, BOP1 ribosomal biogenesis factor (BOP1), was previously reported to affect spindle formation and cause CIN in CRC ^{18,19}, therefore, we selected it for further analysis. *BOP1* and *CCAT2* genes are both located on chromosome 8q24, a region amplified in many cancers ²⁰. BOP1 protein is one of the three components, which includes also PES1 and WDR12 proteins, of the PeBoW complex, a regulator of rRNA processing affecting ribosome biogenesis ²¹.

To explore the interaction between *CCAT2* lncRNA and BOP1 protein, an *in vivo* MS2-pull down assay was conducted in COLO320 cells. BOP1 was retrieved through the *CCAT2*-MS2 construct and not by MS2-empty vector, while WDR12 and PES1 of the PeBoW complex, were only minimally retrieved (**Figure 2A**). To validate these results, RNA immunoprecipitation (RIP) using BOP1, WDR12, and PES1 antibodies was performed. *CCAT2* was identified ~5 and ~11 times higher in the BOP1 immunoprecipitate than PES1 and WDR12 precipitates, respectively (**Figure 2B and Supplementary Figure 2B**). This suggests that BOP1 protein is a strong interactor of *CCAT2* lncRNA, and the WDR12 and PES1 signals are probably identified due to indirect, low stability interactions with BOP1 protein. *In vitro* pull-down, was consistent with the previous results: the biotin-labeled *CCAT2* lncRNA, but not biotin-labeled controls, pulled down the recombinant BOP1 (**Figure 2C**).

The BOP1 protein consists of seven WD40 repeats (from amino acids 411 to 746, **Supplementary Figure 2C**), which are discrete domains that interact with proteins and RNAs, providing platforms to assemble functional complexes²². To characterize the region(s) of BOP1 that directly interacts with *CCAT2* lncRNA, we generated a series of BOP1 truncations with deletion of each WD repeats (**Figure 2D**), and one with a deletion of the nuclear localization signal (NLS). Using RIP assays, we observed that the abundance of *CCAT2* in WD 1, 2, 3, 5, 6, and 7 - truncated BOP1 groups was decreased compared to other groups. This suggested that deletion of any individual WD repeats, except WD 4, abolishes the BOP1-*CCAT2* interaction (**Figure 2D**).

In order to map the RNA sequence of *CCAT2* that interacts with BOP1 protein, RNA pull-down was performed using a set of 10 *CCAT2* segments. Results indicated that segment 3 (nucleotides 333 to 435) interacted directly with BOP1 protein (**Figure 2E**). Although the conservation of *CCAT2* gene is high in mammals (75.4% ± 19.9, n = 66 species) (**Supplementary Figure 2D**), the interacting segment 3 is mostly conserved in primates (more than 90% conservation), than in other mammals (30% - 70%) (**Supplementary Figure 2E**). The secondary structure of the *CCAT2* lncRNA region that spans nucleotide 207 to 492, which includes segment 3, was determined experimentally by SHAPE. Consistent with the results from **Figure 2E**, some active regions were determined, suggesting that segment 3, provides a platform for protein interactions (**Figure 2F and Supplementary Figure 2F and 2G**).

CCAT2* lncRNA up-regulates BOP1 *in vitro* and *in vivo

To investigate the effect of *CCAT2* lncRNA on the PeBoW complex, we verified the expression of the PeBoW complex components in *CCAT2* overexpression clones. In the cell lines with high levels of *CCAT2*, HCT116^{*CCAT2*}, and KM12SM, *BOP1* mRNA levels were four and two times higher while protein levels were eleven and three times higher compared to HCT116^{Empty} and KM12C (**Figure 3A**). In both HCT116 and KM12SM, 50-60% knock-down of *CCAT2* resulted in down regulation of BOP1 protein and mRNA levels (**Figure 3B**).

These results indicated that *CCAT2* lncRNA mainly regulates BOP1 by a post-transcriptional mechanism. To test if *CCAT2* lncRNA affects the stability of BOP1 protein, cyclohexamide (CHX) chase assay was conducted on KM12SM cells with transient *CCAT2* over-expression. Four hours after CHX addition, BOP1 protein expression started decreasing more rapidly in the Empty clone than in the *CCAT2* overexpressing clone (**Figure 3C**). We then checked the intracellular localization of BOP1 protein: as expected, in HCT116^{*CCAT2*} cells, BOP1 was enriched in the nuclear fraction

compared to the HCT116^{Empty} clone, while there was no difference in the cytoplasm (**Figure 3D**). These data were confirmed in DLD-1^{Empty} and DLD-1^{CCAT2} (**Supplementary Figure 3A**).

Using the CCAT2 mouse model ¹¹, we observed that the stable overexpression of *CCAT2* lncRNA in mice leads to the up-regulation of *BOP1* mRNA and protein in healthy colon tissue of CCAT2 mice compared to WT mice, hence this phenomenon is preceding tumor formation (**Figure 3E and Supplementary Figure 3B**). Moreover, we detected a higher protein level of BOP1 in the bone marrow of *CCAT2* mice, who we previously showed to develop MDS and display chromosomal abnormalities ¹¹, compared to WT mice (**Supplementary Figure 3C**). We also checked *BOP1* mRNA level in macroscopically unaffected colon tissues and in polyps from AOM/DSS treated *CCAT2* transgenic mice. We observed that the mRNA level of *BOP1* was further increased in polyps compared to normal colon in *CCAT2* transgenic mice ($P = .0095$) (**Figure 3F**).

In our previous study ⁹, we reported that *CCAT2* up-regulates MYC protein through TCF7L2. We found that MYC is also a predicted transcription factor (TF) for *BOP1* gene (**Supplementary Figure 3D and 3E**). CHIP-Seq data (UCSC Genome Browser Assembly) showed that MYC binds to its specific sequence (CACGTG) located in the 5' region of *BOP1* gene and acts as a TF for *BOP1* ²³ (**Supplementary Figure 3F**). Next, we verified whether MYC could regulate the expression of BOP1 using a doxycycline inducible HCT116 MYC tet-on system. *BOP1* mRNA levels were about 3 times higher 12h after induction of MYC and remained stable until 24h. Accordingly, the protein level of BOP1 increased after 12h, and reached an even higher level 24h after induction (**Supplementary Figure 3G**). In summary, *CCAT2* lncRNA regulates BOP1 mainly at the protein level by direct binding, but also positively regulates its transcription through MYC.

Overexpression of BOP1 promotes CIN

To confirm the role of BOP1 in triggering CIN, we stably overexpressed *BOP1* in HCT116, KM12SM, and HT29 cell lines (**Supplementary Figure 4A and 4B**) and performed cytogenetic analysis. After few passages (5-10), no difference on genomic instability was observed (**Supplementary Figure 4C**). However, after a longer propagation time (>15 passages), BOP1 clones started to present chromosomal aberrations. HCT116 cells with BOP1 overexpression (HCT116^{BOP1}) showed a higher frequency of chromosomal abnormalities (fusions, breaks, and fragmentation) (**Figure 4A panels (i), (ii), and (iii)**) compared to HCT116^{Empty} (31.4% versus 8.3%, $P = .0001$) (**Figure 4B**). The KM12SM^{BOP1} clones showed a higher percentage of aberrant metaphases compared to control cells (38.0% versus 22.0%, $P = .0136$). Specifically, a higher

percentage of polyploidy or tetraploidy was observed in the KM12SM^{BOP1}, indicative of a greater chromosome segregation failure (**Figure 4A panel (iv) and Figure 4B**). Moreover, a significantly higher genomic vulnerability was found in HT29^{BOP1} (28.6% versus 2.9%, $P < .0001$), including c-anaphases (**Figure 4A panel (v) and Figure 4B**).

BOP1 has previously been reported to alter the spindle apparatus and to cause aberrant lagging chromosomes¹⁸. As shown in **Figure 4C**, in HCT116, the percentage of cells with abnormal spindles increased from 12.1% in HCT116^{Empty} clones to 19.7% in HCT116^{BOP1} clones, $P = .0236$ (**Figure 4C**). Results from KM12SM cells were consistent, 21.1% of KM12SM^{Empty} clones showed aberrant spindles, as compared to 40.3% of KM12SM^{BOP1} cells $P < .0001$ (**Figure 4D**). A greater percentage of cells with anaphase bridges was found in the HCT116^{BOP1} clones when compared to controls, 49.0% vs 70.2%, $P = .0036$ (**Figure 4E**). KM12SM^{BOP1} clones displayed a higher frequency of anaphase bridges compared to KM12SM^{Empty} 37.6% vs 63.0%, $P < .0001$ (**Figure 4E**). Therefore, the CIN phenotype induced by BOP1 reproduced the one of its regulator, *CCAT2*.

BOP1 plays an oncogenic role in CRC

Functional assays were conducted to explore the role of BOP1 in CRC. Knocking-down *BOP1* impaired the proliferation of HCT116 and KM12SM (**Figure 5A**). Consistently, the cell viability was higher in HCT116^{BOP1} ($P = .0024$), and in KM12SM^{BOP1} ($P = .0032$) versus controls (**Figure 5B**). Cell colony formation was inhibited after knocking-down BOP1 in HCT116 ($P = .0156$ for siRNA 1 and $P = .0047$ for siRNA 2) (**Figure 5C**), whereas up-regulation of BOP1 promoted colony formation in HCT116 ($P = .0497$) (**Figure 5D**) and KM12SM ($P = .0028$) (**Supplementary Figure 5A**). Fewer cells migrated and invaded into the lower chamber in a transwell assay after BOP1 siRNAs, both in HCT116 ($P = .0175$ for siRNA 1 and $P < .0001$ for siRNA 2) and KM12SM ($P = .0015$ for siRNA 1 and $P = .0038$ for siRNA 2) (**Figure 5E**). Stable over-expression of BOP1 enhanced cell migration and invasion in HCT116 ($P = .013$) and KM12SM ($P = .0339$) (**Figure 5F**). Scratch assays indicated that BOP1 positively regulates cell migration in HCT116: knocking-down BOP1 decreased migration ($P = .0122$ for siRNA 1 and $P = .0031$ for siRNA 2) (**Supplementary Figure 5B**). Collectively, BOP1 protein plays an oncogenic role in CRC, confirming recent findings²⁴ and the BOP1 overexpression phenotype mirrors the *CCAT2* overexpression effects⁹.

BOP1 modulates the function of AURKB

We hypothesized that high levels of *CCAT2* lncRNA would increase the level of ribosomal subunits and subsequently this could affect genomic integrity ²⁵. By performing polysome profiling, we concluded that the function of *CCAT2* lncRNA via BOP1 is ribosome independent (**Supplementary Figure 6A-6C**).

In order to find down-stream targets of the *CCAT2*-BOP1 pathway, we used a genome-wide screen, CINdex analysis ²⁶, on the TCGA CRC cohort. We found that the aurora kinase family and PeBoW complex genes, associated with CIN and positively correlate with each other (**Supplementary Figure 6D** and **Supplementary Table 9**). This assay directed us to investigate aurora kinase family genes.

No difference in the levels of aurora kinase A (AURKA) protein, and of two other proteins reported to induce CIN, CDC20, and BUB1B, were detected between scramble siRNA and *CCAT2* knockdown in KM12SM (**Supplementary Figure 6E**) and BOP1 knockdown in HCT116 (**Supplementary Figure 6F**). We further checked for differences in the levels of aurora kinase B (AURKB) and phosphorylated aurora B (pAURKB) in HCT116^{CCAT2} versus HCT116^{Empty} clones. We observed that the over-expression of *CCAT2* induces higher pAURKB at Thr 232 (active form of AURKB), but no changes in AURKB mRNA and protein (**Figure 6A left panel**). In a second model, both total levels of AURKB mRNA and protein and pAURKB were higher in KM12SM compared to KM12C (**Figure 6A right panel**). AURKB is predominantly activated by autophosphorylation, and does not require the involvement of other kinase, while interaction with other molecules augments the phosphorylation ²⁷. Next, we observed that high BOP1 induces the phosphorylation of AURKB, both in HCT116 and KM12SM (**Figure 6B**) and the knock-down of BOP1 induced the downregulation of AURKB mRNA and protein and of pAURKB (**Figure 6C**). As MYC was reported to be a regulator of *AURKB* ²⁸, we checked if MYC is a TF for *AURKB*. CHIP-Seq data (UCSC Genome Browser on Human Feb. 2009 (GRCh37/hg19) Assembly) showed that MYC binds to CCACGCC located in the 5' region of *AURKB* and acts as a TF for *AURKB* (**Supplementary Figure 6G**). This was confirmed in HCT116 MYC tet-on system: after induction of MYC, the levels of AURKB mRNA and protein and of pAURKB protein increased (**Figure 6D**).

Previously, it was shown that AURKB protein can bind mRNA molecules that stimulate AURKB activity during mitosis ²⁹. To identify whether *CCAT2* RNA forms a complex with AURKB protein, we performed MS2-pull down assay: AURKB protein was retrieved in the *CCAT2*-MS2 but not in the MS2-empty vector transduced HCT116 cells (**Figure 6E**). By using RIP, we confirmed this

complex: *CCAT2* was detected 20 times higher in the AURKB precipitate compared to IgG control ($P < .0001$) (**Supplementary Figure 6H**). In order to determine which *CCAT2* lncRNA segment associates with AURKB protein we did RNase I treatment of the lysate before RIP, so that unbound fragments were digested. Two of the segments were enriched: S8 and S6 (**Supplementary Figure 6I**).

To appreciate if the dysregulation of *CCAT2*-*BOP1*-AURKB pathway is widespread in cancers, we checked for this pathway in GC, which has high CIN rates (50%)³⁰. We performed a non-coding GEA comparing normal gastric samples with peritoneal carcinomatosis samples of GC patients (GSE133590). One of the top up-regulated lncRNA in peritoneal carcinomatosis was *CCAT2* ($P = .0115$) (**Supplementary Figure 7A**). We analyzed the *CCAT2* lncRNA expression in two pairs of GC patients derived xenografts (PDXs) and one GC patient derived organoid (PDO) and in each of them *CCAT2* was up-regulated compared to parental cells (**Supplementary Figure 7B**), showing that successful engraftment, a marker of poor prognosis³¹, is associated with high *CCAT2* levels. Next, we did CINdex analysis using the GC TCGA cohort and identified that aurora family and PeBoW complex genes positively correlated with CIN at chromosome level (**Supplementary Figure 7B and Supplementary Table 10**). Additionally, we used the primary GC cells, AGS, with euploid chromosomal number and KATO III with a tetraploid chromosome number. The RNA expression levels of *CCAT2* and *BOP1* and the protein levels of *BOP1*, the other components of the PeBoW complex and pAURKB were higher in KATO III compared to AGS (**Supplementary Figure 7C**). These data imply that the identified mechanism relates to CIN more generally.

***CCAT2* and *BOP1* are overexpressed in MSS CRC**

To assess the clinical relevance of our findings, we examined multiple patient cohorts. Firstly, we used the **TCGA CRC cohort (Cohort A)** as a screening cohort and identified significantly higher expression of *BOP1*, *PES1*, and *WDR12* mRNAs in tumor versus normal tissue ($P < .0001$) (**Figure 7A**). It is known that MSS/MSI-L CRC cancers (analyzed together as MSS) are CIN positive and MSI-H (referred to as MSI) are CIN negative³². Therefore, we compared the mRNA expression of PeBoW complex components in MSS versus MSI CRC. Only the mRNA level of *BOP1* was significantly higher in MSS versus MSI ($P < .0001$) and *PES1* and *WDR12* showed no differences between the subgroups ($P = .8115$ and $P = .2333$) (**Figure 7B**). We were not able check for *CCAT2* lncRNA in this cohort, as *CCAT2* is not polyadenylated.

In a second cohort of CRC tumors and paired adjacent normal tissues (**Cohort B**) we measured the RNA expression of *CCAT2*, *BOP1*, *PES1*, and *WDR12*: all were significantly overexpressed in tumor versus normal tissues (**Supplementary Figure 8A**). We also identified a significant positive correlation between *CCAT2* lncRNA and *BOP1* mRNA in tumor tissues ($r = 0.6296$) (**Supplementary Figure 8B**). Regarding MSS versus MSI comparison, there were insufficient patients in the MSI group for this analysis. We identified that *CCAT2* and *BOP1* expression levels remained unchanged in MSI tumors versus paired normal tissues ($P = .7422$ and $P = .5649$, respectively), but significantly increased in MSS versus paired normal tissues ($P < .0001$ for both genes) (**Supplementary Figure 8C**).

In a third group, **Cohort C**, we confirmed these data: *CCAT2* lncRNA and the mRNA level of all three PeBoW components were highly expressed in tumor versus adjacent normal tissues ($P < .0001$) (**Figure 7C and Supplementary Figure 8D**). We also checked for the correlation between *BOP1* mRNA and *CCAT2* lncRNA expression in normal and tumor tissues; the correlation between the two transcripts increased from $r = 0.3050$ in normal tissues to an $r = 0.5252$ in cancer (**Supplementary Figure 8E and 8F**). Because of an ample MSI sub-group, we compared the expression of *CCAT2* lncRNA and PeBoW mRNAs between MSI and MSS. Only *CCAT2* and *BOP1*, but not *PES1* or *WDR12*, were up-regulated in MSS ($P = .001$ and $P = .03$, respectively) (**Figure 7D and Supplementary Figure 8G**).

Additionally, we used **Cohort D**, with ample MSI subgroup, and we established that only *CCAT2* and *BOP1* were up-regulated in MSS versus MSI ($P < .0001$ and $P = .03$, respectively) (**Figure 7E and Supplementary Figure 8H**). The RNA expression levels of *CCAT2* and *BOP1* were positively correlated in tumor tissues ($r = 0.6263$), implying co-regulation (**Figure 7F**). High levels of *CCAT2* or *BOP1* were associated with worse overall survival (OS) ($P < .0001$ and $P = .003$, respectively) (**Figure 7G**). Additionally, high levels of *PES1* and *WDR12* mRNAs were prognostic for shorter OS ($P = .0007$ and $P = .0004$, respectively) (**Supplementary Figure 8I**). Similarly, increased transcription levels of *CCAT2* and *BOP1* predicted shorter recurrence free survival (RFS) ($P < .0001$ for both) (**Figure 7H**). *PES1* and *WDR12* proved to have a comparable prognostic value ($P < .0001$ and $P = .0002$, respectively) (**Supplementary Figure 8J**).

Cohort D had follow-up data for all patients. Univariate analysis revealed that high *CCAT2* lncRNA and *BOP1* mRNA levels were significantly associated with shorter OS and RFS (for *CCAT2*: HR: 6.1, 95%CI: 2.79-13.31, $P < .0001$ and HR: 4.78, 95%CI: 2.74-8.09, $P < .0001$, respectively; for

BOP1: HR: 3.01, 95%CI: 1.38-6.55, $P = .006$ and HR: 2.77, 95%CI: 1.65–4.60, $P = .0002$, respectively) (**Supplementary Table 11**). Multivariate analysis revealed that high *CCAT2* and *BOP1* were independent factors for predicting poor OS and RFS (for *CCAT2*: HR: 5.51, 95%CI: 2.48-12.27, $P < .0001$ and HR: 4.85, 95% CI: 2.76-8.28, $P < .0001$, respectively; for *BOP1*: HR: 3.12, 95%CI: 1.42–6.84, $P = .005$ and HR: 2.67, 95%CI: 1.59–4.45, $P = .0003$, respectively) (**Supplementary Table 12**).

Finally, to assess if our findings are present at the protein level, we used **Cohort E**. We previously showed that the expression of *CCAT2* is higher in tumor tissues of each of these patients compared to their normal tissue¹⁰. We assessed the protein expression of BOP1, AURKB, and pAURKB and identified high protein levels of BOP1 and pAURKB in tumor tissue compared to normal mucosae for 60% (6/10) of the pairs, all six being MSS CRC (**Figure 7I**). We also identified that *CCAT2* lncRNA and BOP1 protein are upregulated in MSS PDX compared to MSI PDX (**Supplementary Figure 8K**). Collectively, these results prove that *CCAT2* and the PeBoW complex are oncogenes and only *CCAT2* and BOP1 are specifically overexpressed in MSS CRC.

Discussion

CIN correlates with patient survival in CRC³³ and multiple other cancers³⁴. Therefore, understanding the mechanisms underpinning CIN is essential to discover new therapies. Dozens of proteins are involved in chromosome segregation³⁵. Many of them have recently been evaluated as therapeutic targets, but none of the proposed treatments have reached approval. We propose that targeting ncRNAs involved in chromosomal segregation errors might provide an alternative approach to inhibiting CIN. We present compelling new data supporting the involvement of the lncRNA *CCAT2* in the development of CIN.

First, we showed that high *CCAT2* lncRNA is sufficient to induce early premalignant modifications. *CCAT2* mice, after AOM/DSS treatment, have significantly more polyps and the degree of colon glands' hyperplasia and dysplasia is higher compared to WT mice. Additionally, a high *CCAT2* background induces CIN in organoids established from healthy mouse colon, before tumor formation. We demonstrated that *CCAT2* lncRNA induces CIN via BOP1 in two ways: through an "indirect transcriptional mechanism", probably via c-MYC, a TF promoting *BOP1* gene expression, and by a "direct post-transcriptional mechanism", by binding the mature BOP1 protein, prolonging its half-life. The genes within this pathway (*CCAT2*, *MYC*, and *BOP1*) are located on the

well-studied, oncogenic chromosomal amplicon 8q24. In support of our experimental data, we showed that *BOP1* mRNA and *CCAT2* lncRNA expression correlate positively, in CRC patient cohorts. These results led us to the conclusion that *CCAT2* lncRNA is an important factor that induces the up-regulation of BOP1 in cancer and promotes CIN.

Second, we discovered that *CCAT2* lncRNA and BOP1 are abnormal in three cancer models, CRC, GC, and in the *in vivo* *CCAT2* transgenic mice treated with AOM/DSS. These results suggest that the new mechanism identified could represent a general model of CIN initiation.

Third, by using one independent genome-wide screening method – CINdex in TCGA CRC cohort, we hypothesized that *CCAT2* lncRNA via BOP1 induces CIN through aurora kinase family proteins. Indeed, the expression of *CCAT2* lncRNA or BOP1 correlated with the phosphorylation of AURKB suggesting that *CCAT2* lncRNA acts as an adaptor, promoting interaction of BOP1 and AURKB, bringing them in physical proximity. Together, our findings concerning the *CCAT2* – BOP1 – AURKB pathway expression and function describe a new mechanism of CIN (**Figure 7J**).

lncRNAs and ribosomal biogenesis proteins have rarely been studied in the context of CIN. Several studies have emerged reporting *BOP1* as an oncogene that can induce CIN. Killian *et al.* showed that the depletion of *BOP1* in CRC cells increased the number of aberrant mitotic cells¹⁹. The same group analyzed the expression of *BOP1* in CRC patients and observed that high *BOP1* was tumor specific. Other studies revealed that *BOP1* overexpression increased the number of multipolar spindles¹⁸. In rectal cancer patients, *BOP1* was shown to be overexpressed in samples with gain of the 8q chromosome arm and steadily increased from adenoma to carcinoma, implying a tumorigenic role³⁶. None of the studies explored the upstream pathways that regulate BOP1, or the precise mechanism by which BOP1 induces CIN. On the other hand, AURKB, is one of the key regulators of mitosis³⁷, increased activation of AURKB is present in multiple cancer types and correlates with CIN³⁸. The variety of interactions that facilitate the post-transcriptional modifications that activate AURKB are not fully deciphered. Hence, it is crucial to understand new mechanisms that regulate AURKB function and *CCAT2* via BOP1 appears to be a novel pathway activating AURKB.

In conclusion, this study presents a new mechanism in which the lncRNA, *CCAT2*, induces CIN, an early tumorigenic event. This pathway reveals new potential therapeutic targets for CIN.

Figure Legends

Figure 1. *CCAT2* lncRNA induces CIN and activates pathways associated with ribosomal proteins. **(A)** Cytogenetic analysis showing chromosomal aberrations in HCT116^{CCAT2} cells (left) and KM12SM cells (right). Red arrows indicate breaks, blue arrows indicate fusions and green arrows indicate fragments. **(B)** The frequency of aberrant metaphases in HCT116^{Empty} versus HCT116^{CCAT2} and KM12C versus KM12SM. At least 35 metaphases were analyzed for each clone. **(C)** Immunofluorescence images and **(D)** frequency of abnormal spindle (upper lane) and anaphase bridge (lower lane) in HCT116^{CCAT2} cells. At least 200 interphase cells were analyzed for each clone. **(E)** Cytogenetic analysis showing chromosomal aberrations in organoids from WT (left) and *CCAT2* mice (right). Blue arrow indicates fusions. **(F)** The frequency of aberrant metaphases in organoids from WT versus *CCAT2* mice. At least 35 metaphases were analyzed for each organoid. **(G)** Schematic illustration of the AOM/DSS colon cancer model. **(H)** Images of colon mucosa from WT and *CCAT2* mice after treatment with AOM/DSS. Red delineation indicates polyps' area. **(I)** Total number of polyps, total surface area of colon polyps, and average polyp diameter size in WT and *CCAT2* transgenic mice at the end of the AOM/DSS treatment (n = 7 per group). **(J)** H&E images of the colon from WT and *CCAT2* transgenic mice after treatment with AOM/DSS. Black arrows indicate polyps. **(K)** Largest size polyp according to H&E analysis in WT and *CCAT2* transgenic mice. **(L)** The percentage of WT and *CCAT2* transgenic mice with grade 1-2 versus grade 3-4 hyperplasia, and **(M)** with normal glands versus dysplastic glands. **(N)** IPA analysis showing significantly enriched pathways in *CCAT2* transgenic mouse model (left Y axis represents negative log *P* values; right Y axis represents the ratio of molecules in the dataset mapping to the number of molecules in the canonical pathways) (left panel). Venn diagram showing overlapping genes related to the ribosomal proteins from the canonical pathways (right panel). Mean ± SD. (***P* < .01).

Figure 2. *CCAT2* lncRNA interact with BOP1. **(A)** Schematic illustration of MS2-pull down assay (left panel) and immuno-blotting results of BOP1, PES1, and WDR12 (right panel). **(B)** RIP assay was performed to check the enrichment of *CCAT2* lncRNA in COLO320. **(C)** *In vitro* RNA pull-down using GST-tagged *CCAT2* lncRNA and recombinant BOP1 protein. **(D)** Determination of the interaction between ΔBOP1 domains and *CCAT2* lncRNA by *in vitro* RNA pull down. **(E)** *In vitro* RNA pull-down using multiple *CCAT2* lncRNA segments (S1 to S10). **(F)** SHAPE assay showing the

structure of the *CCAT2* lncRNA region from nucleotide 207 to 492. Blue arrows indicate the start and the end of segment 3. Mean \pm SD. (**P* < .05), (***P* < .01).

Figure 3. *CCAT2* lncRNA up-regulates BOP1 in vitro and in vivo. (A) Expression of PeBoW complex components in HCT116^{Empty} and HCT116^{CCAT2} (left panel), and in KM12C and KM12SM (right panel). (B) Expression of PeBoW complex components in HCT116 WT (left panel) and KM12SM (right panel) after *CCAT2* knock-down. (C) The half-life of BOP1 protein in KM12SM cells with transient *CCAT2* overexpression or empty vector (left panel). Data from three experiments were quantified and are depicted as a graphic (right panel). (D) The nuclear and cytoplasmic localization of PeBoW complex in HCT116^{Empty} and HCT116^{CCAT2}. (E) Expression of *CCAT2* lncRNA and PeBoW complex components in the colon of *CCAT2* mice. (F) The expression of *BOP1* in normal colon tissues and colon polyps of *CCAT2* mice after AOM/DSS treatment (n = 7). Mean \pm SD. (ns, not significant), (**P* < .05), (***P* < .01); (***)*P* < .001, (****)*P* < .0001).

Figure 4. Overexpression of BOP1 promotes CIN. (A) Cytogenetic analysis showing chromosomal aberrations in cells with overexpression of BOP1. In panels (i), (ii) and (iii) are representative images of HCT116^{BOP1}, with fusion (blue arrow), break (red arrow), and fragments (green arrows). In panel (iv) is an image of KM12SM^{BOP1} with polyploidy and acentric chromosomes (black arrows) and fusion (blue arrow), and in panel (v) is an image of HT29^{BOP1} with c-anaphase morphology. (B) The frequency of cells exhibiting chromosome abnormalities in HCT116, KM12SM, and HT29 Empty versus BOP1 overexpressed clones. At least 35 metaphases were analyzed for each clone. (C, D) Images and frequencies of abnormal spindles in HCT116 (C) and KM12SM (D) with BOP1 overexpression. At least 200 interphase nuclei were analyzed for each clone. (E, F) Images and frequency of anaphase bridges in HCT116 (E) and KM12SM (F) with BOP1 overexpression. At least 200 cells were analyzed for each clone. Mean \pm SD. (**P* < .05), (***P* < .01), (****)*P* < .0001).

Figure 5. BOP1 plays an oncogenic role in CRC. (A) Proliferation rate of HCT116 (left) and KM12SM (right) after siRNA knock-down of BOP1. (B) Proliferation rate of HCT116^{Empty} and HCT116^{BOP1} (left) and KM12SM^{Empty} and KM12SM^{BOP1} (right). (C, D) Representative images of

colony formation assay in HCT116 with BOP1 knock-down **(C)** and HCT116 with stable overexpression of BOP1 **(D)**. Quantitative analysis of colony numbers (right side of panels C and D). **(E)** Invasion potential of HCT116 and KM12SM cells after transfection with BOP1 siRNA. Representative images of invasion assay for HCT116 (upper panel) and KM12SM (lower panel). Quantitative analysis of invading cell (right panel). **(F)** Invasion potential in cells with stable overexpression of BOP1. Representative images of invasion assay for HCT116 (upper panel) and KM12SM (lower panel). Quantitative analysis of invading cell (right panel). Mean \pm SD. (* $P < .05$), (** $P < .01$); (***) $P < .001$), (****) $P < .0001$).

Figure 6. BOP1 modulates the function of AURKB. **(A)** Expression of AURKB and pAURKB in HCT116^{Empty} and HCT116^{CCAT2} (left panel) and KM12C and KM12SM (right panel). **(B)** Expression of BOP1, AURKB, and pAURKB analyzed in HCT116^{Empty} and HCT116^{BOP1} (left panel) and KM12SM^{Empty} and KM12SM^{BOP1} (right panel). **(C)** Expression of BOP1, AURKB, and pAURKB analyzed in HCT116 (left panel) and KM12SM (right panel) after BOP1 knock-down with siRNA. **(D)** Expression of BOP1 and AURKB at 0, 6, 12, 18, and 24 hours in HCT116 cells with inducible c-MYC expression system. **(E)** MS2-pull down assay to identify if AURKB interacts with MS2-labeled *CCAT2* in HCT116. Mean \pm SD. (ns, not significant), (** $P < .01$); (***) $P < .001$), (****) $P < .0001$).

Figure 7. CCAT2 and BOP1 are overexpressed in MSS CRC. **(A)** The expression levels of PeBoW complex in Cohort A. **(B)** The expression levels of the PeBoW complex in MSI and MSS primary CRC in Cohort A. **(C)** The expression of *CCAT2* lncRNA and *BOP1* mRNA in tumor and adjacent normal tissues from Cohort C. **(D)** The expression of *CCAT2* lncRNA and *BOP1* mRNA in MSI and MSS CRC from Cohort C. **(E)** The expression of *CCAT2* lncRNA and *BOP1* mRNA in MSI and MSS CRC from Cohort D. **(F)** Correlation between the RNA expression of *CCAT2* and *BOP1* in patients from Cohort D. **(G)** Kaplan–Meier OS curves of CRC patients from Cohort D, *CCAT2* lncRNA (left panel) and *BOP1* mRNA (right panel). **(H)** Kaplan–Meier RFS curves of CRC patients from Cohort D, of *CCAT2* lncRNA (left panel) and *BOP1* mRNA (right panel). Time is expressed in days. **(I)** Western blot analysis of BOP1, AURKB, and pAURKB protein expression in paired CRC samples (**Cohort E**). N=normal tissue, T=tumor tissue, N/A=not available microsatellite status. The samples in which both BOP1 and pAURKB proteins are up-regulated in tumor versus normal tissues are marked with red stars. **(J)** A model of *CCAT2* involvement in CIN (red arrows – new interactions; black

arrows – available data). Data are represented as violin plots. (ns) not significant, ($*P < .05$), ($**P < .01$); ($***P < .001$), ($****P < .0001$).

References

1. Gordon DJ, Resio B, Pellman D. Causes and consequences of aneuploidy in cancer. *Nat Rev Genet* 2012;13:189-203.
2. Boveri M. Über Mitosen bei einseitiger Chromosomenbindung. *Jenaische Zeitschrift für Naturwissenschaft* 1903;37:401-443.
3. Negrini S, Gorgoulis VG, Halazonetis TD. Genomic instability--an evolving hallmark of cancer. *Nat Rev Mol Cell Biol* 2010;11:220-8.
4. Gronroos E, Lopez-Garcia C. Tolerance of Chromosomal Instability in Cancer: Mechanisms and Therapeutic Opportunities. *Cancer Res* 2018;78:6529-6535.
5. **Galimberti F, Thompson SL**, Ravi S, et al. Anaphase catastrophe is a target for cancer therapy. *Clin Cancer Res* 2011;17:1218-22.
6. Hoffelder DR, Luo L, Burke NA, et al. Resolution of anaphase bridges in cancer cells. *Chromosoma* 2004;112:389-97.
7. Bakhom SF, Cantley LC. The Multifaceted Role of Chromosomal Instability in Cancer and Its Microenvironment. *Cell* 2018;174:1347-1360.
8. Dragomir MP, Kopetz S, Ajani JA, et al. Non-coding RNAs in GI cancers: from cancer hallmarks to clinical utility. *Gut* 2020;69:748-763.
9. **Ling H, Spizzo R**, Atlasi Y, et al. CCAT2, a novel noncoding RNA mapping to 8q24, underlies metastatic progression and chromosomal instability in colon cancer. *Genome Res* 2013;23:1446-61.
10. Redis RS, Vela LE, Lu W, et al. Allele-Specific Reprogramming of Cancer Metabolism by the Long Non-coding RNA CCAT2. *Mol Cell* 2016;61:520-534.
11. Shah MY, Ferracin M, Pileczki V, et al. Cancer-associated rs6983267 SNP and its accompanying long noncoding RNA CCAT2 induce myeloid malignancies via unique SNP-specific RNA mutations. *Genome Res* 2018;28:432-447.
12. Pellagatti A, Boulwood J. The molecular pathogenesis of the myelodysplastic syndromes. *Eur J Haematol* 2015;95:3-15.
13. Maslov AY, Vijg J. Genome instability, cancer and aging. *Biochim Biophys Acta* 2009;1790:963-9.
14. Bayani J, Selvarajah S, Maire G, et al. Genomic mechanisms and measurement of structural and numerical instability in cancer cells. *Seminars in Cancer Biology* 2007;17:5-18.
15. Gerling M, Glauben R, Habermann JK, et al. Characterization of chromosomal instability in murine colitis-associated colorectal cancer. *PLoS One* 2011;6:e22114.
16. Roux PP, Topisirovic I. Regulation of mRNA translation by signaling pathways. *Cold Spring Harb Perspect Biol* 2012;4.
17. Kim TH, Leslie P, Zhang Y. Ribosomal proteins as unrevealed caretakers for cellular stress and genomic instability. *Oncotarget* 2014;5:860-71.
18. Killian A, Sarafan-Vasseur N, Sesboue R, et al. Contribution of the BOP1 gene, located on 8q24, to colorectal tumorigenesis. *Genes Chromosomes Cancer* 2006;45:874-81.
19. **Killian A, Le Meur N**, Sesboue R, et al. Inactivation of the RRB1-Pescadillo pathway involved in ribosome biogenesis induces chromosomal instability. *Oncogene* 2004;23:8597-602.
20. **Beroukhi R, Mermel CH**, Porter D, et al. The landscape of somatic copy-number alteration across human cancers. *Nature* 2010;463:899-905.
21. Rohmoser M, Holzel M, Grimm T, et al. Interdependence of Pes1, Bop1, and WDR12 controls nucleolar localization and assembly of the PeBoW complex required for maturation of the 60S ribosomal subunit. *Mol Cell Biol* 2007;27:3682-94.
22. Neer EJ, Schmidt CJ, Nambudripad R, et al. The ancient regulatory-protein family of WD-repeat proteins. *Nature* 1994;371:297-300.
23. Kent WJ, Sugnet CW, Furey TS, et al. The human genome browser at UCSC. *Genome Res* 2002;12:996-1006.

24. Qi J, Yu Y, Akilli Ozturk O, et al. New Wnt/beta-catenin target genes promote experimental metastasis and migration of colorectal cancer cells through different signals. *Gut* 2016;65:1690-701.
25. Grummt I. The nucleolus-guardian of cellular homeostasis and genome integrity. *Chromosoma* 2013;122:487-97.
26. **Song L, Bhuvaneshwar K**, Wang Y, et al. CINdex: A Bioconductor Package for Analysis of Chromosome Instability in DNA Copy Number Data. *Cancer Inform* 2017;16:1176935117746637.
27. Yasui Y, Urano T, Kawajiri A, et al. Autophosphorylation of a newly identified site of Aurora-B is indispensable for cytokinesis. *J Biol Chem* 2004;279:12997-3003.
28. den Hollander J, Rimpi S, Doherty JR, et al. Aurora kinases A and B are up-regulated by Myc and are essential for maintenance of the malignant state. *Blood* 2010;116:1498-505.
29. Jambhekar A, Emerman AB, Schweidenback CT, et al. RNA stimulates Aurora B kinase activity during mitosis. *PLoS One* 2014;9:e100748.
30. Cancer Genome Atlas Research N. Comprehensive molecular characterization of gastric adenocarcinoma. *Nature* 2014;513:202-9.
31. DeRose YS, Wang G, Lin YC, et al. Tumor grafts derived from women with breast cancer authentically reflect tumor pathology, growth, metastasis and disease outcomes. *Nat Med* 2011;17:1514-20.
32. Simons CC, Hughes LA, Smits KM, et al. A novel classification of colorectal tumors based on microsatellite instability, the CpG island methylator phenotype and chromosomal instability: implications for prognosis. *Ann Oncol* 2013;24:2048-56.
33. Watanabe T, Kobunai T, Yamamoto Y, et al. Chromosomal instability (CIN) phenotype, CIN high or CIN low, predicts survival for colorectal cancer. *J Clin Oncol* 2012;30:2256-64.
34. **Jamal-Hanjani M, Wilson GA, McGranahan N**, et al. Tracking the Evolution of Non-Small-Cell Lung Cancer. *N Engl J Med* 2017;376:2109-2121.
35. Carter SL, Eklund AC, Kohane IS, et al. A signature of chromosomal instability inferred from gene expression profiles predicts clinical outcome in multiple human cancers. *Nature Genetics* 2006;38:1043-1048.
36. Lips EH, van Eijk R, de Graaf EJ, et al. Integrating chromosomal aberrations and gene expression profiles to dissect rectal tumorigenesis. *BMC Cancer* 2008;8:314.
37. **Carmena M, Wheelock M**, Funabiki H, et al. The chromosomal passenger complex (CPC): from easy rider to the godfather of mitosis. *Nat Rev Mol Cell Biol* 2012;13:789-803.
38. Munoz-Barrera M, Monje-Casas F. Increased Aurora B activity causes continuous disruption of kinetochore-microtubule attachments and spindle instability. *Proc Natl Acad Sci U S A* 2014;111:E3996-4005.

Figure 1

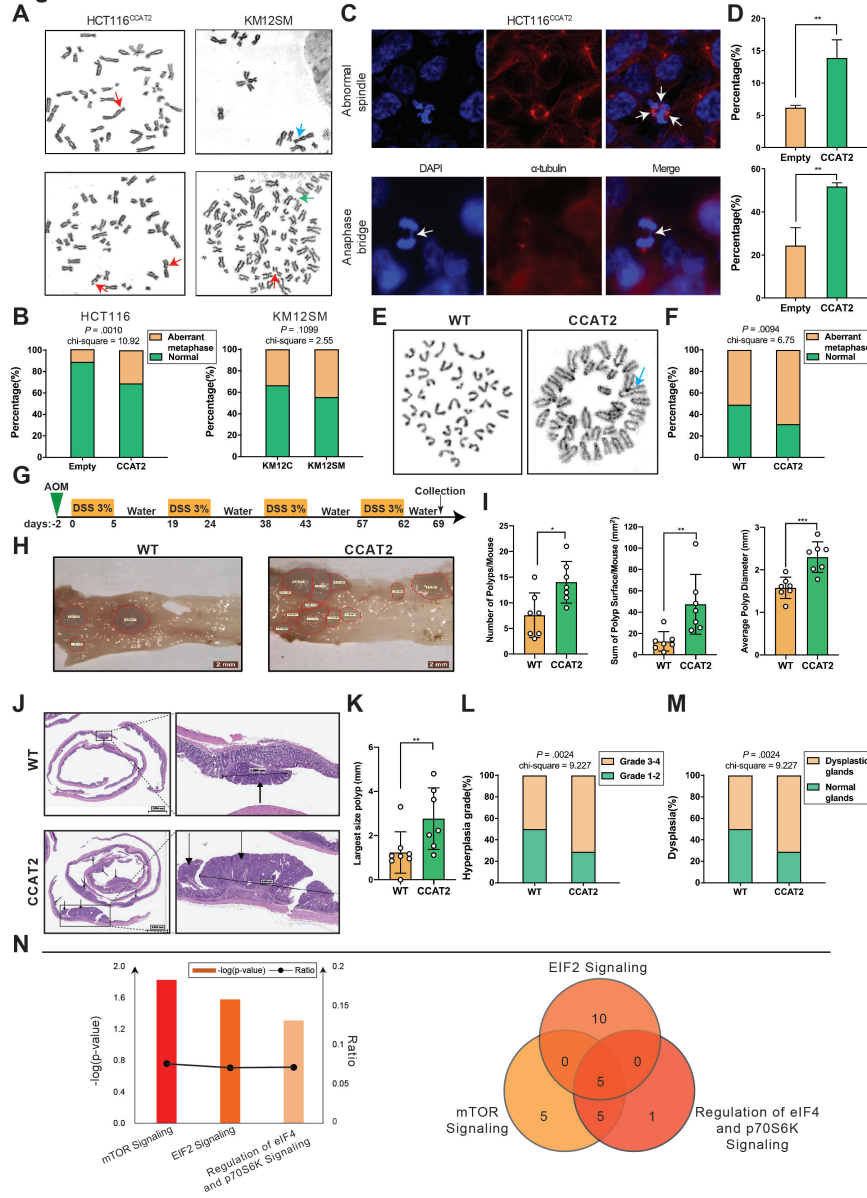


Figure 2

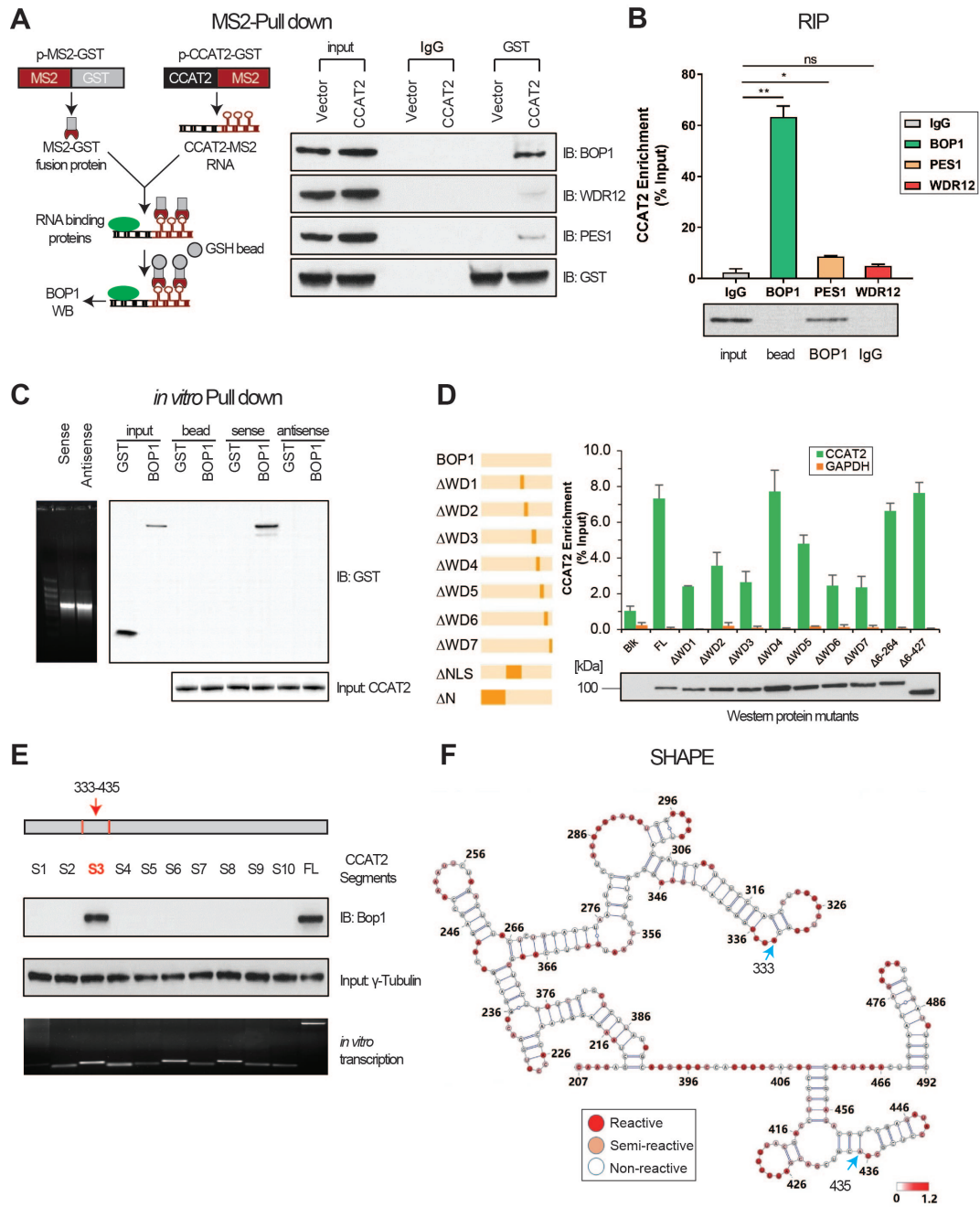
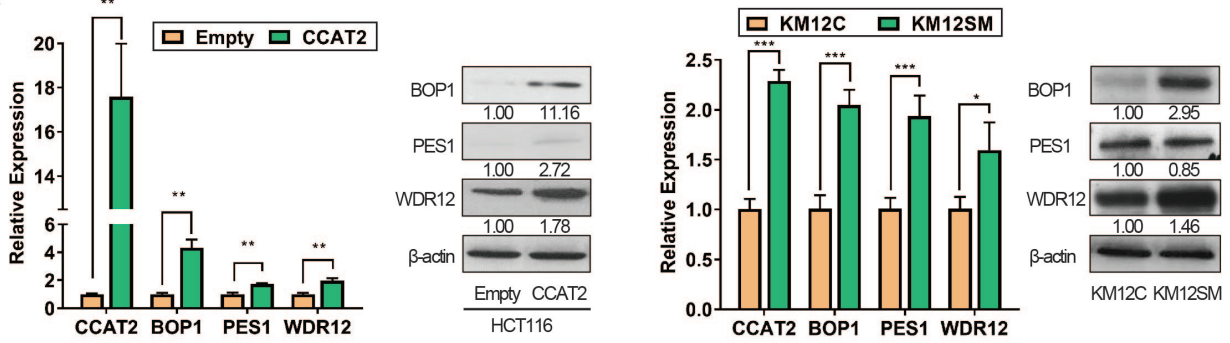
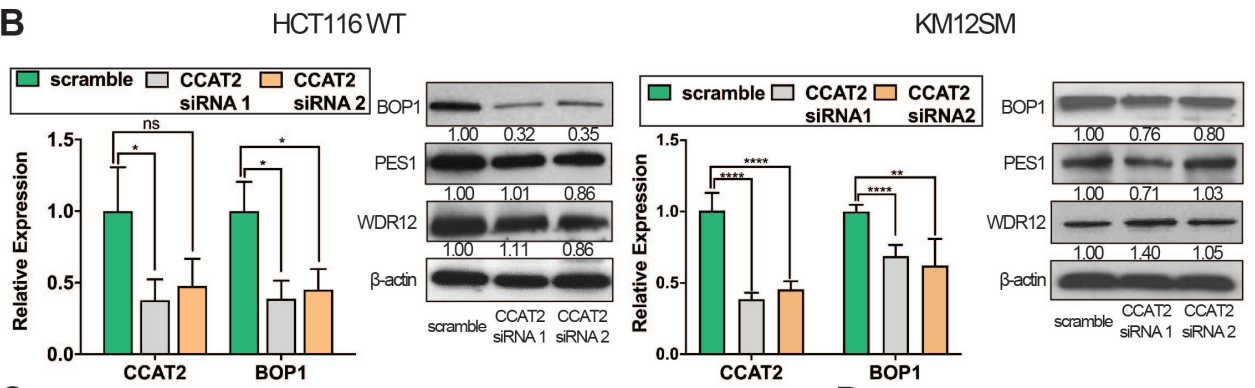


Figure 3

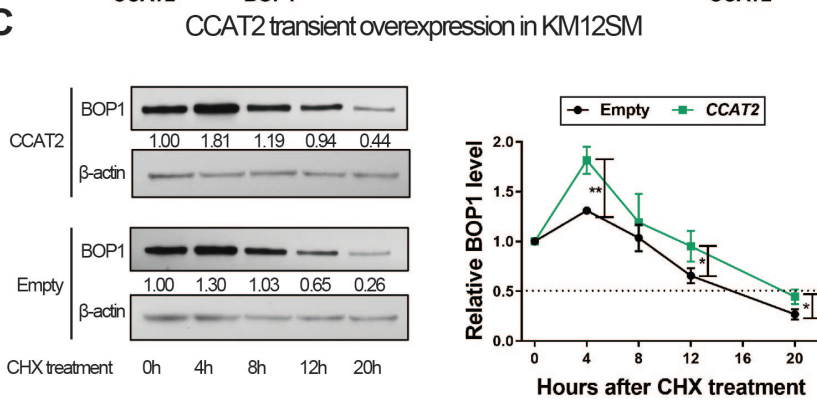
A



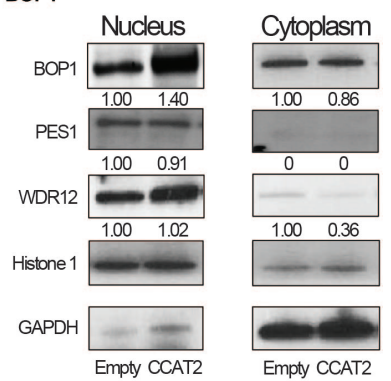
B



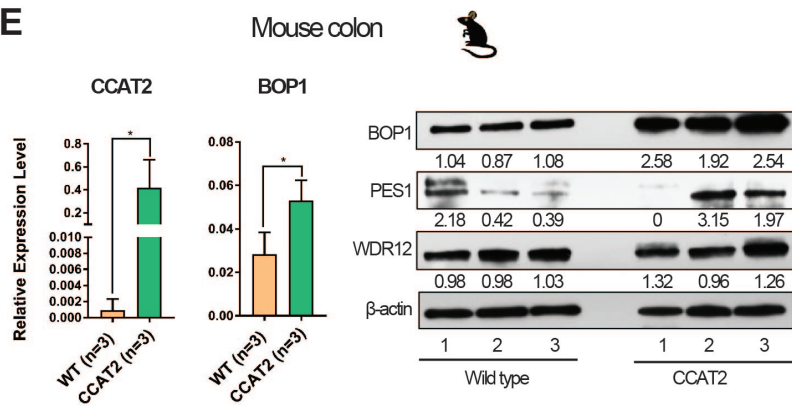
C



D



E



F

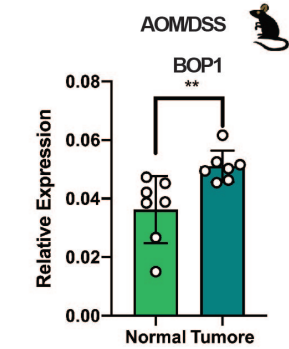
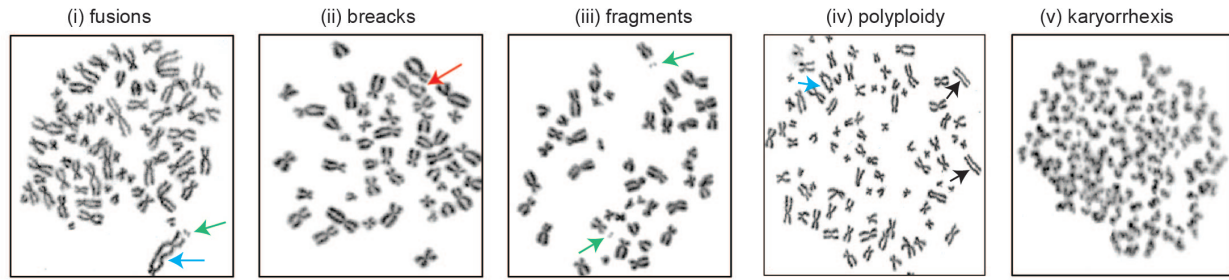


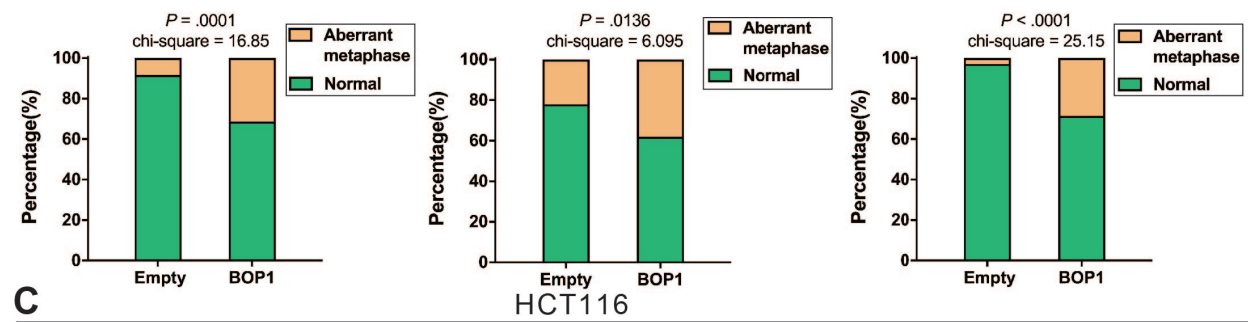
Figure 4

A

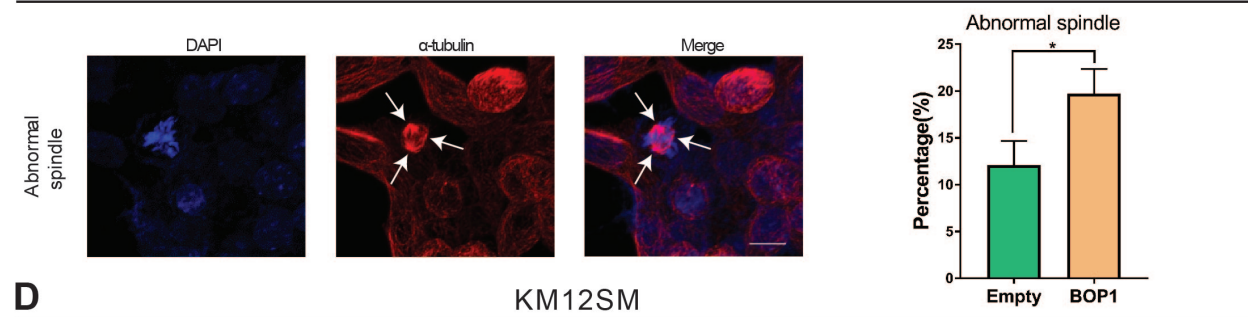
cytogenetics



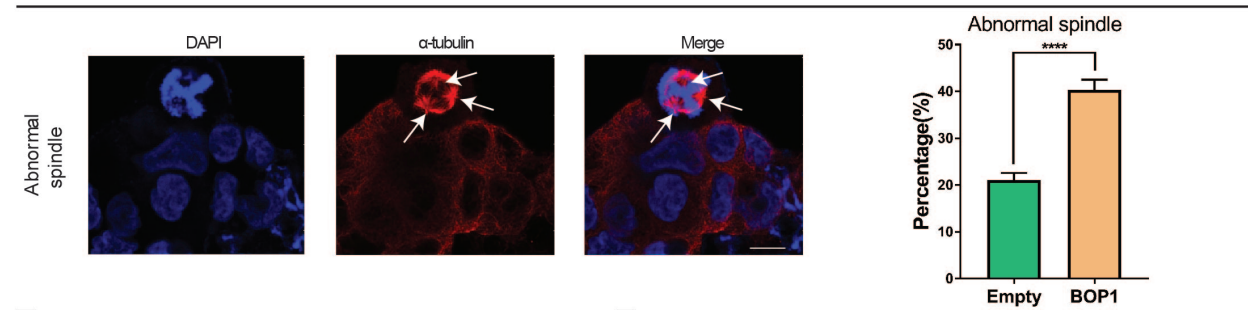
B



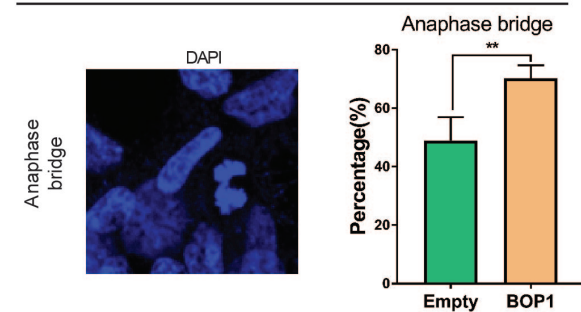
C



D



E



F

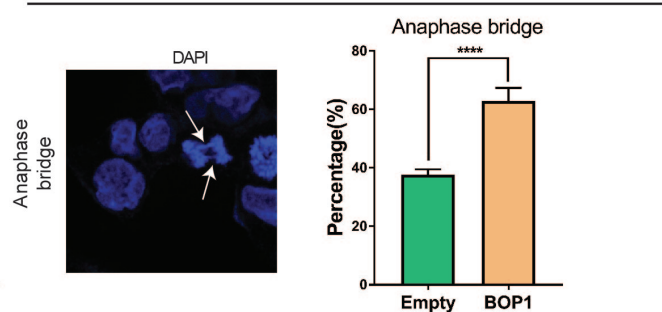


Figure 5

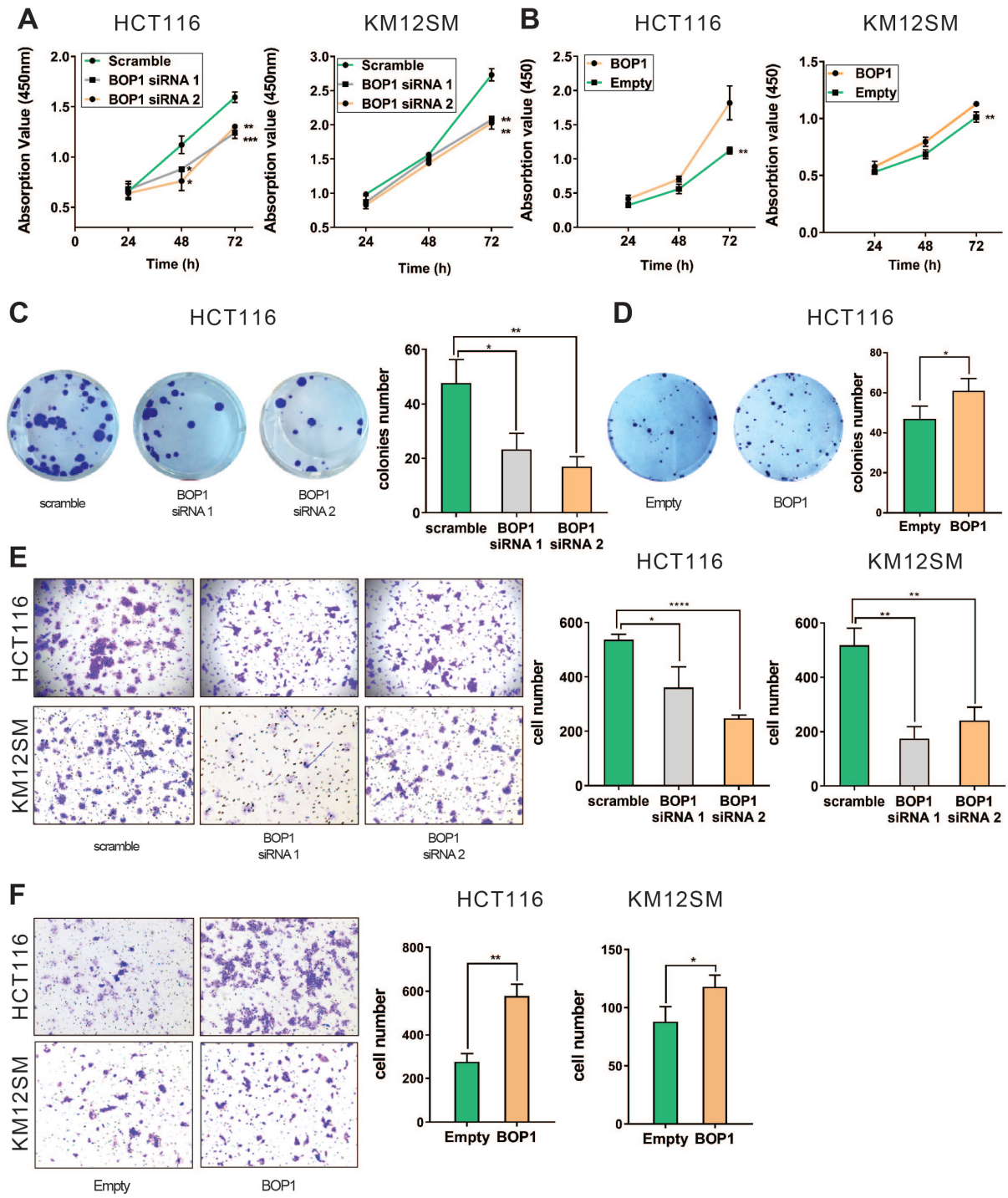
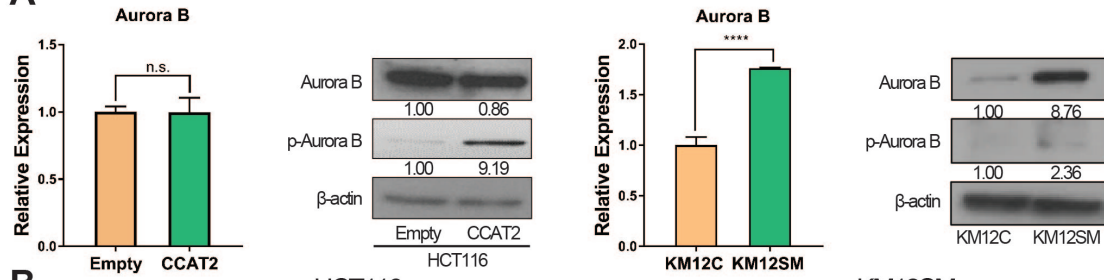
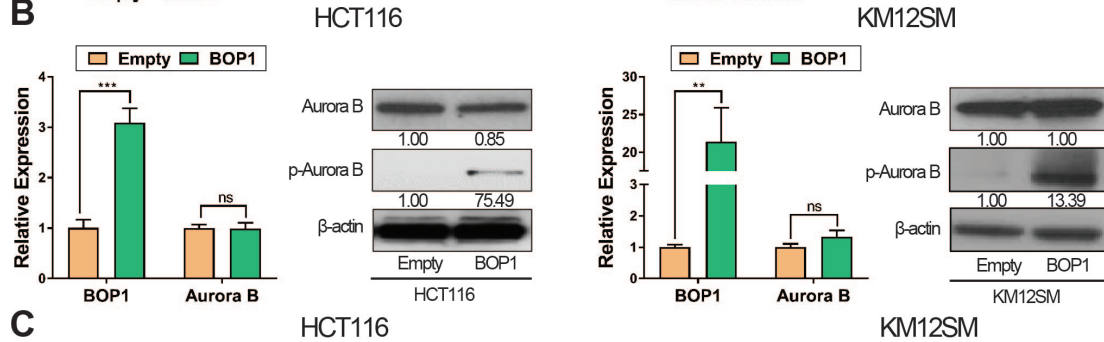


Figure 6

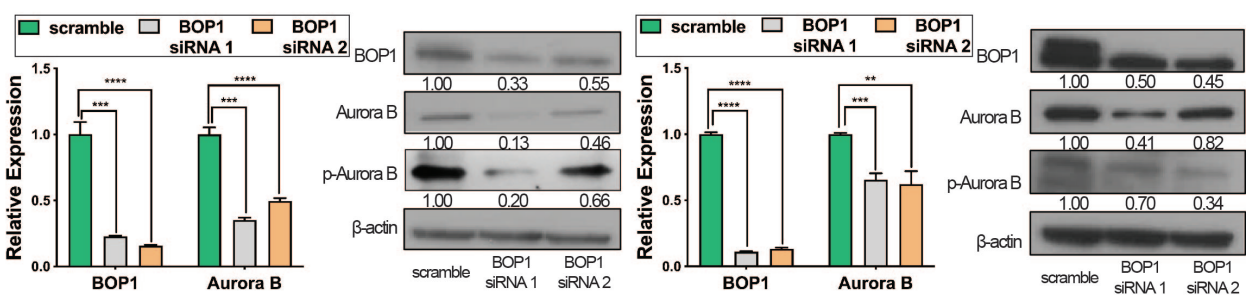
A



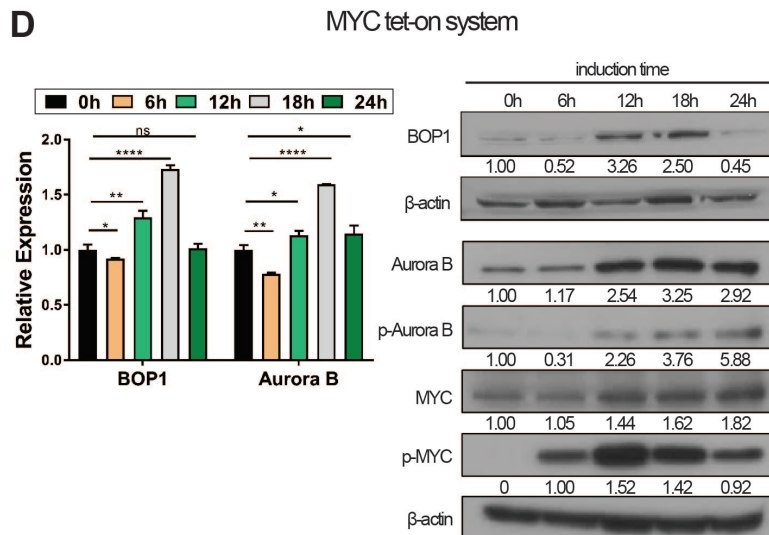
B



C



D



E

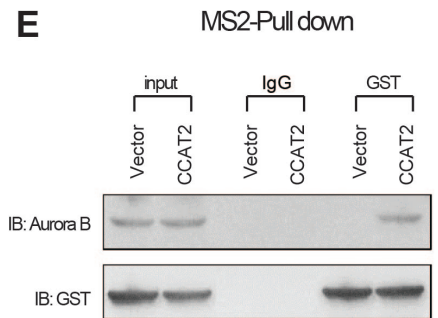
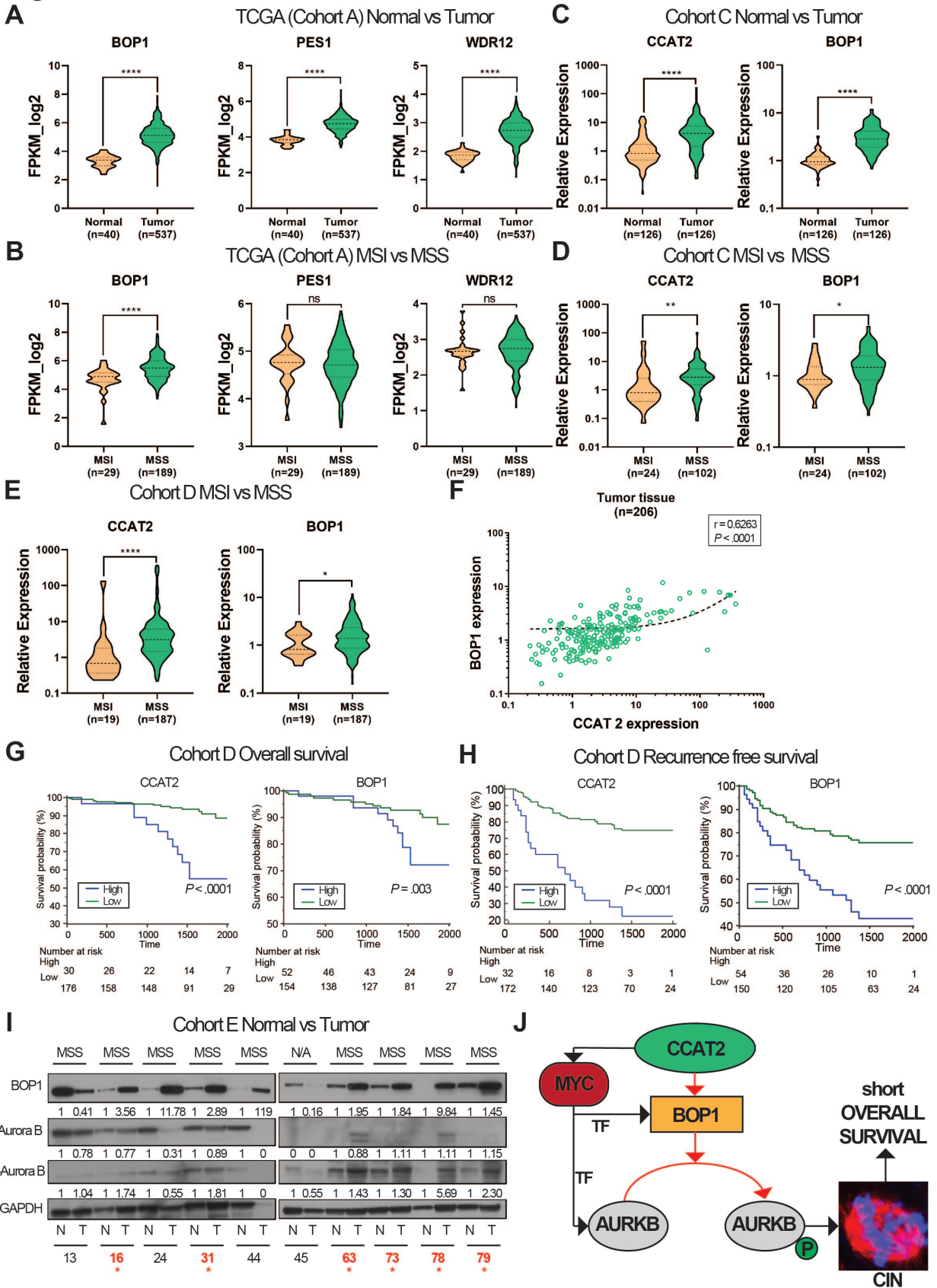


Figure 7



What you need to know:

Background and Context: High expression of the colon cancer associated transcript 2 gene (*CCAT2*), which encodes a long noncoding RNA (lncRNA), associates with chromosome instability, but little is known about how *CCAT2* lncRNA regulates this cancer enabling characteristic.

New Findings: Colorectal cancer cells overexpress *CCAT2* lncRNA, which promotes chromosome instability by stabilizing and inducing expression of BOP1 and activation of aurora kinase B.

Limitations: In this study pharmacological targeting of *CCAT2* lncRNA was not assessed. Further studies are needed to analyze the targetability of *CCAT2* lncRNA and associated toxicity.

Impact: Strategies to target this pathway might be developed for treatment of patients with microsatellite stable colorectal tumors.

Lay Summary: The authors identified a gene product that causes chromosomes to become unstable in colon cells, promoting development of colorectal cancer.

Supplementary materials and methods

The Long Noncoding RNA *CCAT2* induces chromosomal instability through BOP1 - AURKB signaling

Baoqing Chen, Mihnea P. Dragomir, Linda Fabris, Recep Bayraktar, Erik Knutsen, Xu Liu, Changyan Tang, Yongfeng Li, Tadanobu Shimura, Tina Catela Ivkovic, Mireia Cruz De los Santos, Simone Anfossi, Masayoshi Shimizu, Maitri Y. Shah, Hui Ling, Peng Shen, Asha S. Multani, Barbara Pardini, Jared K. Burks, Hiroyuki Katayama, Lucas C. Reineke, Longfei Huo, Muddassir Syed, Shumei Song, Manuela Ferracin, Eiji Oki, Bastian Fromm, Cristina Ivan, Krithika Bhuvaneshwar, Yuriy Gusev, Koshi Mimori, David Menter, Subrata Sen, Takatoshi Matsuyama, Hiroyuki Uetake, Catalin Vasilescu, Scott Kopetz, Jan Parker-Thornburg, Ayumu Taguchi, Samir M. Hanash, Leonard Girnita, Ondrej Slaby, Ajay Goel, Gabriele Varani, Mihai Gagea, Chunlai Li, Jaffer A. Ajani, George A. Calin

Supplementary Material and Methods

Supplementary figure 1-8

Supplementary tables 1-12

Supplementary References

Supplementary Material and Methods

Cell culture

Human colon cancer cell lines HCT116, KM12C, KM12SM, COLO320, DLD-1, HT29 and gastric cancer cell lines AGS and KATO-III (**Supplementary Table 7**) were obtained from the American Type Culture Collection. Of note, KM12SM cell is the spontaneous liver metastasis of the KM12C cells¹. HCT116 and HT29 cells were cultured in McCoy's 5A, COLO320, DLD-1, AGS and KATO-III in RPMI-1640, KM12C and KM12SM in DMEM with 4.5 g/L glucose (10% fetal bovine serum and 1 % antibiotics) at 37°C with 5% CO₂ and 95% humidity. All cell lines were validated by the Characterized Cell Line Core at The University of Texas MD Anderson Cancer Center using STR DNA fingerprinting.

CCAT2 transgenic mice

CCAT2 transgenic mice were generated as previously described². The mice used for this study were both females and males of 7-9 months of age. Briefly, a human 1.7-kb cDNA of *CCAT2* was cloned into a vector backbone which contained the CAG promoter, eGFP reporter gene and an IRES element. The *CCAT2*-vector was inserted randomly into the genome of C57BL/6N mice by pronuclear injection by the MDACC Genetically Engineered Mouse Facility. The founders were mated with WT C57BL/6N mice. Pups were selected for presence of the transgene by PCR on tail-extracted DNA according to standard protocols. All the protocols and experiments were conducted according to the guidelines of the MDACC Institutional Animal Care and Use Committee.

AOM/DSS mouse model

Because of the sex-related differences in the chemically induced colorectal cancer model³, 7-8-week-old male mice of C57BL/6N strain⁴⁻⁶, wild-type or *CCAT2* transgenic, were used. Azoxymethane (AOM) was purchased from the Sigma-Aldrich (St Louis, MO). Colitis-grade Dextran Sodium Sulfate (DSS) with a molecular weight of 36000–50 000 was purchased from MP Biochemicals. All mice were initially treated with a single intraperitoneal injection of AOM (10 mg/kg of body weight). Two days after AOM administration, the mice received 3% DSS in their drinking water for 5 days, followed by a 2-week rest period without DSS. This scheme was repeated for a total of four DSS administrations. Mice were sacrificed one week after the last DSS administration. At this time, mice were dissected, the colon was excised and flushed with saline solution. The entire colon length from the cecum to rectum was cut open longitudinally exposing

the mucosa for gross examination and taking pictures with Leica camera dissecting microscope for counting and measuring the mucosal polyps. Frozen tissue samples of grossly detected polyps and of normal colon mucosa were collected. Subsequently, the colon was fixed in 10% neutral buffered formalin for histopathological examination.

Histopathologic Evaluation

Two longitudinal serial sections of each colon were prepared histologically and examined microscopically by an ACVP certified veterinary pathologist. Histopathological evaluation included counting and size measurement of polyps (colon adenomas), and grading of hyperplastic and dysplastic changes of colonic glands with a score from 1 to 4 (1 = minimal, 2 = mild, 3 = moderate, 4 = marked). The entire colon from cecum to rectum was collected at necropsy and then was open longitudinally and gently flushed with PBS solution for cleaning the feces. The colon was attached to index-card paper for exposing the mucosa and photographing the entire colonic mucosa with the Leica stereomicroscope and camera for gross counting of the polyps. Then the colon tissue was immersed in 10% neutral buffered formalin for 48 hour fixation. Fixed colon tissues were arranged in "Swiss rolls" and cut longitudinally in 2 halves which were processed and embedded in paraffin blocks, from which 4- μ m thick sections were cut and stained with hematoxylin and eosin (H&E). H&E stained slides were scanned with Aperio AT2 scanner for microscopic examination and histomorphometric evaluation of colonic polyps.

Murine colon crypts isolation and murine colon organoid culture

Crypts were isolated and colon organoids were established as previously described⁷⁻⁹. Approximately 10 cm of colon was harvested from WT and CCAT2 transgenic mice, respectively. The colon was washed with cold PBS (without Ca²⁺ and Mg²⁺), opened laterally and cut into 2-mm pieces. The pieces were washed again several times with cold PBS with penicillin/streptomycin (Gibco, 15140122) until were clear. Then, tissue fragments were subjected to enzymatic digestion in 2 ml digestion medium containing 2 mg ml⁻¹ collagenase IV (Sigma-aldrich, C5138), 0.1 mg ml⁻¹ dispase type II (Sigma-Aldrich, D4693), 10 μ M Y-27632 (StemCell, 72304), 100 U/100 μ g ml⁻¹ penicillin/streptomycin and 10% FBS in DMEM medium (Gibco, 11995065), on an orbital shaker at room temperature for 30 minutes. The tissue mixture was then filtered through a 70- μ m cell strainer into a 50 ml conical tube, and centrifuged at 200 x *g* for five minutes at 4°C. The pellets were resuspended in 10 ml cold DMEM medium containing penicillin/streptomycin and FBS, and centrifuged again at 200 x *g* for five minutes at 4°C.

Isolated crypts were counted using a hemacytometer with an inverted microscope, and embedded in growth factor-reduced Matrigel (Corning, catalog # 356231), diluted 3:4 in organoid culture media and seeded into 24-well plates (Corning™ 3526) at a density of 250–500 crypts in 50 µl total volume per well, and overlaid with 500 µl organoid culture media onto the Matrigel after incubation for 20 minutes at 37 °C.

Fresh medium was added every 2 or 3 days. Colon organoids were observed and treated at proper times. Outgrowing organoids were passaged every 7-days after mechanical and TrypLE™ Express (Gibco, 12604021) disruption. The organoids were washed several times with centrifugation at 200 g at 4 °C. The pellets were suspended in Matrigel with a dilution ration 1:4 and seeded as described above.

Murine colon organoids were cultured in Advanced DMEM/F12 medium (Gibco, 12634010) containing 10 mM HEPES (Invitrogen, 15630-056), 1% GlutaMAX (Invitrogen, 35050), 100 U/100 µg ml⁻¹ penicillin/streptomycin, supplemented with 50 ng ml⁻¹ human EGF (PeproTech, 315-09), 200 ng ml⁻¹ Noggin (PeproTech, 250-38), 500 ng ml⁻¹ R-spondin (BioLegend, 783606), 1 mM *N*-acetyl-L-cysteine (Sigma-Aldrich, A9165), 1× N2 (Gibco, 17502-048), 1× B27 (Gibco, 17504-044), 10 nM gastrin (Sigma-Aldrich, G9145), 10 mM Nicotinamide (Sigma-Aldrich, N0636), 10 µM Chiron (Sigma-Aldrich, SML1046), 500 nM A83-01 (StemCell, 72024), 10 µM SB202190 (Sigma-Aldrich, S7067), 10 µM Y-27632, 10 nM prostaglandin E2 (Selleck Chemicals, S3003), and 1× Primocin (InvivoGen, ant-pm-1)]. Organoids cell viability was measured every three days after treatment by using CellTiter-Glo® 3D Cell viability assay (Promega, G9683) according to manufacturer's instruction.

Gastric cancer PDX and PDO

GA-080417 cell line (referred to as #1) was established directly from patient ascites by culturing the ascites cells in RPMI (7% FBS, 1% antibiotics) and expanding them for more than 10 passages. This cell line was then injected to SCID mice by both subcutaneous (1x10⁴ ~1x10⁵) and orthotopic (1x10⁵) administration to investigate their tumorigenicity. GA-080417 cells can grow into tumors after both subcutaneous and orthotopic injection.

In contrast, GA-082517 cell line (referred to as #3) was established from PDX tumor that was generated by subcutaneous injection of GA-082517 patient ascites cells. Tumor cells were disassociated from PDX tumor tissue and cultured in RPMI (7% FBS, 1% antibiotics) followed by

about 10 passages. The GA-082517 cell line was tested for tumorigenicity by both subcutaneous ($1 \times 10^3 \sim 1 \times 10^5$) and orthotopic (1×10^5) administration in SCID mice and was found to have tumor growth through both administration routes.

GA-051816 cell line (referred to as #2) was previously reported, for more detail refer to Song et al. ¹⁰.

Colon cancer PDX

Colon cancer PDX were established as previously described ¹¹. About 6-8-weeks old female NOD.Cg-Prkdcscid Il2rgtm1Wjl/SzJ (NSG) mice were maintained in the MDACC animal facilities following standard animal regulation and strict health control. Rodent care and housing were in accordance with institutional guidelines and regulations as well as according to Institutional Animal Care and Use Committee approved animal protocols. Patient tumor (PX) specimens acquired at MDACC were engrafted into NSG mice. One tumor fragment ($\sim 50 \text{ mm}^3$) per mouse was implanted subcutaneously into the flanks of mice anesthetized under 2–4 % isoflurane/O₂ inhalation. Primary tumor xenografts (P0) growth was monitored and documented twice a week, with the date of first palpable growth noted. When tumor burden reached 1500 mm^3 , mice were euthanized for tumor collection. Sections of these tumors were transplanted into new mice for PDX establishment (P1). Tumor samples at each passage were collected for histology, protein, and genomic analysis. Several PDX samples were collected in freezing media (CryoStor CS10) for storage in liquid nitrogen.

Patient sample collection

Cohort A (TCGA colorectal cancer cohort) consisted of 537 CRC cases with clinical and mRNA expression information. Among them 40 had mRNA data for matched normal tissues. The clinical information was retrieved from ¹². The information regarding the MSS/MSI status for 275 patients was obtained from the Cancer Genome Atlas ¹³. The clinical characteristics were listed in **Supplementary Table 1**. For this cohort of patients, fragments per kilobase millions (FPKM) quantification mRNA-seq data from the Genomic Data Commons Data Portal (<https://portal.gdc.cancer.gov/>) for *BOP1*, *PES1* and *WDR12* genes were downloaded and log₂ transformed.

For **Cohort B**, RNA samples from frozen cancer and matched non-neoplastic tissues of resected specimen from 100 CRC patients were obtained from the Department of Surgery and Science

(Department of Surgery II), Kyushu University Hospital. Non-neoplastic tissues were obtained from the resected specimen and were sufficiently far enough from the primary tumor. Histological diagnosis was made according to the World Health Organization criteria and pathological staging was done in accordance to the tumor-node-metastasis (TNM) classification system. Cases with stage IV were patients with synchronous distant metastasis when undergoing surgery. The details of the patient's clinical characteristics were listed in the **Supplementary Table 2**.

Cohort C consisted of RNA samples isolated from tumor and adjacent normal colon tissue samples of a total of 126 CRC patients from the Department of Comprehensive Cancer Care, Masaryk Memorial Cancer Institute, Czech Republic. Cohort C was composed of 24 MSI-H and 102 MSS (MSS/MSI-L) sporadic CRC patients. pTNM classification of the patients was done based on pathology reports and histological slides (**Supplementary Table 3**). The patients underwent standard surgical procedure and adjuvant therapy was added when necessary (stage II with risk factors or stage III). In case of advanced disease at the time of diagnosis, patients received adjuvant treatment according to the oncologist choice, following the recommendations of national guidelines.

In the **Cohort D**, a total of 206 fresh frozen tissue specimens, which encompassed primary colorectal adenocarcinoma tissues from 19 MSI-H and 187 MSS (MSI-L and MSS) cancer patients, were collected from Tokyo Medical and Dental University, Japan. Patients undergoing resection of their primary tumor that was histologically confirmed to be a stage II and III CRC and classified as MSI-H or MSS (MSI-L and MSS) were included in this study. Details of the clinical and pathological features of the included patients are shown in **Supplementary Table 4**.

Cohort E consisted of 10 paired samples, normal colon mucosa and colon tumor. The samples were obtained from the Ruder Boskovic Institute, Croatia. Tissue samples were obtained from fresh surgical specimens frozen in liquid nitrogen and stored at -80°C. The samples were histologically confirmed prior to use. Nine out of ten samples were classified as MSS and for one sample the status was not available (N/A). The *CCAT2* expression for this cohort was previously reported¹⁴.

CIN index (CINdex) analysis

Segmented copy number data (as on hg19 reference genome), along with RNA-seq gene expression counts from TCGA Colon Adenocarcinoma (COAD) and TCGA Stomach Adenocarcinoma

(STAD) patients were downloaded from the Broad Institute Firebrowse platform (<http://firebrowse.org/>). An intersection was done to select only those 280 COAD tumor samples that had both copy number and gene expression data. An intersection was done to select only those 412 STAD tumor samples that had both copy number and gene expression data.

Bioconductor package CINdex (<http://bioconductor.org/packages/CINdex/>)¹⁵ was applied on the segmented copy number data which enabled to characterize genome-wide DNA copy number alterations as a measure of chromosomal instability. This package calculated genomic instability at the chromosome and cytoband level. Only data from autosomes were considered for this analysis. A threshold of 2.25 and 1.75 in the un-normalized setting was used to define gains and losses respectively.

The chromosome CIN and gene expression data from 280 COAD and 412 STAD patients were shifted by 1, respectively 2 and then converted to the log base 2 scale. A Pearson correlation analysis was performed between the chromosome CIN and the gene expression data and results with a p-value less than 0.05 were short listed for further inspection. A customized correlogram table was plotted where each cell represented a correlation between two variables. Positive correlation was represented by orange color while negative correlation represented by purple colors. The cells were colored white if p-value of a correlation test was not significantly different from zero. All analyses were performed using the R statistical platform (<https://www.r-project.org/>).

Genomic instability analysis

Chromosome analyses were performed as previously reported². Cells/mouse organoids were plated into 10 mm plates. After reaching 60-70% confluence, cells were first exposed to colcemid (0.04 mg/mL) for 1-2 hours at 37°C and to hypotonic treatment (0.075 M KCl) for 20 min at room temperature. Afterwards, cells were fixed in a methanol and acetic acid mixture (3:1 by volume) for 15 min and washed three times with the fixative. Air-dried preparations were made and the slides were stained with 4% Giemsa. The slides were analyzed for chromosomal aberrations, including chromosome and chromatid breaks, fusions, fragments and tetraploidy. A minimum of 35 metaphases were analyzed from each sample. Images were captured using a Nikon 80i microscope equipped with karyotyping software from Applied Spectral Imaging, Inc. Carlsbad, CA, USA.

Immunofluorescence staining

Cells were cultured in 8-well chamber slides (Ibidi). To check the aberrant spindles, cells were synchronized by culturing in the medium with nocodazole (100ng/ml) for 14 hours and then were released to process to G2/M phase by removal of nocodazole. Cells were fixed with 4% paraformaldehyde for 30 min at room temperature and then washed with PBS for three times, followed by blocking and permeabilization with blocking buffer, which includes 4% BSA and 0.3% Triton X-100, for 1 hour at room temperature. For the analysis of the spindle apparatus, cells were incubated overnight at 4°C with mouse anti- α -tubulin (1:16000; CST) and then with anti-mouse secondary antibodies (Alexa Fluor 647; Invitrogen) for 1 hour at room temperature. Slides were finally mounted with mounting medium containing DAPI (Abcam). For analyzing the anaphase bridges, cells were cultured, fixed, blocked, and permeabilized with same procedure and reagents. Then, the cells were stained with DAPI (Abcam 1:5000) directly, and washed three times with PBS to remove the background signal. Images were acquired with the Spin Disc Confocal microscope (Andor).

Plasmids and constructs

Mammalian expression vectors for full-length *CCAT2* and a series of mutants were constructed by subcloning the gene sequences into pCDNA3.1 (+) backbone (Life Technologies), pBabe retroviral expression vector, or MS2-24x-pCND4 vector. The full-length FLAG-tagged BOP1 human expression vector was purchased from Origene (#RC204016), and GST-tagged recombinant human BOP1 protein was purchased from Novus Biologicals. The BOP1 and *CCAT2* truncated mutants were generated by using QuikChange II XL Site-Direct Mutagenesis Kit (Agilent Technologies, #200522). All constructs were confirmed by DNA sequencing at Sequencing and Microarray Facility (SMF), UT MD Anderson Cancer Center.

RNA interference

CCAT2, *BOP1*, or negative control siRNAs were purchased from Ambion. Cells were seeded into six-well plates. When the cells reached 50-70% confluence, they were transfected with 25 nM of the corresponding siRNA by Lipofectamine 2000 (Life Technologies) according to the manufacturer's protocol. RNA and proteins were collected at 48h (in the *BOP1* knock-down experiments) or 72h (in the *CCAT2* knock-down experiments) after transfection. qRT-PCR and Western blot were used to check the efficiency of knock-down.

Generation of stable clones

HCT116 cells with *CCAT2* stable overexpression (HCT116^{CCAT2}) were established by transfecting pcDNA 3.1 *CCAT2*-expression vector with Lipofectamine 2000 (Invitrogen, ThermoFisher Scientific) as previously described¹⁶. Empty clone was generated by transfection with the empty pcDNA3.1 vector (HCT116^{Empty}). In our previous papers^{14, 16} these clones were termed: empty (E) and overexpressed clone 1 (OC1). DLD-1^{Empty} and DLD-1^{CCAT2} were established using the same above-mentioned method.

The cell culture supernatants with lentivirus carrying BOP1 were purchased from the MDACC shRNA and ORFeome Core of The University of Texas MD Anderson Cancer Center. HCT116, KM12SM, and HT29 cells were plated into six-well plates. Cells were infected by the cell-free supernatants containing lentivirus with 10 µg/µL polybrene (Sigma) for 48 hours and then switched to normal medium with Blasticidin S for 72 hours. Cells with successful transduction showed green fluorescence. Flow cytometry was used to select the green fluorescence-positive cells. We termed the clones with BOP1 overexpression HCT116^{BOP1}, KM12SM^{BOP1}, and HT29^{BOP1}.

For MYC tet-on stable clones, we first generated the HCT116 tetracycline reverse transcriptional activator (rtTA) stable clones by transducing with CMV-rtTA lentivirus and selected by neomycin (Sigma), as the activation of genes downstream of TetO induced by doxycycline is rtTA dependent. Then the stable HCT116 rtTA clones were transduced with tet-on C-MYC lentivirus and selected by puromycin (Sigma). CMV-rtTA lentivirus and inducible tet-on C-MYC lentivirus were purchased from Cellomics Technology.

RNA extraction, cDNA synthesis and quantitative real-time PCR

Total RNA was isolated using Direct-zol kit (Zymo research) following the manufacturer's protocol. Then, the cDNA was synthesized using High-Capacity cDNA Reverse Transcription Kit (Thermo Fisher Scientific) according to the manufacturer's protocol. qRT-PCR was performed using SsoAdvanced™ Universal SYBR Green Supermix real-time PCR kit (Bio-Rad). Primers were synthesized by Integrated DNA Technologies (sequences are listed in **Supplementary Table 5**). The relative gene expression levels were calculated using the $2^{-\Delta\Delta Ct}$ method. The geometric mean of *GAPDH*, *β-actin*, and U6 snRNA were used as normalizer for *in vitro* studies; *mActb* and *Rplpo* mRNAs were used as housekeeping genes for *in vivo* experiments while for clinical samples we used *β-actin* or geometric mean of *GAPDH*, *β-actin*, and U6 snRNA as normalizer. The absolute RNA

expression of the house keeping genes showed minimal and non-statistical difference between the groups we compared.

Whole or cytosolic/nuclear protein fractionation and Western blot

Protein lysates from whole-cell pellets samples were generated using Cell Lysis Buffer (Cell Signaling Technology) that contains protease and phosphatase inhibitor cocktails (Sigma-Aldrich). Cytosolic and nuclear protein fractionations were performed by utilizing of the NER Nuclear and Cytoplasmic Extraction Reagents kit (ThermoFisher Scientific) according to the manufacturer's protocol. Protein concentration was quantified by Bradford assay (Bio-Rad). In total, 20 ug of proteins were loaded on 4-20% acrylamide Criterion™ TGX™ precast gels (Bio-Rad) and transferred to nitrocellulose membranes by semi-dry method. The membranes were incubated with the corresponding primary antibodies (listed in **Supplementary Table 6**) overnight and then incubated with the appropriate HRP-conjugated secondary antibody. Immunoreactivity was detected by incubation with ECL SuperSignal West Femto substrate (ThermoFisher Scientific), and then detected by the autoradiographic film.

Cytosolic and nuclear RNA fractionation

RNA was isolated from cellular fractions according to the previously described protocol ¹⁷. Briefly, the cell pellet was resuspended in 380 ul Hypotonic lysis buffer (HLB: 10 mM Tris (pH 7.5), 10 mM NaCl, 3 mM MgCl₂, 0.3% (vol/vol) NP-40 and 10% (vol/vol) glycerol) and the mixture was incubated on ice for 10 min. The cells were centrifuged at 1,000 x g at 4 °C for 3 min; the supernatant, which is the cytoplasmic fraction, was transferred to another tube. RNA precipitation solution (RPS: 0.5 ml of 3 M sodium acetate (pH 5.5) with 9.5 ml of ethanol) was added and the mixture was stored at -20 °C for over 1h. The remaining pellet (the nuclear fraction) was washed three times with HLB by centrifuging at 200 x g at 4°C for 2 min. TRIzol was added over the nuclear pellet and RNA was extracted using Direct-zol kit (Zymo research) following the manufacturer's protocol. The cytoplasmic fraction, after 1h, was centrifuged at 18,000 x g at 4 °C for 15 min. The pellet was washed in 70% ethanol and centrifuged again at 18,000 x g at 4 °C for 5 min. After air drying, 1 ml of TRIzol was added to the pellet and RNA was extracted. The lncRNA *NEAT1* was used as a positive control for nuclear enrichment.

γ-H2AX assay

This assay was performed with and without Bleomycin treatment. HCT116^{Empty} and HCT116^{CCAT2} overexpressed cells were cultured for 24 hours in 8-well chamber slides (Ibidi). In the case of Bleomycin treatment, 10 µg/ml of Bleomycin was added for two hours at 37°C. Treated and untreated cells were then washed three times with PBS and fixed by incubating them in ice cold methanol for 5 minutes at room temperature. This step was followed by blocking and permeabilization with 1% BSA-PBST at 37°C for 30 minutes. Next, the cells were incubated overnight at 4°C with the primary antibody of H2AX (rabbit polyclonal IgG) followed by one-hour incubation at room temperature with secondary antibody, goat polyclonal IgG conjugated with FITC. Finally, cells were stained with Hoechst 33342, before adding the cover slip. Images were acquired with the Spin Disc Confocal microscope (Andor).

Cellular Senescence Staining

HCT116^{Empty} and HCT116^{CCAT2} cells were seeded in 6-well plates to a seeding density of 3×10^5 cells per mL, and a final chamber volume of 1 mL. When the cells reached 70-80% confluence, were stained for senescence using a β -Galactosidase Staining Kit (Cell Signaling Technology #9860) following the manufactures instructions. Cells were mounted for analysis with 70% glycerol. All the cells from the circumference of three wells were analyzed for each clone.

SHAPE Analysis

RNA secondary structure probing was started by mixing stock *CCAT2* RNA and folding buffer (200 mM NaCl, 100 mM HEPES, 0.2 mM EDTA, pH 8.0), followed by incubation at 37°C with refolding buffer for 30 min (100 mM NaCl, 50 mM HEPES, 16.5 mM MgCl₂, pH 8.0). The SHAPE reaction was then started by adding NMIA (+) (32.5mM, 65mM or 130mM), or DMSO as control (-). Samples were then incubated for 45 min at 37°C, precipitated with ethanol and glycogen. Reverse transcription was performed using Super Script III reverse transcriptase (Invitrogen). Electrophoresis on an 8% (vol/vol) polyacrylamide gel was then performed to separate fragments. Band-intensities were visualized by gel electrophoresis or capillary electrophoresis and were quantified using SAFA, version 1.1 Semi-Automated Footprinting Analysis¹⁸. SHAPE reactivity data from capillary and gel electrophoresis were incorporated as a SHAPE constraint file in the RNA structure folding program, and the 20 lowest energy structures based on those constraints were generated^{19,20}. Structures were calculated with RNAstructure default secondary structure options. Each structure image presented in this manuscript was rendered using VARNA.

Cycloheximide Chase Assay

Protein half-life studies were performed as previously described²¹. Cells were cultured in six-well plates and then transfected with *CCAT2* or empty vector for 24 hours and then cultured with cycloheximide (CHX, 100µg/ml), which blocks the translation of mRNA. After culturing with cycloheximide for 0, 4, 8, 12, and 20 hours, the cells were collected and lysed with lysis buffer (CST) for protein extraction. The degradation of BOP1 was then detected by Western blotting analysis.

Proliferation assay

Cell Counting Kit-8 (Enzo) was used to determine the cell viability according to the manufacturer's protocol. Cells were seeded at a density of 2500 cells per well in 96-well plates overnight. For the proliferation assay in knock-down experiments, cells were transfected with the corresponding siRNA and then seeded in 96-well plates. After culturing for 0, 24, 48 and 72 hours, 10ul of CCK8 was added to each well and then incubated at 37°C for 2 hours. The absorbance values at 450 nm were measured to represent the cell viability.

MTT assay - 5- Fluorouracil.

In vitro chemoresistance to 5-Fluorouracil (5-FU) of HCT116^{CCAT2} clones versus HCT116^{Empty} was assessed by MTT. Briefly, cells were plated 24 hours prior to treatment in 96-well microculture plates. After 24 hours, 3 different doses of 5-FU were added (2, 20 and 40 µM) to the supernatant without changing the medium. After 48 hours, the MTT reagent (Sigma) was added to each well and incubated for 3 hours at 37°C. The optical density (OD) was read at 570 nm on a microplate spectrophotometer and growth values (%) were calculated as followed (OD treated cells /OD untreated cells) x 100.

MTS assay - oxaliplatin

Cell viability of oxaliplatin treated HCT116^{CCAT2} clones versus HCT116^{Empty} cells was measured by The CellTiter 96[®] AQueous One Solution Cell Proliferation Assay (Promega). Cells were seeded in 100 µl medium into 96-well plates and incubated for 24 hours at 37°C before treatment. The cells were treated with different concentrations of oxaliplatin: 2, 20 and 40 µM (Selleckchem) for 48h. At the end of treatment, 20 µl of MTS solution was added to each well of the plate and the optical density (OD) at 490 nm was then measured using microplate reader and growth values (%) were calculated as followed (OD treated cells /OD untreated cells) x 100.

Colony formation assay

Around 500 HCT116 cells with BOP1 knock-down or overexpression and KM12SM cells with BOP1 overexpression were plated into 6-well or 12-well plates. For the knock-down experiments models, corresponding siRNAs were added and then incubated for 48 to 72 hours. Cells were then cultured with new medium for 10-14 days. The colonies were fixed with 4% paraformaldehyde solution, stained with crystal violet. Colonies with more than 50 cells were counted.

Invasion and scratch assay

Cells in serum-free media were seeded into precoated Matrigel 24-well invasion chambers (8 mm; 24 wells; BD Biosciences) according to the manufacturer's protocol. In the bottom well, 700 μ l of medium with 20% FBS was added to serve as chemoattractant. Twenty-four hours after seeding, cells at the top of the insert well were removed by swabbing, the cells that penetrated the membrane and were located on the bottom side of the insert well were fixed with paraformaldehyde, stained with crystal violet, and counted. For scratch assay, cells were seeded in 6-well plates and cultured to reach around 90-100% confluency. A scratch was made by scratching a line across the bottom of each well using a 20 μ L pipette tip. The detached cells were then removed by washing with PBS. Migration into the open area was recorded at 48 hours after scratching.

Polysome profiling

Polysome profiling was done in accordance with previously published protocols^{22, 23}. Briefly, 10⁶ cells were treated 10 minutes at 37°C with cycloheximide at 100 μ g/ml. Cells were then trypsinized and collected under ice cold conditions. Cell lysates were prepared using dounce homogenization with 50 strokes of the dounce. The lysate was then precleared at 1200xg for 10 minutes, and equal OD254 units were loaded onto a 17-50% sucrose gradient. The sucrose gradients were fractionated on a gradient fractionator using a UA-6 detection system (Teledyne ISCO). For experiments to quantify absolute amounts of 40S and 60S subunits, a modified procedure was followed essentially as described²⁴. In this procedure, the lysis buffer consisted of 20mM Tris-HCl, pH 7.5, 100mM KCl, and 5mM MgCl₂, and the sucrose was mixed into that buffer for pouring the sucrose gradients. Lysates were precleared as described above, and EDTA was added to a final concentration of 50mM prior to fractionating.

***In vitro* RNA-protein binding assay**

Biotin-labeled full-length and truncated fragments of *CCAT2* RNA were transcribed *in vitro* with a Biotin RNA Labeling Mix Kit (Roche) and T7 or SP6 RNA polymerase (Ambion) using the PCR products as a template, treated with RNase-free DNase I (Ambion). The reaction mix was then purified with an RNA Clean & Concentrator kit (Zymo Research) and the purified biotinylated RNA was denatured at 95°C for 2 min, cooled on ice for 2 min, and then transferred in RNA structure/folding buffer at 30°C for 30 min to allow proper RNA secondary structure formation.

The RNA-protein binding assays were performed using Pierce™ Magnetic RNA-Protein Pull-Down Kit (Thermo Scientific) according to the manufacturer's instructions. Briefly, magnetic Dynabeads M-280 Streptavidin beads were washed three times with washing buffer and then immediately subjected to capture *in vitro* transcribed RNA (2 µg) as described above. To pull down recombinant proteins, the RNA-captured beads were incubated with recombinant proteins (1 µg) in binding buffer for 1 hour at RT. Beads were washed three times and boiled in 1 x reducing sample buffer. The retrieved proteins were analyzed by Western blotting.

MS2 pull-down assay

The pCCAT2-MS2, pEmpty-MS2, and pMS2-GST vectors were generated as previously reported¹⁴. HCT116 cells were plated into 15mm plates. After reaching 60-70% confluence, the cells were co-transfected with pCCAT2-MS2 vector or pEmpty-MS2, and pMS2-GST vector using Lipofectamine 2000 (Invitrogen, ThermoFisher Scientific). Forty-eight hours after transfection, cells were harvested and proteins were collected and quantified. In total, 1000 µg (2 µg/µl) lysate was incubated with GSH agarose beads (GE Healthcare) for 3 hours at 4°C, followed by 3 times washing with cell-lysis buffer to remove unspecific bound proteins. Beads were then suspended in SDS buffer and heated. Bound proteins were detected by Western blotting.

RNA immunoprecipitation

EZ-Magna RIP RNA-Binding Protein Immunoprecipitation Kit (Merck Millipore) was used according to the manufacturer's protocol. Cells were harvested and lysed in the RIP buffer containing the protease inhibitor. Cell lysates were then incubated with the buffer containing magnetic beads conjugated with anti-BOP1 (Abcam), anti-PES1 (Santa Cruz), anti-WDR12 (Abcam), anti-AURKB or IgG as a negative control at 4°C overnight and then washed with washing buffer for three times to remove the unspecific bounds. RNA was then isolated using the phenol:chloroform:isoamyl alcohol method and further used for cDNA synthesis and qRT-PCR to

test the presence of *CCAT2*. For *CCAT2* segments - Aurora Kinase B interaction, UV crosslinked cells were used. The lysates were treated with RNase I for exactly 3 min at 37°C then immediately transferred on ice and centrifuged. The supernatant was incubated with magnetic beads conjugated with anti-AURKB overnight. After immunoprecipitation, RNA was purified with phenol:chloroform:isoamyl alcohol to prepare cDNA. Then, *CCAT2* segment specific primers were applied to perform qRT-PCR.

Gene expression analysis (GEA)

For the mouse GEA, total RNA was extracted from bone marrow (BM) cells of WT and *CCAT2* transgenic mice. Labeling and hybridization of mRNAs were performed according to Affymetrix protocols. Briefly, 5 µg of total RNA was reverse transcribed with an oligo(dT) primer that has a T7 RNA polymerase promoter at the 5' end. Second-strand synthesis was followed by cRNA production with incorporation of biotinylated ribonucleotides using the BioArray High Yield RNA Transcript Labeling Kit T3 (Enzo Life Sciences). The labeled cRNA was fragmented and hybridized to Affymetrix GeneChip Mouse Genome 230 4.0 arrays. GeneSpring GX software v.13 (Agilent Technologies) was used for probe set summarization and robust multiarray average (RMA) normalization procedures. The differentially expressed genes were selected to have a >1.5-fold change difference between the compared groups (average value), a <10% FDR using Benjamini-Hochberg corrected moderated t-test and $P < .05$.

***In silico* analysis of genomic evolution**

Genomic conservation was analyzed by downloading Multiz Alignments of 100 Vertebrates from the UCSC Genome Browser (GRCh38/hg38 Assembly, chr22:46,492,389-,46,493,270). Sequence identity was determined using the CLC Genomic Workbench 8.5.4. A phylogenetic tree was generated (Algorithm = UPGMA, Distance measure = Jukes-Cantor, Bootstrap = 100 Replicates), and identity was calculated by summarizing the distance from *Homo sapiens*.

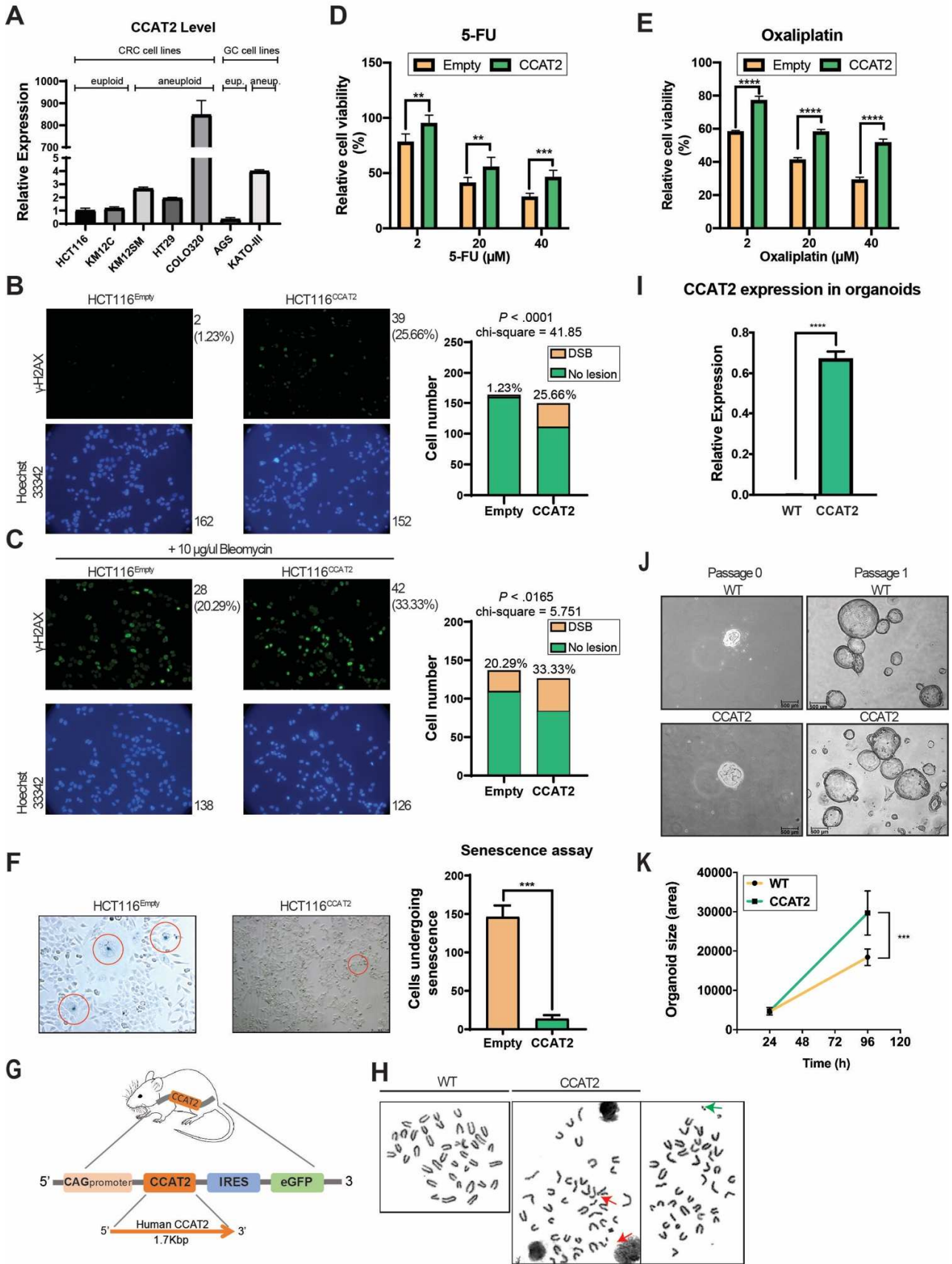
Statistical and survival analysis

Statistical analyses were carried out with GraphPad Prism 7 and SPSS software. To determine whether the data followed a normal Gaussian distribution, the Shapiro-Wilk normality test was performed. P values were determined with a paired/unpaired t-test (normal distribution) or the Wilcoxon matched-pairs signed rank test for paired non-normal distribution data and the Mann-Whitney-Wilcoxon for un-paired data (non-normal distribution). Linear correlation between gene

expressions was performed using Pearson correlation coefficient (normal distribution) or nonparametric Spearman correlation (non-normal distribution). All tests were two-sided, and P values < 0.05 were considered statistically significant.

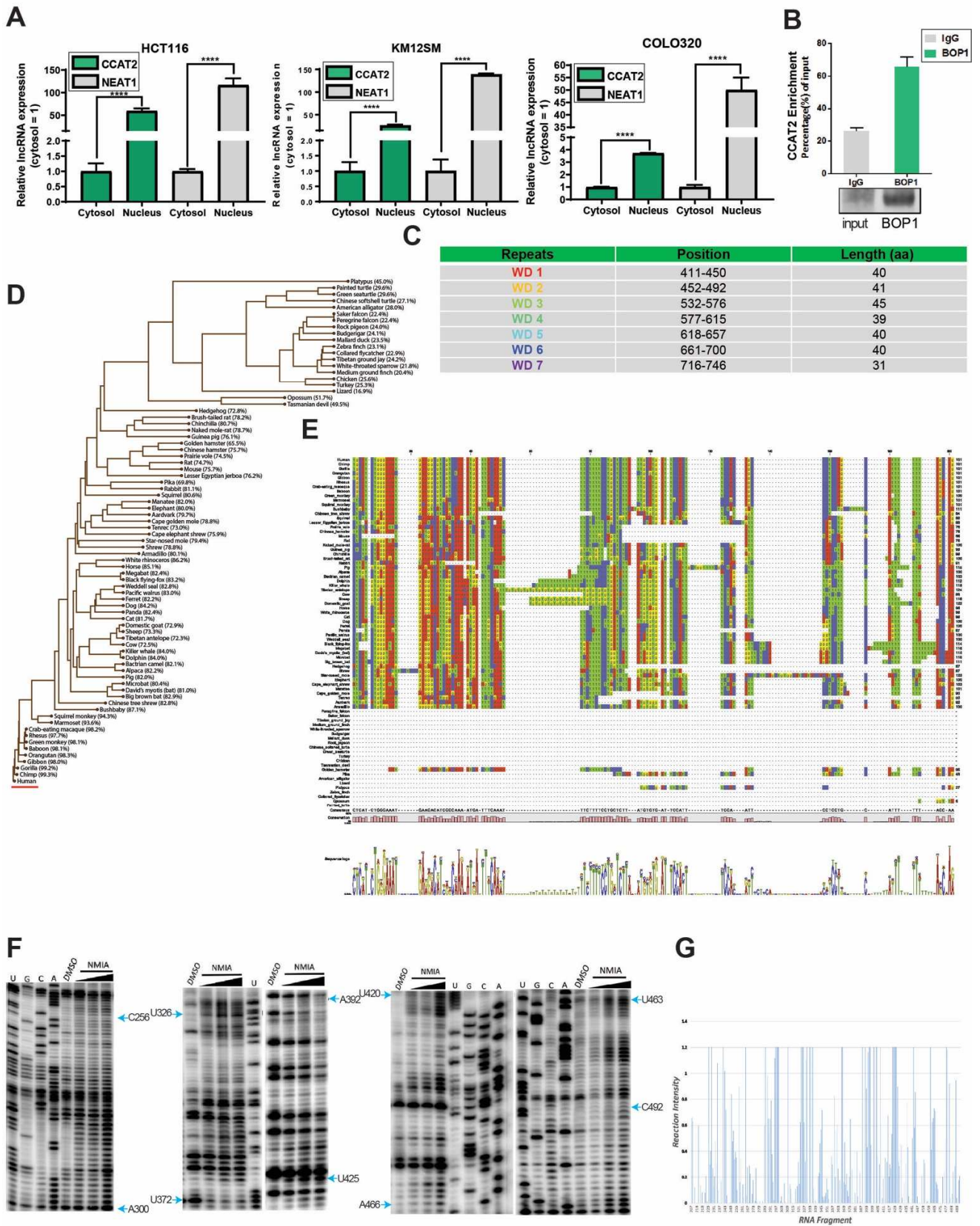
The Kaplan-Meier method was used to plot and evaluate patients' prognostic outcome. Receiver operating characteristic (ROC) curves with Youden's Index for overall survival/recurrence free survival were established to determine optimal cut-off values for *CCAT2*, *BOP1*, *PES1* and *WDR12*. The log-rank test was performed for statistical univariate analysis of prognostic variables. In multivariate analyses, a Cox proportional hazard model was used to identify parameters with a statistically significant influence on survival.

Supplementary Figure 1



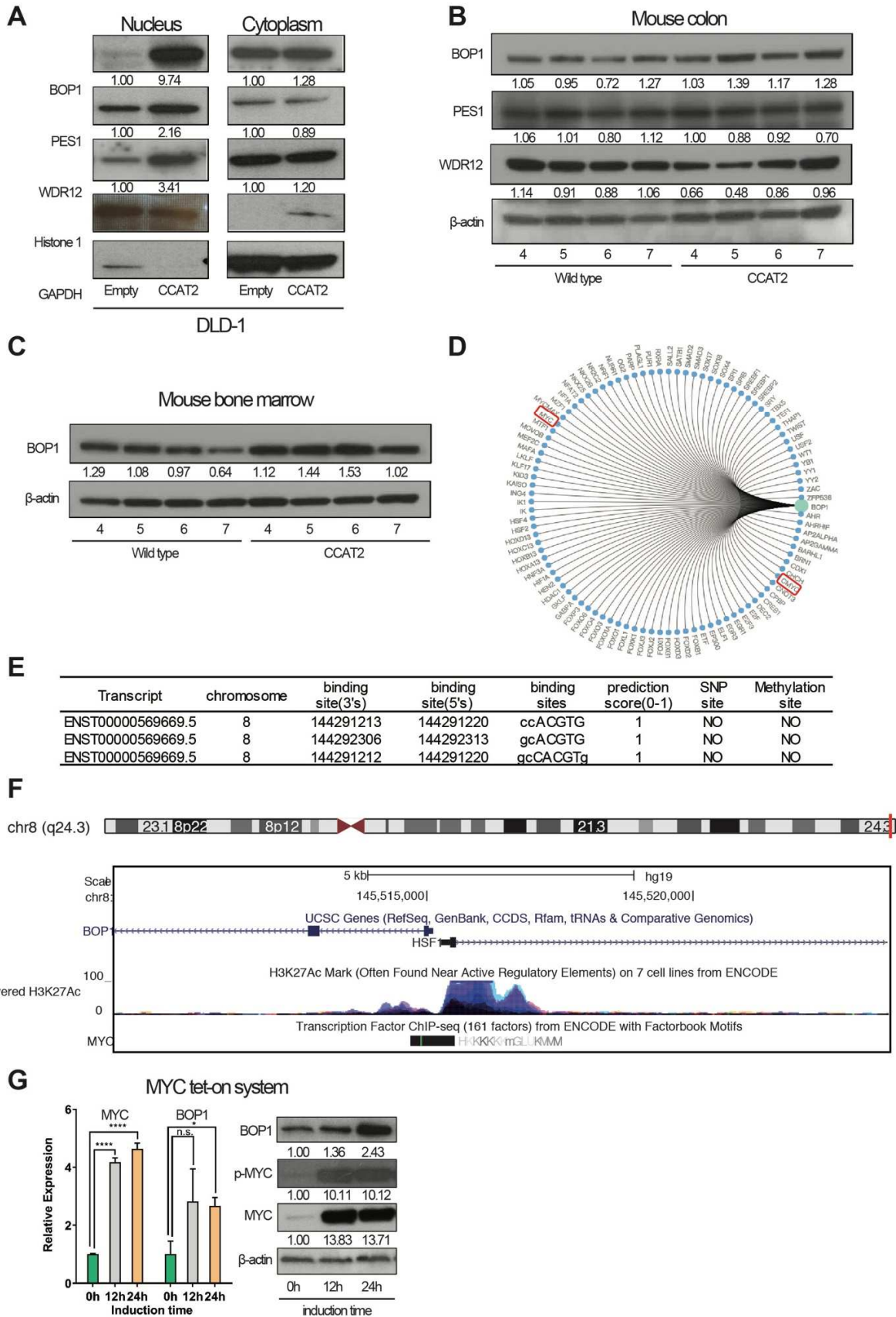
Supplementary Figure 1. Related to Figure 1. **A.** *CCAT2* expression in colorectal cancer (CRC) and gastric cancer (GC) cell lines used in the present study. **B.** Images of the γ -H2AX assay for double strand breaks (DSB) without Bleomycin treatment in HCT116^{Empty} and HCT116^{CCAT2}. **C.** Images of the γ -H2AX assay for DSB after 2 hours of exposure to 10 μ g/ml of Bleomycin in HCT116^{Empty} and HCT116^{CCAT2}. **D.** Effect of 5-Fluorouracil (5-FU) on cell proliferation of HCT116^{Empty} and ^{CCAT2} clones. Cells were treated with three different concentrations of 5-FU (2, 20 and 40 μ M) and after 48 hours cell viability was determined using the MTT assay. **E.** Effect of oxaliplatin on cell proliferation of HCT116^{Empty} and ^{CCAT2} clones. Cells were treated with three different concentrations of oxaliplatin (2, 20 and 40 μ M) and after 48 hours cell viability was determined using the MTS assay. **F.** Representative images (in red circles) for senescence assay in HCT116^{Empty} and HCT116^{CCAT2} and the corresponding statistical analysis. **G.** Schematic representation of *CCAT2*-plasmid inserted into the mouse genome. **H.** Representative metaphase from the bone marrow of WT mice and *CCAT2* transgenic mouse model that developed myelodysplastic syndrome. Red arrows indicate chromosomal breaks and green arrows chromosomal fragments. **I.** *CCAT2* expression in colon organoids from WT and *CCAT2* transgenic mice. **J.** Representative inverted microscopy images of colon organoids of WT and *CCAT2* transgenic mouse model immediately after they were established and after 1 passage. **K.** Proliferation rate of colon organoids from WT and from *CCAT2* transgenic mice. Data are represented as mean values \pm SD. (***P* < .001), (*****P* < .0001). Student's t test.

Supplementary Figure 2



Supplementary Figure 2. Related to Figure 2. **A.** The nuclear and cytoplasmic localization of *CCAT2* and *NEAT1* (positive control) in HCT116, KM12SM and COLO320 cells as measured by qRT-PCR. **B.** RIP assays showing that BOP1 interacts with *CCAT2* in HCT116 cells. The qRT-PCR results of RIP assays are shown in the upper panel. Western-blot data, to check the immunoprecipitation efficiency, are shown in the lower panel. **C.** The positions and length of the seven WD repeats of BOP1. **D.** Evolutionary conservation of full length *CCAT2* (*Homo sapiens* is underlined in red). **E.** Conservation of the motif 3 of *CCAT2*. **F.** Representative gels for the SHAPE probing of *CCAT2* 330-430 fragment with different primers. Lanes from left to right were gels probed with primer 1, 2, 3, 4, 5. U, G, C, A sequencing reactions performed using dideoxy-terminating nucleotides. Control in DMSO; NMIA concentration gradient from 32.5 mmol to 130 mmol. **G.** Quantification of the SHAPE probing data gels for *CCAT2* 330-430 fragment. Band intensities visualized by gel electrophoresis were quantified using SAFA, version 1.1. (**** $P < .0001$). Student's t test.

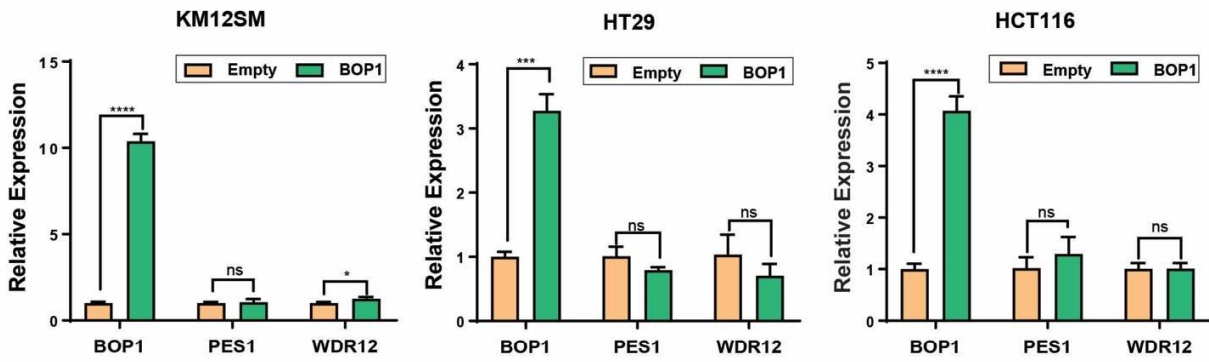
Supplementary Figure 3



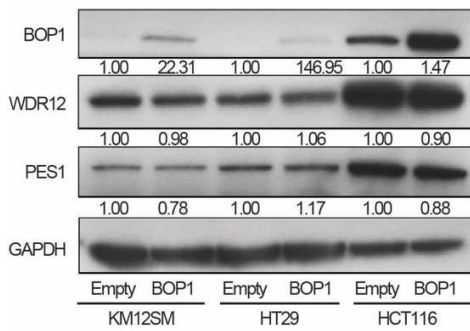
Supplementary Figure 3. Related to Figure 3. **A.** The nuclear and cytoplasmic localization of PES1, BOP1, and WDR12 (PeBoW) complex was determined by Western-blot of fractionated protein lysate from DLD-1^{Empty} and DLD-1^{CCAT2} cells. **B.** The protein expression of PeBoW complex components in the colon of CCAT2 transgenic mice (WT = 4, CCAT2 = 4). **C.** The protein expression of BOP1 in the bone marrow of CCAT2 transgenic mice (WT = 4, CCAT2 = 4). **D.** MYC is one of the predicted transcription factors of *BOP1* (from GCBI GENERADAR). **E.** Predicted binding sites of MYC around the genomic location of *BOP1*. **F.** CHIP-Seq data (UCSC Genome Browser on Human Feb. 2009 (GRCh37/hg19) Assembly) showing MYC (Cluster Score (out of 1000): 1000, Position: chr8:145514703-145515524, Band: 8q24.3, Genomic Size: 822) binding site in the genomic region around *BOP1*. **G.** The expression of BOP1, MYC and p-MYC at 0, 12 and 24 hours in HCT116 cells with an inducible c-MYC expression system. Data are represented as mean values \pm SD. (ns, not significant), (* $P < .05$), (**** $P < .0001$). Student's t test.

Supplementary Figure 4

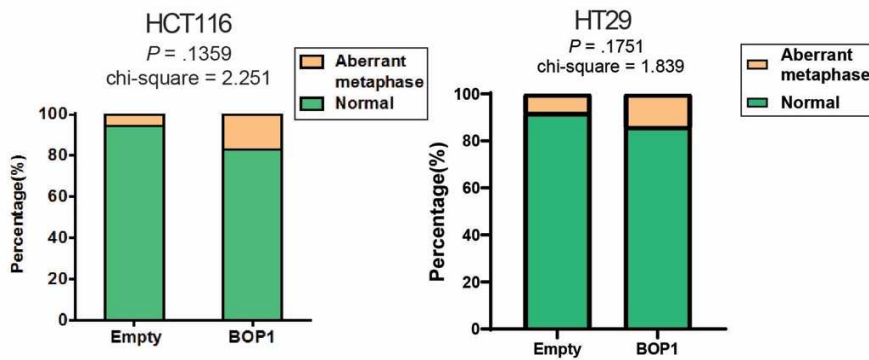
A



B



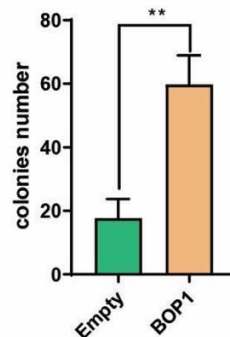
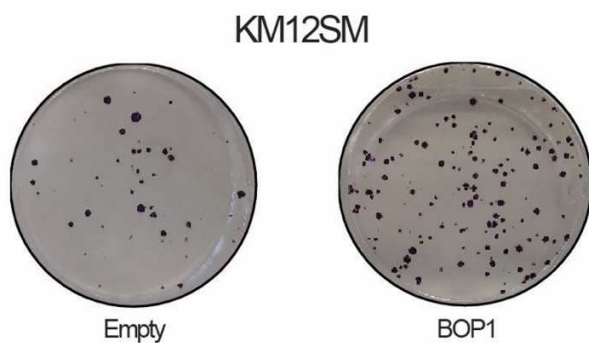
C



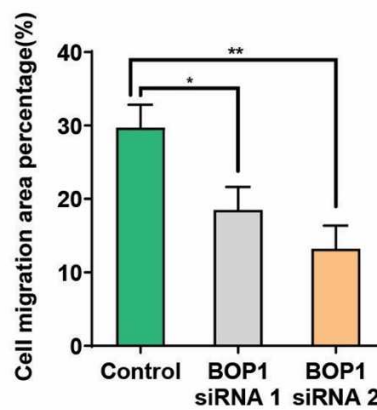
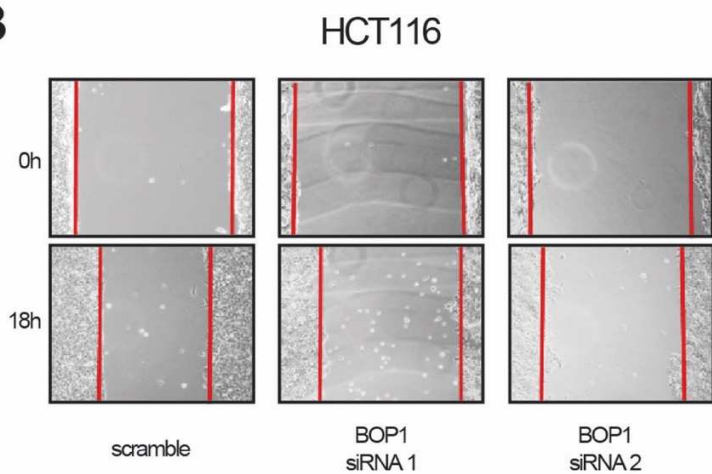
Supplementary Figure 4. Related to Figure 4. **A.** mRNA expression of PES1, BOP1, and WDR12 (PeBoW) complex members in KM12SM, HT29 and HCT116 Empty and BOP1 clones analyzed by qRT-PCR. **B.** Protein expression of PeBoW complex members in KM12SM, HT29 and HCT116 Empty and BOP1 clones analyzed by Western blot. **C.** Cytogenetic analysis showing that the frequency of cells exhibiting chromosome abnormalities (including chromosomal breaks, fusions and polyploidy) in HCT116 and HT29 Empty versus BOP1 clones after a short-term of passaging (5-10) has no significant difference. At least 35 interphase nuclei were analyzed for each clone. Data are represented as mean values \pm SD. (ns, not significant), ($*P < .05$), ($***P < .001$), ($****P < .0001$). Student's t test.

Supplementary Figure 5

A

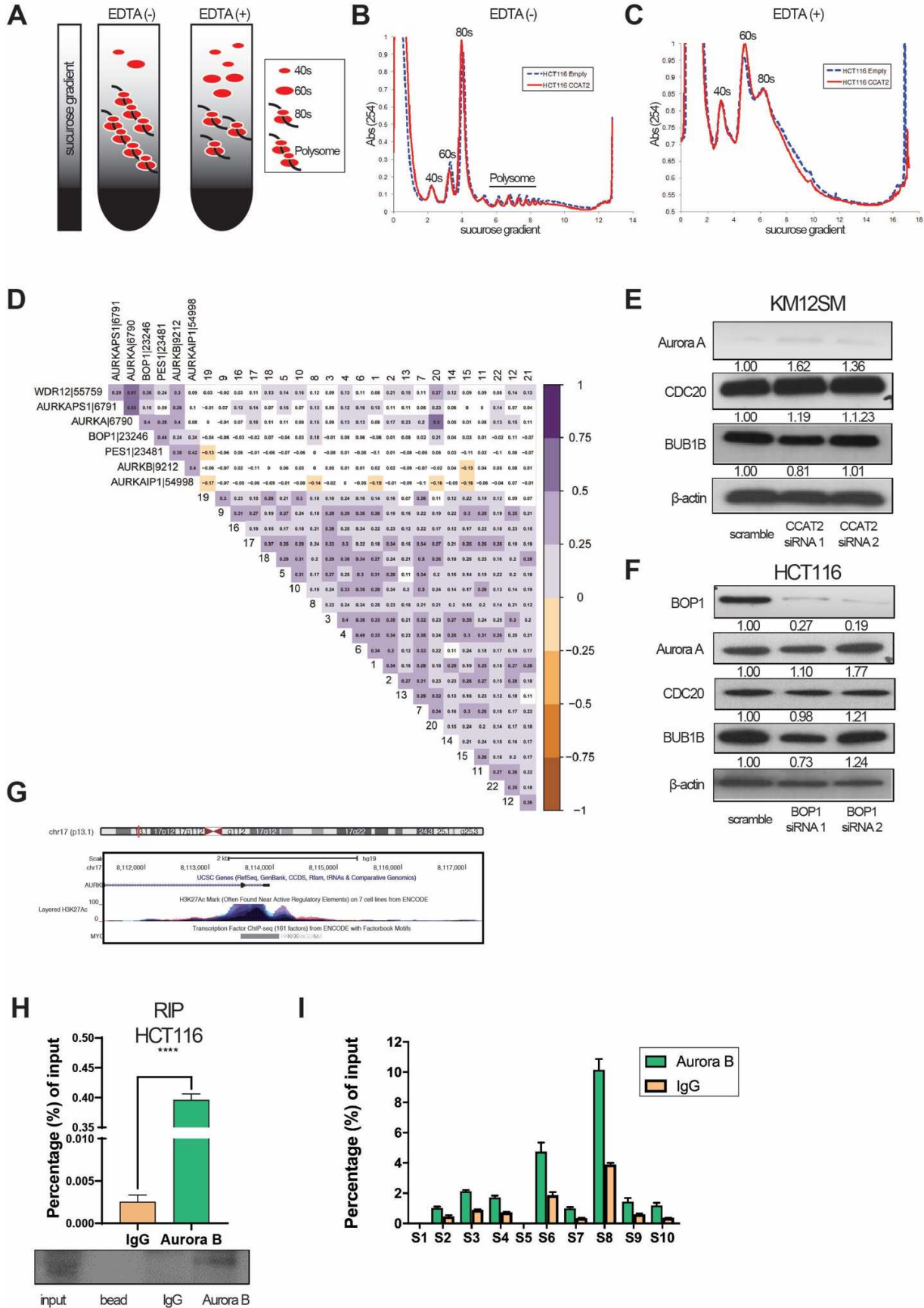


B



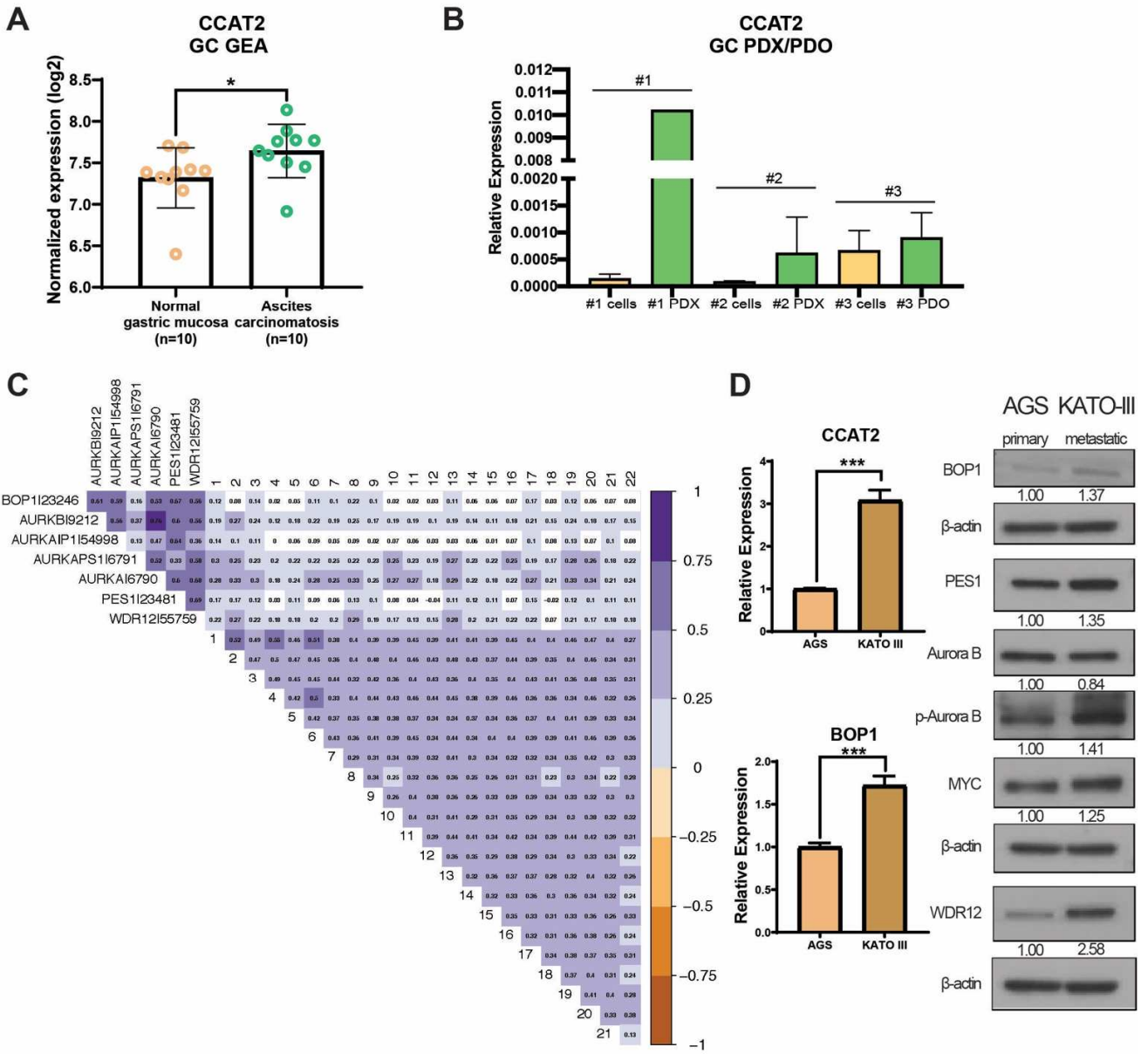
Supplementary Figure 5. Related to Figure 5. **A.** Up-regulation of *BOP1* increases the number of colonies in KM12SM^{BOP1} clones. **B.** Scratch assay showed that transient BOP1 knock-down inhibits the migration capacity of HCT116. Data are represented as mean values \pm SD. (* $P < .05$), (** $P < .01$). Student's t test.

Supplementary Figure 6



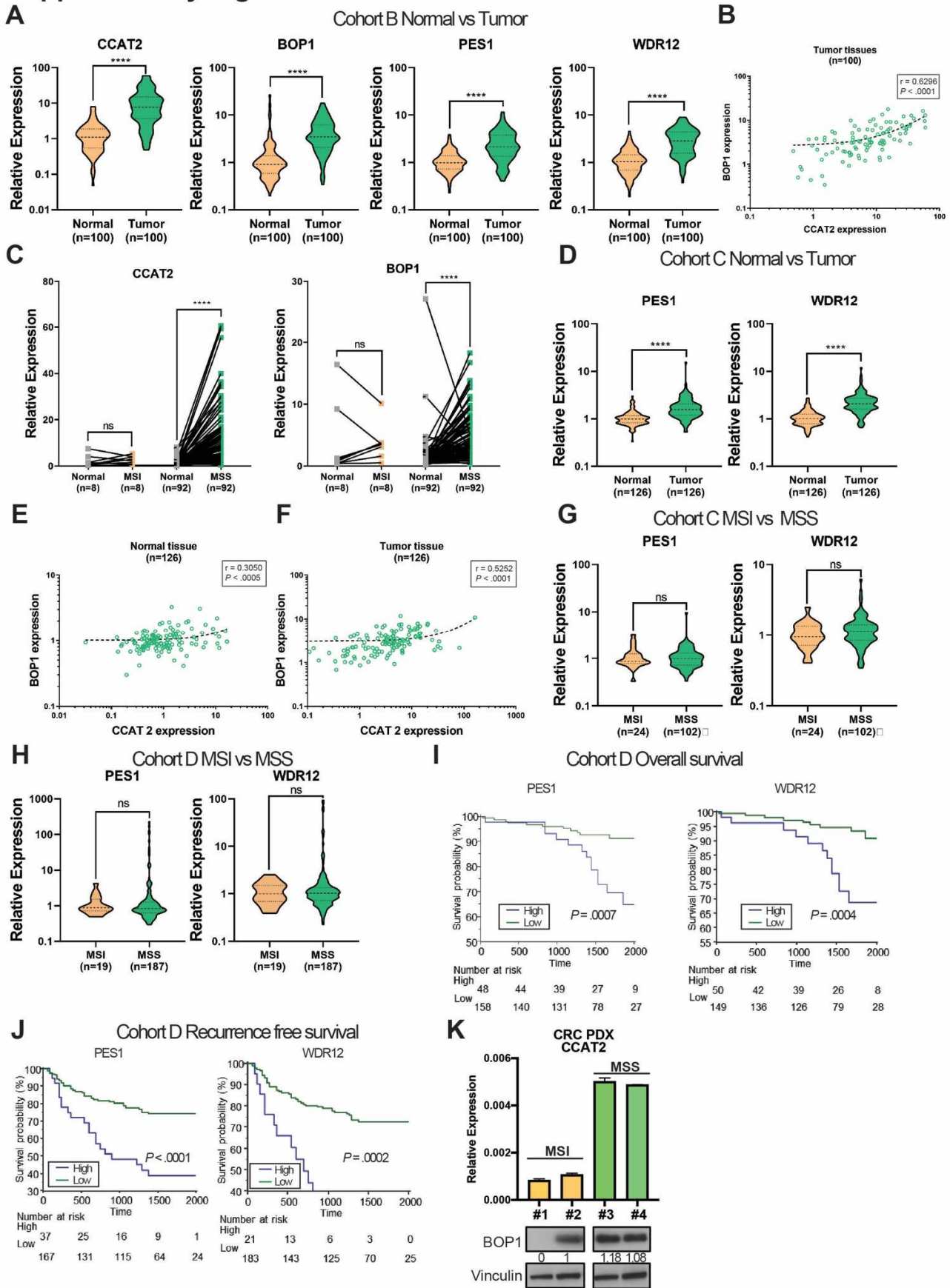
Supplementary Figure 6. Related to Figure 6. **A.** Schematic representation of Ribosome profiling analysis with or without EDTA. **B.** Ribosome profiling analysis without EDTA of HCT116^{Empty} and HCT116^{CCAT2} cells. **C.** Ribosome profiling analysis with EDTA of HCT116^{Empty} and HCT116^{CCAT2} cells. **D.** Correlation matrix between the Aurora family gene expression, PES1, BOP1, and WDR12 (PeBoW) complex components gene expression and index of CIN at whole chromosome level in the CRC cohort from TCGA database. **E.** The protein levels of key regulators of the chromosomal segregation mechanism (AURKA, CDC20, and BUB1B) were determined by Western blot in KM12SM cells after *CCAT2* knock-down. **F.** The protein levels of key regulators of the chromosomal segregation mechanism (AURKA, CDC20, and BUB1B) were determined by Western blot in HCT116 cells after BOP1 knock-down. **G.** CHIP-Seq data (UCSC Genome Browser on Human Feb. 2009 (GRCh37/hg19) Assembly) showing MYC (Cluster Score (out of 1000): 595, Position: chr17:8113496-8114099, Band: 17p13.1, Genomic Size: 604) binding site in the 5' region of *AURKB*. **H.** RIP assay followed by qRT-PCR was performed to check the interaction of *CCAT2* with *AURKB*. HCT116 cell lysates were precipitated with *AURKB* antibodies and IgG was used as negative control, and were analyzed by Western blot. **I.** RNase I digestion followed by RIP assay, quantified by qRT-PCR to detect which *CCAT2* segment interacts with *AURKB*. (**** $P < .0001$). Student's t test.

Supplementary Figure 7



Supplementary Figure 7. Related to Figure 6. **A.** Log₂ normalized expression of *CCAT2* obtained from GEA comparing normal gastric mucosa with malignant ascites from GC patients. **B.** *CCAT2* expression in cells derived from GC patients and paired PDX/PDO **C.** Correlation matrix between the Aurora family gene expression, PES1, BOP1, and WDR12 (PeBoW) complex components gene expression and index of CIN at whole chromosome level in the GC cohort from TCGA database. **D.** The expression of *CCAT2*, PeBoW complex members, AURKB, pAURKB and MYC analyzed by qRT-PCR and Western blot in gastric cancer cell lines. AGS is a gastric cancer cell line derived from primary tumor and KATO III is derived from metastatic lymph nodes. Data are represented as mean values \pm SD. (* $P < .05$), (** $P < .001$), (*** $P < .0001$). Student's t test.

Supplementary Figure 8



Supplementary Figure 8. Related to Figure 7. **A.** RNA expression of *CCAT2*, *BOP1*, *PES1* and *WDR12* in 100 paired primary CRC tumor tissues and the adjacent non-tumor colon/rectum was analyzed by qRT-PCR (**Cohort B**). The expression of the RNA has been normalized to β -actin. Wilcoxon test for non-normal distributed paired samples was performed. **B** Spearman correlation between the expression of the lncRNA *CCAT2* and the mRNA *BOP1* in tumor tissues in **Cohort B**. **C.** *BOP1* and *CCAT2* expression in paired normal and MSI (MSI-H) or normal and MSS (MSS/MSI-L) CRC tissues. Wilcoxon test for non-normal distributed paired samples was performed. **D.** *PES1* and *WDR12* expression in adjacent normal and tumor tissues from **Cohort C**. Wilcoxon test for non-normal distributed paired samples was performed. **E.** Spearman correlation between the expression of the lncRNA *CCAT2* and the mRNA *BOP1* in normal tissues in **Cohort C**. **F.** Spearman correlation between the expression of the lncRNA *CCAT2* and the mRNA *BOP1* in tumor tissue in **Cohort C**. **G.** *PES1* and *WDR12* expression in MSI (MSI-H) and MSS (MSS/MSI-L) tumors of **Cohort C**. Mann-Whitney test for non-normal distributed un-paired samples was performed. **H.** *PES1* and *WDR12* expression in MSI (MSI-H) and MSS (MSS/MSI-L) tumors of **Cohort D**. Mann-Whitney test for non-normal distributed un-paired samples was performed. **I.** Kaplan–Meier overall survival curves and **J.** recurrence free survival curves of CRC patients from the **Cohort D**, expressing high (blue) or low (green) levels of *PES1* and *WDR12*. Time is expressed in months. **K.** The expression of the lncRNA *CCAT2* and the protein expression of BOP1 in two MSI PDX (#1 and #2) and two MSS PDX (#3 and #4). Data are represented as violin plots. (ns, not significant), (**** $P < .0001$). Student's t test and Mann–Whitney–Wilcoxon test.

Supplementary Table 1. Clinical and pathological characteristics of the **Cohort A** (TCGA CRC cohort).

Variable		n
Gender	male	280
	female	257
Age	median (range)	66 (31-90)
Tumor location	right side colon	184
	left side colon	192
	rectum	49
UICC Stage	I	92
	II	201
	III	154
	IV	73
MSI/MSS status	MSS	150
	MSI-L	39
	MSI-H	29
	missing	319

Supplementary Table 2. Clinical and pathological characteristics of **Cohort B**.

Variable		n
Gender	male	66
	female	34
Age	median (range)	64 (33-85)
Tumor location	right side colon	22
	left side colon	29
	rectum	49
Differentiation grade	well	56
	moderate	36
	poor	3
	others	5
T stage	T1	17
	T2	12
	T3	63
	T4	8
Lymph node metastasis	negative	48
	positive	52
Distant metastasis	M0	91
	M1	9
UICC Stage	I-II	45
	III	46
	IV	9
Lymphatic invasion	negative	65
	positive	35
Venous invasion	negative	65
	positive	35
MSI/MSS status	MSS	82
	MSI-L	10
	MSI-H	8

Supplementary Table 3. Clinical and pathological characteristics of **Cohort C**.

Variable		n
Gender	male	76
	female	50
Age	median (range)	64 (30-84)
Tumor location	proximal	47
	distal	79
Differentiation grade	well (G1)	32
	moderate (G2)	68
	poor (G3)	19
	other (missing, G4, multiple grades)	7
T stage	T1	1
	T2	22
	T3	95
	T4	8
Lymph node metastasis	negative	69
	positive	57
Distant metastasis	M0	91
	M1	35
UICC Stage	I	17
	II	42
	III	32
	IV	35
MSI/MSS status	MSI	24
	MSS	102

Supplementary Table 4. Clinical and pathological characteristics of **Cohort D**.

Variable		n
Gender	male	120
	female	86
Age at operation	median (range)	70 (33-93)
Tumor location	right side colon	47
	left side colon	79
	rectum	80
Tumor size (mm)	median (range)	45 (10-140)
Histological type	intestinal	184
	diffuse	22
T stage	T2	9
	T3	141
	T4	56
Lymph node metastasis	negative	111
	positive	95
UICC Stage	II	111
	III	95
Lymphatic invasion	negative	92
	positive	114
Venous invasion	negative	21
	positive	185
MSI/MSS status	MSI	19
	MSS	187

Supplementary Table 5. Primers and siRNAs used in this study.

Gene	Sequence	Description
CCAT2 F1 (human)	5' GGGCACTAGACTGGGAATTAG 3'	PCR Primer
CCAT2 R1 (human)	5' AGGGAGCTGAGATAGGAAGAG 3'	PCR Primer
BOP1 F2 (human)	5' GCCACAAGATGCACGTACCT 3'	PCR Primer
BOP1 R2 (human)	5' TTCCTGGATGAAGCGTCCGTA 3'	PCR Primer
PES1 F (human)	5' GGGCATTATCCCATGAACC 3'	PCR Primer
PES1 R (human)	5' CACCTTGTATTCACGGAACCTGT 3'	PCR Primer
WDR12 F (human)	5' CAGAGGAATGGATCTTGACTGGT 3'	PCR Primer
WDR12 R (human)	5' CAGTGTAGGGCTTTCACCTTGT 3'	PCR Primer
BOP1-del6-264 F (human)	5' GCGGGTTCGCGGATGGGCTGGATCC 3'	PCR Primer
BOP1-del6-264 R (human)	5' GGATCCAGCCATCCGCAACCCGCC 3'	PCR Primer
BOP1-delWD1 F (human)	5' CCTGGTCTACAGGGTTCCCGTGGGG 3'	PCR Primer
BOP1-delWD1 R (human)	5' CCCCACGGGAACCTGTAGACCAGG 3'	PCR Primer
BOP1-delWD2 F (human)	5' CGCTGTGTGAGGACTGTTGGCAGCACAGATCAG 3'	PCR Primer
BOP1-delWD2 R (human)	5' CTGATCTGTGCTGCCAACAGTCCTCACACAGCG 3'	PCR Primer
BOP1-delWD3 F (human)	5' CGGCTGCGCATCCGACCCACGGA 3'	PCR Primer
BOP1-delWD3 R (human)	5' TCCGTGGCTGCGGATGCGCAGCCG 3'	PCR Primer
BOP1-delWD4 F (human)	5' CAGAGTCCGTTCCGCCTGATGCCAACTGC 3'	PCR Primer
BOP1-delWD4 R (human)	5' GCAGTTGGGCATCAGGCGGAACGGACTCTG 3'	PCR Primer
BOP1-delWD5 F (human)	5' CTCACCAAGAAGCTGATGATGCTGAGACACCACAAG 3'	PCR Primer
BOP1-delWD5 R (human)	5' CTTGTGGTGTCTCAGCATCATCAGTCTTCTGGTGAG 3'	PCR Primer
BOP1-delWD6 F (human)	5' ATACAGGATGCTGAGAAAACCCCTTGCTGGTGC 3'	PCR Primer
BOP1-delWD6 R (human)	5' GCACCAGCAAGGGTTTCTCAGCATCCTGTAT 3'	PCR Primer
BOP1-del265-427 F (human)	5' GGTGCACGCCATCAAGCTGGTTTCAGGCTCTG 3'	PCR Primer
BOP1-del265-427 R (human)	5' CAGAGCCTGAAACCAGCTTGATGGCGTGCACC 3'	PCR Primer
CCAT2-EcoRI F (human)	5' CCGgaattcccagggtgatcaggtggact 3'	PCR Primer
CCAT2-SalI R (human)	5' CGGgtcgagctcttctgggctgatgttgc 3'	PCR Primer
CCAT2q-1 F (human)	5' TAATACGACTCACTATAGACCCAGCAAGTTTCTCAGGA 3'	PCR Primer
CCAT2q-1 R (human)	5' CATTTCAGCAATCAGGTCAA 3'	PCR Primer
CCAT2q-2 F (human)	5' TAATACGACTCACTATAGAGACCCAAGAGGGAGGTATCA 3'	PCR Primer
CCAT2q-2 R (human)	5' TGGCTCTTGACTTCCAGTCC 3'	PCR Primer
CCAT2q-3 F (human)	5' TAATACGACTCACTATAGAACTTTCCAGCCTCGTTCT	PCR Primer
CCAT2q-3 R (human)	5' GGCTGTGGAAGTGAATCAT	PCR Primer
CCAT2q-4 F (human)	5' TAATACGACTCACTATAGCTCCATAGAGCCTGCAGAGG	PCR Primer
CCAT2q-4 R (human)	5' ATTGGTCAGAGGTGGAGCTG 3'	PCR Primer

CCAT2q-5 F (human)	5' TAATACGACTCACTATAGCAGCAGATGAAAGGCACTGA 3'	PCR Primer
CCAT2q-5 R (human)	5' CTCCTCCCCACATAAAAT 3'	PCR Primer
CCAT2q-6 F (human)	5' TAATACGACTCACTATAGACCCAGCAAGTTTCTCAGGA 3'	PCR Primer
CCAT2q-6 R (human)	5' CACAGTTATTGCCTGGAGCA 3'	PCR Primer
CCAT2q-7 F (human)	5' TAATACGACTCACTATAGGGCATGCCCTACGTAAGTTC 3'	PCR Primer
CCAT2q-7 R (human)	5' TTTGGGGTAGGTCAGGAAT 3'	PCR Primer
CCAT2q-8 F (human)	5' TAATACGACTCACTATAGTGCATTGGTGAGCTGTGTTT 3'	PCR Primer
CCAT2q-8 R (human)	5' ATGGTGCTGCTGGTAGCTTT 3'	PCR Primer
CCAT2q-9 F (human)	5' TAATACGACTCACTATAGGCCATAATCATCCCTGAGGA 3'	PCR Primer
CCAT2q-9 R (human)	5' CACCCAGAGAGATGACACC 3'	PCR Primer
CCAT2q-10 F (human)	5' TAATACGACTCACTATAGTTGTTGGGGTTTGATCCTTT 3'	PCR Primer
CCAT2q-10 R (human)	5' CAAGCACTTGAGCACACAT 3'	PCR Primer
Aurora B F (human)	5' ACAGACGGCTCCATCTGGCCT 3'	PCR Primer
Aurora B R (human)	5' GGCAGCTGTGGGCTGGACATT 3'	PCR Primer
c-MYC F (humane)	5' GGCTCCTGGCAAAGGTCA 3'	PCR Primer
c-MYC R (humane)	5' CTGCGTAGTTGTGCTGATGT 3'	PCR Primer
β -actin F (human)	5' CATGTACGTTGCTATCCAGGC 3'	PCR Primer
β -actin R (human)	5' CTCCTTAATGTCAGCAGCAT 3'	PCR Primer
U6 F (human)	5' CTCGCTTCGGCAGCACA 3'	PCR Primer
U6 R (human)	5' AACGCTTCAGGAATTTGCGT 3'	PCR Primer
GAPDH F (human)	5' CTGGGCTACACTGAGCACC 3'	PCR Primer
GAPDH R (human)	5' AAGTGGTCGTTGAGGGCAATG 3'	PCR Primer
BOP1 F (mouse)	5' CAGCTCTGATGAGGAGGACATTCGGAAC 3'	PCR Primer
BOP1 R (mouse)	5' CAACCTGCTCATCAGTTAGCCG 3'	PCR Primer
mACTB F (mouse)	5' CCTGTGCTGCTCACCGAGGC 3'	PCR Primer
mACTB R (mouse)	5' GACCCGCTCTCCGGAGTCCATC 3'	PCR Primer
HPRT1 F (mouse)	5' ACATTGTGGCCCTCTGTGTG 3'	PCR Primer
HPRT1 R (mouse)	5' TTATGTCCCCGTTGACTGA 3'	PCR Primer
siRNA	Target Sequence/Producer ID	
CCAT2 siRNA 1	5' AGGTGTAGCCAGAGTTAAT 3'	siRNA target sequence
CCAT2 siRNA 2	5' AGGAAGAGGTTAAGCAATT 3'	siRNA target sequence
BOP1 siRNA 1	s198254	Producer ID
BOP1 siRNA 2	s198255	Producer ID

Supplementary Table 6. Antibodies used in this study.

Antibodies	Product information
BOP1 (rabbit)	Abcam (ab86982)
BOP1 (mouse)	Santa Cruz (SC-390672)
BOP1 (IP)	Abcam (ab86652)
WDR12	Abcam (ab95070)
PES1	Abcam(ab88543)
PES1 (IP)	Santa Cruz (SC-166300)
MYC	Millipore (06-340)
pSer62 cMyc	Cell Signaling Technologies 13748
Aurora Kinase B (rabbit)	Cell Signaling Technologies 3094
Aurora Kinase B (mouse)	Santa Cruz (SC-65987)
P Thr232 Aurora Kinase B	Invitrogen PA5-38557
γ -tubulin	Cell Signaling Technologies 3873T
β -actin	Cell Signaling Technologies 3700T
GAPDH	Santa Cruz (SC51905)
Histone H1	Santa Cruz (SC34464)

Supplementary Table 7. Cell lines used in this study (colon cancer and gastric cancer cell lines).

Cell line	CCAT2 expression*	CIN	Modal chromosome no.	TP53	References
HCT116	Low	-	45/46	WT	25, 26
KM12C	Low	-	45	H179R	1, 27, 28
KM12SM	High	+	75-82	H179R	1, 27, 28
COLO320	Very high	+	51	R248W	29
HT29	High	+	70 (3n)	R273H	25, 30
AGS	Low	-	49	WT	31-33
KATO-III	High	+	tetraploid range	Genomic deletion	31, 34, 35

CIN: chromosomal instability. * - see Supplementary Figure 1A for data.

Supplementary Table 8. List of proteins identified by mass spectrometry to specifically bind to *CCAT2* after MS2 pull-down assay *

Accession	Gene	Subcellular location	# interaction hits by Mass Spec
B4DX30	ACSL5	Nucleus, Mitochondria	2
E9PRN9	BOP1	Nucleus, Nucleoli	1
B4DDM6	BUB3	Nucleoplasm	1
H3BTZ5	CNN2	Nucleoplasm, Actin filaments, Cytosol	1
B4DLW8	DDX5	Nucleoplasm	4
Q13347	EIF3I	Nucleoplasm, Cytosol	2
H7BY36	EWSR1	Nucleus, Nucleoli	2
Q8IW50-7	FAM219A	Nucleoplasm, Golgi apparatus, Vesicles	1
B4DY13	GTPBP4	Nucleoli	2
O94992	HEXIM1	Nucleoplasm, Vesicles	1
O60814	HIST1H2BK	Nucleoplasm, Cytosol	10
Q5T7C4	HMGB1	Nucleus	1
H7C1J8	HNRNPA3	Nucleoplasm	1
P25205	MCM3	Nucleoplasm	6
Q15233-2	NONO	Nucleoplasm	2
H0Y653	NOP56	Nucleoli fibrillar center	1
G3V1R4	NSUN2	Nucleus	3
K7ELW0	PARK7	Nucleus, Cytosol	2
E7ETC2	PPP3CA	Nucleoplasm, Cytosol	2
H0YMZ1	PSMA4	Nucleus, Vesicles, Cytosol	2
P28074	PSMB5	Nucleus, Centrosome	2
Q06124-2	PTPN11	Nucleus, Nucleoli, Actin filaments, Cytosol	1
K7EIJ4	RANBP3	Nucleoplasm	1
B4DWG0	RCBTB2	Nucleus, Golgi apparatus	1
I3L4R8	RPA1	Nucleoplasm	1
P40429	RPL13A	Nucleoli, Cytosol	1
F8VUA6	RPL18	Nucleoli, Endoplasmic reticulum, Cytosol	2
E9PKZ0	RPL8	Nucleoli, Endoplasmic reticulum, Cytosol	2
G3XAA9	RPS6KA4	Nucleus, Cytosol	1
K7EPT6	TAF15	Nucleoplasm	2
G3V448	TMX1	Nucleoli, Endoplasmic reticulum	1
Q13263	TRIM28	Nucleoplasm	10
J3KT19	USP10	Nucleoplasm, Cytosol	1
B1AHC7	XRCC6	Nucleoplasm	7
P27348	YWHAQ	Nucleoplasm, Cytosol	4
C9JN71	ZNF878	Nucleus, Nucleoli	3

* - MS2 Empty Pull down in all the instances gave 0 hits.

Supplementary Table 9. CINdex analysis at the chromosome level of the CRC TCGA cohort and correlation between the genes of the Aurora family, PeBoW complex and CIN at chromosomal level.

Chr. number	Gene	Correlation Test - T statistic	P-value	Correlation coefficient	Confidence interval 1	Confidence interval 2
20	AURKA	9.7	3.20E-19	0.501	0.41	0.58
20	WDR12	4.6	6.50E-06	0.266	0.15	0.37
13	AURKA	4.0	7.97E-05	0.234	0.12	0.34
20	AURKAPS1	4.0	8.80E-05	0.232	0.12	0.34
2	WDR12	3.6	0.0003271	0.213	0.10	0.32
20	BOP1	3.5	0.0005195	0.206	0.09	0.32
20	AURKC	-3.4	0.0007570	-0.200	-0.31	-0.08
7	AURKA	3.3	0.0009951	0.196	0.08	0.31
8	BOP1	3.1	0.0019504	0.184	0.07	0.30
7	AURKC	-3.1	0.0019925	-0.184	-0.29	-0.07
19	AURKAIP1	-2.9	0.0045704	-0.169	-0.28	-0.05
2	AURKA	2.8	0.0052080	0.167	0.05	0.28
17	AURKA	2.8	0.0060698	0.164	0.05	0.28
13	AURKC	-2.7	0.0067611	-0.162	-0.27	-0.05
20	AURKAIP1	-2.7	0.0069726	-0.161	-0.27	-0.04
10	WDR12	2.7	0.0070027	0.161	0.04	0.27
6	AURKAPS1	2.7	0.0078359	0.159	0.04	0.27
15	AURKAIP1	-2.7	0.0081522	-0.158	-0.27	-0.04
13	WDR12	2.5	0.0127088	0.149	0.03	0.26
8	AURKA	2.5	0.0129917	0.148	0.03	0.26
12	AURKA	2.5	0.0133298	0.148	0.03	0.26
1	AURKAIP1	-2.5	0.0137918	-0.147	-0.26	-0.03
5	AURKAPS1	2.5	0.0138759	0.147	0.03	0.26
8	AURKAIP1	-2.4	0.0160611	-0.144	-0.26	-0.03
5	WDR12	2.4	0.0164290	0.143	0.03	0.26
12	AURKC	-2.4	0.0174374	-0.142	-0.25	-0.03
17	AURKAPS1	2.4	0.0187027	0.140	0.02	0.25
22	AURKAPS1	2.3	0.0202989	0.139	0.02	0.25
12	WDR12	2.3	0.0223718	0.136	0.02	0.25
15	AURKC	-2.3	0.0241227	-0.135	-0.25	-0.02
8	AURKAPS1	2.3	0.0244076	0.134	0.02	0.25
6	AURKA	2.2	0.0252607	0.134	0.02	0.25
19	PES1	-2.2	0.0258461	-0.133	-0.25	-0.02
15	AURKB	-2.2	0.0261202	-0.133	-0.25	-0.02
4	AURKA	2.2	0.0261782	0.133	0.02	0.25
1	AURKAPS1	2.2	0.0277008	0.132	0.01	0.25
18	WDR12	2.2	0.0278869	0.131	0.01	0.24
21	WDR12	2.2	0.0310365	0.129	0.01	0.24
22	AURKA	2.1	0.0337156	0.127	0.01	0.24
4	WDR12	2.1	0.0355162	0.126	0.01	0.24
14	WDR12	2.1	0.0378901	0.124	0.01	0.24
8	AURKC	-2.1	0.0379421	-0.124	-0.24	-0.01
16	AURKAPS1	2.0	0.0417412	0.122	0.00	0.24
4	AURKAPS1	2.0	0.0429808	0.121	0.00	0.23

AURKA, aurora kinase A; AURKAIP1, aurora kinase A interacting protein 1; AURKAPS1, aurora kinase A pseudogene 1; AURKB, aurora kinase B, BOP1, BOP1 ribosomal biogenesis factor; PES1 pescadillo ribosomal biogenesis factor 1; WDR12, WD repeat domain 12.

Supplementary Table 10. CINdex analysis at the chromosome level of the GC TCGA cohort and correlation between the genes of the Aurora family, PeBoW complex and CIN at chromosomal level.

Chr. number	Gene	Correlation Test - T statistic	P value	Correlation coefficient	Confidence Interval 1	Confidence Interval 2
20	AURKA	7.39	8.05E-13	0.34	0.25	0.43
8	AURKA	7.14	4.33E-12	0.33	0.24	0.42
19	AURKA	7.01	9.73E-12	0.33	0.24	0.41
2	AURKA	6.98	1.18E-11	0.33	0.24	0.41
1	AURKAPS1	6.41	3.91E-10	0.30	0.21	0.39
3	AURKA	6.34	6.23E-10	0.30	0.21	0.38
8	WDR12	6.09	2.64E-09	0.29	0.20	0.37
13	AURKA	6.08	2.83E-09	0.29	0.20	0.37
1	AURKA	5.95	5.70E-09	0.28	0.19	0.37
6	AURKA	5.91	7.11E-09	0.28	0.19	0.37
19	AURKAPS1	5.88	8.39E-09	0.28	0.19	0.37
13	WDR12	5.81	1.24E-08	0.28	0.18	0.36
17	AURKA	5.71	2.20E-08	0.27	0.18	0.36
13	AURKAPS1	5.68	2.54E-08	0.27	0.18	0.36
10	AURKA	5.67	2.74E-08	0.27	0.18	0.36
2	WDR12	5.65	3.01E-08	0.27	0.18	0.36
2	AURKB	5.58	4.27E-08	0.27	0.17	0.35
11	AURKA	5.58	4.31E-08	0.27	0.17	0.35
20	AURKAPS1	5.45	8.49E-08	0.26	0.17	0.35
16	AURKAPS1	5.32	1.74E-07	0.25	0.16	0.34
7	AURKA	5.27	2.24E-07	0.25	0.16	0.34
10	AURKAPS1	5.26	2.33E-07	0.25	0.16	0.34
2	AURKAPS1	5.25	2.39E-07	0.25	0.16	0.34
7	AURKAPS1	5.22	2.88E-07	0.25	0.16	0.34
8	AURKB	5.20	3.21E-07	0.25	0.16	0.34
9	AURKA	5.14	4.32E-07	0.25	0.15	0.33
22	AURKA	5.10	5.16E-07	0.24	0.15	0.33
3	AURKB	5.08	5.83E-07	0.24	0.15	0.33
19	AURKB	5.00	8.52E-07	0.24	0.15	0.33
5	AURKA	4.99	8.99E-07	0.24	0.15	0.33
14	AURKAPS1	4.89	1.45E-06	0.23	0.14	0.32
9	AURKAPS1	4.85	1.74E-06	0.23	0.14	0.32
3	AURKAPS1	4.83	1.97E-06	0.23	0.14	0.32
11	AURKAPS1	4.76	2.69E-06	0.23	0.14	0.32
3	WDR12	4.67	4.05E-06	0.22	0.13	0.31
5	AURKAPS1	4.61	5.49E-06	0.22	0.13	0.31
1	WDR12	4.60	5.67E-06	0.22	0.13	0.31
16	AURKA	4.60	5.71E-06	0.22	0.13	0.31
6	AURKB	4.59	6.00E-06	0.22	0.13	0.31
15	AURKAPS1	4.58	6.22E-06	0.22	0.13	0.31
8	AURKAPS1	4.55	7.06E-06	0.22	0.13	0.31
14	AURKA	4.55	7.08E-06	0.22	0.13	0.31
8	BOP1	4.52	8.02E-06	0.22	0.12	0.31
16	WDR12	4.50	8.93E-06	0.22	0.12	0.31
22	AURKAPS1	4.50	8.99E-06	0.22	0.12	0.31
6	AURKAPS1	4.48	9.86E-06	0.22	0.12	0.31
17	WDR12	4.47	1.00E-05	0.22	0.12	0.31
21	AURKA	4.44	1.18E-05	0.21	0.12	0.30
18	AURKA	4.34	1.81E-05	0.21	0.12	0.30
15	WDR12	4.28	2.33E-05	0.21	0.11	0.30
17	AURKB	4.27	2.40E-05	0.21	0.11	0.30
19	WDR12	4.25	2.64E-05	0.21	0.11	0.30
4	AURKAPS1	4.19	3.42E-05	0.20	0.11	0.29
6	WDR12	4.13	4.45E-05	0.20	0.11	0.29
14	WDR12	4.12	4.58E-05	0.20	0.10	0.29
7	WDR12	4.06	0.0001	0.20	0.10	0.29

13	AURKB	3.98	0.0001	0.19	0.10	0.28
7	AURKB	3.95	0.0001	0.19	0.10	0.28
11	AURKB	3.89	0.0001	0.19	0.09	0.28
1	AURKB	3.88	0.0001	0.19	0.09	0.28
12	AURKAPS1	3.87	0.0001	0.19	0.09	0.28
9	WDR12	3.87	0.0001	0.19	0.09	0.28
17	AURKAPS1	3.85	0.0001	0.19	0.09	0.28
10	AURKB	3.84	0.0001	0.19	0.09	0.28
21	AURKAPS1	3.79	0.0002	0.18	0.09	0.28
4	AURKA	3.78	0.0002	0.18	0.09	0.28
22	WDR12	3.77	0.0002	0.18	0.09	0.27
5	WDR12	3.73	0.0002	0.18	0.09	0.27
21	WDR12	3.69	0.0002	0.18	0.08	0.27
15	AURKA	3.68	0.0003	0.18	0.08	0.27
16	AURKB	3.64	0.0003	0.18	0.08	0.27
20	AURKB	3.64	0.0003	0.18	0.08	0.27
12	AURKA	3.64	0.0003	0.18	0.08	0.27
4	WDR12	3.63	0.0003	0.18	0.08	0.27
5	AURKB	3.62	0.0003	0.18	0.08	0.27
18	AURKAPS1	3.60	0.0004	0.17	0.08	0.27
20	WDR12	3.58	0.0004	0.17	0.08	0.27
21	AURKB	3.58	0.0004	0.17	0.08	0.27
9	AURKB	3.56	0.0004	0.17	0.08	0.27
17	BOP1	3.50	0.0005	0.17	0.07	0.26
2	PES1	3.49	0.0005	0.17	0.07	0.26
10	WDR12	3.43	0.0007	0.17	0.07	0.26
1	PES1	3.40	0.0008	0.17	0.07	0.26
22	AURKB	3.16	0.0017	0.15	0.06	0.25
12	WDR12	3.15	0.0018	0.15	0.06	0.25
18	AURKB	3.03	0.0026	0.15	0.05	0.24
17	PES1	2.99	0.0030	0.15	0.05	0.24
14	AURKB	2.86	0.0044	0.14	0.04	0.23
1	AURKAIP1	2.82	0.0050	0.14	0.04	0.23
3	BOP1	2.77	0.0058	0.14	0.04	0.23
11	WDR12	2.60	0.0097	0.13	0.03	0.22
8	PES1	2.59	0.0100	0.13	0.03	0.22
19	AURKAIP1	2.58	0.0101	0.13	0.03	0.22
1	BOP1	2.55	0.0112	0.12	0.03	0.22
4	AURKB	2.53	0.0119	0.12	0.03	0.22
19	BOP1	2.47	0.0138	0.12	0.02	0.22
14	PES1	2.47	0.0139	0.12	0.02	0.22
19	PES1	2.45	0.0149	0.12	0.02	0.21
3	PES1	2.44	0.0152	0.12	0.02	0.21
5	PES1	2.29	0.0225	0.11	0.02	0.21
22	PES1	2.27	0.0235	0.11	0.02	0.21
13	PES1	2.27	0.0236	0.11	0.02	0.21
15	PES1	2.25	0.0249	0.11	0.01	0.20
13	BOP1	2.25	0.0250	0.11	0.01	0.20
3	AURKAIP1	2.24	0.0254	0.11	0.01	0.20
6	BOP1	2.17	0.0307	0.11	0.01	0.20
15	AURKB	2.16	0.0314	0.11	0.01	0.20
21	PES1	2.15	0.0321	0.11	0.01	0.20
17	AURKAIP1	2.13	0.0336	0.10	0.01	0.20
9	PES1	2.13	0.0337	0.10	0.01	0.20
9	BOP1	2.11	0.0354	0.10	0.01	0.20
20	PES1	2.10	0.0364	0.10	0.01	0.20
12	AURKB	2.08	0.0379	0.10	0.01	0.20
2	AURKAIP1	2.07	0.0389	0.10	0.01	0.20
21	AURKAIP1	2.05	0.0409	0.10	0.00	0.20
7	BOP1	1.99	0.0473	0.10	0.00	0.19

Supplementary Table 11. Univariate analysis for overall survival and recurrence free survival using log-rank test for patients from **Cohort D**.**Overall Survival**

variable	Univariate analysis		
	HR	95%CI	P-value
Age \geq 70	3.1	1.39-7.59	0.005
Male	0.83	0.39-1.84	0.65
Tumor location rectum yes/no	1.83	0.85-4.03	0.12
Tumor size > 45 mm	1.04	0.48-2.28	0.91
Poorly differentiated histology	1.53	0.45-4.01	0.45
T Stage greater than T4	1.07	0.43-2.40	0.88
Lymph node metastasis positive	2.18	1.01-5.12	0.049
Lymphatic invasion positive	1.53	0.70-3.58	0.3
Venous invasion positive	0.67	0.26-2.30	0.49
UICC stage 3	2.18	0.99-5.12	0.051
MSI patients yes/no	1.28	0.30-3.69	0.69
CCAT2 high expression	6.1	2.79-13.31	<0.0001
BOP1 high expression	3.01	1.38-6.55	0.006
PES1 high expression	3.52	1.62-7.74	0.002
WDR12 high expression	3.15	1.44-6.86	0.004

Recurrence Free Survival

variable	Univariate analysis		
	HR	95%CI	P-value
Age \geq 70	1.14	0.68-1.89	0.62
Male	0.95	0.57-1.61	0.85
Tumor location rectum yes/no	2.63	1.58-4.47	0.0002
Tumor size > 45 mm	1.08	0.65-1.79	0.77
Poorly differentiated histology	1.05	0.44-2.16	0.9
T Stage greater than T4	1.54	0.89-2.59	0.12
Lymph node metastasis positive	1.88	1.13-3.18	0.02
Lymphatic invasion positive	1.38	0.83-2.36	0.22
Venous invasion positive	1.05	0.49-2.72	0.92
UICC stage 3	1.88	1.13-3.18	0.02
MSI patients yes/no	3.41	1.06-20.79	0.04
CCAT2 high expression	4.78	2.74-8.09	<0.0001
BOP1 high expression	2.77	1.65-4.60	0.0002
PES1 high expression	2.94	1.70-4.96	0.0002
WDR12 high expression	4.07	2.18-7.17	<0.0001

HR, Hazard Ratio; CI, Confidence Interval. Bold indicates a statistically significant result.

Supplementary Table 12. Multivariate analysis for overall survival and recurrence free survival in patients from **Cohort D** using Cox proportional hazard model.

CCAT2 and other clinical factors

Overall Survival

variable	Univariate analysis			Multivariate analysis		
	HR	95%CI	P-value	HR	95%CI	P-value
Age \geq 70	3.1	1.39-7.59	0.005	2.41	1.05-6.01	0.04
Lymph node metastasis positive	2.18	1.01-5.12	0.049	2.42	1.10-5.69	0.03
CCAT2 high expression	6.1	2.79-13.31	<0.0001	5.51	2.48-12.27	<0.0001

Recurrence Free Survival

variable	Univariate analysis			Multivariate analysis		
	HR	95%CI	P-value	HR	95%CI	P-value
Tumor location rectum yes/no	2.63	1.58-4.47	0.0002	2.37	1.41-4.08	0.001
Lymph node metastasis positive	1.88	1.13-3.18	0.02	2.03	1.21-3.45	0.007
UICC stage 3	1.88	1.13-3.18	0.02			
MSI patients yes/no	3.41	1.06-20.79	0.04	0.5	0.08-1.66	0.29
CCAT2 high expression	4.78	2.74-8.09	<0.0001	4.85	2.76-8.28	<0.0001

HR, Hazard Ratio; CI, Confidence Interval. Bold indicates a statistically significant result.

BOP1 and other clinical factors

Overall Survival

variable	Univariate analysis			Multivariate analysis		
	HR	95%CI	P-value	HR	95%CI	P-value
Age \geq 70	3.1	1.39-7.59	0.005	3.06	1.36-7.49	0.006
Lymph node metastasis positive	2.18	1.01-5.12	0.049	2.6	1.18-6.12	0.02
BOP1 high expression	3.01	1.38-6.55	0.006	3.12	1.42-6.84	0.005

Recurrence Free Survival

variable	Univariate analysis			Multivariate analysis		
	HR	95%CI	P-value	HR	95%CI	P-value
Tumor location rectum yes/no	2.63	1.58-4.47	0.0002	2.38	1.42-4.09	0.001
Lymph node metastasis positive	1.88	1.13-3.18	0.02	1.87	1.12-3.18	0.02
UICC stage 3	1.88	1.13-3.18	0.02			
MSI patients yes/no	3.41	1.06-20.79	0.04	0.52	0.08-1.73	0.32
BOP1 high expression	2.77	1.65-4.60	0.0002	2.67	1.59-4.45	0.0003

HR, Hazard Ratio; CI, Confidence Interval. Bold indicates a statistically significant result.

References

1. Morikawa K, Walker SM, Nakajima M, et al. Influence of organ environment on the growth, selection, and metastasis of human colon carcinoma cells in nude mice. *Cancer Res* 1988;48:6863-71.
2. Shah MY, Ferracin M, Pileczki V, et al. Cancer-associated rs6983267 SNP and its accompanying long noncoding RNA CCAT2 induce myeloid malignancies via unique SNP-specific RNA mutations. *Genome Res* 2018;28:432-447.
3. Lee SM, Kim N, Son HJ, et al. The Effect of Sex on the Azoxymethane/Dextran Sulfate Sodium-treated Mice Model of Colon Cancer. *J Cancer Prev* 2016;21:271-278.
4. Parang B, Barrett CW, Williams CS. AOM/DSS Model of Colitis-Associated Cancer. *Methods Mol Biol* 2016;1422:297-307.
5. Suzuki R, Kohno H, Sugie S, et al. Strain differences in the susceptibility to azoxymethane and dextran sodium sulfate-induced colon carcinogenesis in mice. *Carcinogenesis* 2006;27:162-9.
6. Gerling M, Glauben R, Habermann JK, et al. Characterization of chromosomal instability in murine colitis-associated colorectal cancer. *PLoS One* 2011;6:e22114.
7. Sato T, Vries RG, Snippert HJ, et al. Single Lgr5 stem cells build crypt-villus structures in vitro without a mesenchymal niche. *Nature* 2009;459:262-5.
8. Sato T, Stange DE, Ferrante M, et al. Long-term expansion of epithelial organoids from human colon, adenoma, adenocarcinoma, and Barrett's epithelium. *Gastroenterology* 2011;141:1762-72.
9. Miyoshi H, Stappenbeck TS. In vitro expansion and genetic modification of gastrointestinal stem cells in spheroid culture. *Nat Protoc* 2013;8:2471-82.
10. Song S, Wang Z, Li Y, et al. PPARdelta Interacts with the Hippo Coactivator YAP1 to Promote SOX9 Expression and Gastric Cancer Progression. *Mol Cancer Res* 2020;18:390-402.
11. Katsiampoura A, Raghav K, Jiang ZQ, et al. Modeling of Patient-Derived Xenografts in Colorectal Cancer. *Mol Cancer Ther* 2017;16:1435-1442.
12. Liu J, Lichtenberg T, Hoadley KA, et al. An Integrated TCGA Pan-Cancer Clinical Data Resource to Drive High-Quality Survival Outcome Analytics. *Cell* 2018;173:400-416 e11.
13. Cancer Genome Atlas N. Comprehensive molecular characterization of human colon and rectal cancer. *Nature* 2012;487:330-7.
14. Redis RS, Vela LE, Lu W, et al. Allele-Specific Reprogramming of Cancer Metabolism by the Long Non-coding RNA CCAT2. *Mol Cell* 2016;61:520-534.
15. Song L, Bhuvaneshwar K, Wang Y, et al. CINdex: A Bioconductor Package for Analysis of Chromosome Instability in DNA Copy Number Data. *Cancer Inform* 2017;16:1176935117746637.
16. Ling H, Spizzo R, Atlasi Y, et al. CCAT2, a novel noncoding RNA mapping to 8q24, underlies metastatic progression and chromosomal instability in colon cancer. *Genome Res* 2013;23:1446-61.
17. Gagnon KT, Li L, Janowski BA, et al. Analysis of nuclear RNA interference in human cells by subcellular fractionation and Argonaute loading. *Nat Protoc* 2014;9:2045-60.
18. Reuter JS, Mathews DH. RNAstructure: software for RNA secondary structure prediction and analysis. *BMC Bioinformatics* 2010;11:129.
19. Das R, Laederach A, Pearlman SM, et al. SAFA: semi-automated footprinting analysis software for high-throughput quantification of nucleic acid footprinting experiments. *RNA* 2005;11:344-54.
20. Deigan KE, Li TW, Mathews DH, et al. Accurate SHAPE-directed RNA structure determination. *Proc Natl Acad Sci U S A* 2009;106:97-102.
21. Zhou P. Determining protein half-lives. *Methods Mol Biol* 2004;284:67-77.
22. Pereboom TC, Bondt A, Pallaki P, et al. Translation of branched-chain aminotransferase-1 transcripts is impaired in cells haploinsufficient for ribosomal protein genes. *Experimental Hematology* 2014;42:394-403.
23. Reineke LC, Cheema SA, Dubrulle J, et al. Chronic starvation induces noncanonical pro-death stress granules. *J Cell Sci* 2018;131.
24. Dassi E. *Post-Transcriptional Gene Regulation*: New York: Springer Science and Business, 2016.

25. Ahmed D, Eide PW, Eilertsen IA, et al. Epigenetic and genetic features of 24 colon cancer cell lines. *Oncogenesis* 2013;2:e71.
26. Knutsen T, Padilla-Nash HM, Wangsa D, et al. Definitive molecular cytogenetic characterization of 15 colorectal cancer cell lines. *Genes Chromosomes Cancer* 2010;49:204-23.
27. Camps J, Morales C, Prat E, et al. Genetic evolution in colon cancer KM12 cells and metastatic derivatives. *Int J Cancer* 2004;110:869-74.
28. Leroy B, Girard L, Hollestelle A, et al. Analysis of TP53 mutation status in human cancer cell lines: a reassessment. *Hum Mutat* 2014;35:756-65.
29. Quinn LA, Moore GE, Morgan RT, et al. Cell lines from human colon carcinoma with unusual cell products, double minutes, and homogeneously staining regions. *Cancer Res* 1979;39:4914-24.
30. Chen TR, Drabkowski D, Hay RJ, et al. WiDr is a derivative of another colon adenocarcinoma cell line, HT-29. *Cancer Genet Cytogenet* 1987;27:125-34.
31. Yao Y, Tao H, Kim JJ, et al. Alterations of DNA mismatch repair proteins and microsatellite instability levels in gastric cancer cell lines. *Lab Invest* 2004;84:915-22.
32. Barranco SC, Townsend CM, Jr., Casartelli C, et al. Establishment and characterization of an in vitro model system for human adenocarcinoma of the stomach. *Cancer Res* 1983;43:1703-9.
33. Cheng LL, Itahana Y, Lei ZD, et al. TP53 genomic status regulates sensitivity of gastric cancer cells to the histone methylation inhibitor 3-deazaneplanocin A (DZNep). *Clin Cancer Res* 2012;18:4201-12.
34. Sekiguchi M, Sakakibara K, Fujii G. Establishment of cultured cell lines derived from a human gastric carcinoma. *Jpn J Exp Med* 1978;48:61-8.
35. Yokozaki H. Molecular characteristics of eight gastric cancer cell lines established in Japan. *Pathol Int* 2000;50:767-77.